Università della Calabria

Dottorato di Ricerca in Ingegneria Chimica e dei Materiali
SCUOLA DI DOTTORATO " PITAGORA " IN SCIENZE INGEGNERISTICHE

Tesi

Modelling study of vanadium based alloys and crystalline porous materials for gas separation membranes

Settore Scientifico Disciplinare CHIM07 – Fondamenti chimici delle tecnologie

Supervisor

Dr. Giorgio DE LUCA

Prof. Efrem CURCIO

Candidato

Jenny BORISOVA EVTIMOVA

Ciclo XXVIII

Il Coordinatore del Corso di Dottorato

Ch.mo Prof. Raffaele MOLINARI

A.A. 2014-2015

European Commission
ERASMUS MUNDUS

UNIVERSITÀ DELLA CALABRIA

Universidad Zaragoza

UNIVERSITÉ DE MONTPELLIER

Modelling study of vanadium based alloys and crystalline porous materials for gas separation membranes

Dissertation

by

Jenny Borisova Evtimova

ACADEMIC YEAR 2014-2015

European Commission
ERASMUS
MUNDUS

EUDIME

UNIVERSITÀ
DELLA CALABRIA

Universidad
Zaragoza
1542

UNIVERSITÉ
DE MONTPELLIER

ACKNOWLEDGEMENT

The financial support of The Education, Audiovisual and Culture Executive Agency – EACEA/European Commission within the "Erasmus Mundus Doctorate in Membrane Engineering – EUDIME" (ERASMUS MUNDUS Programme 2009-2013, FPA n. 2011-0014, SGA n. 2012-1719) is kindly acknowledged.

ACADEMIC YEAR 2014-2015

Abstract

Gas membrane separation is an attractive technology that is often superior to other more conventional procedures for separation of gaseous species in terms of energy consumption and environmental impact. A key factor for membrane separations is the membrane itself with its properties, which determine the overall performance of the process. One essential membrane characteristic is the transport selectivity. High separation factors are especially difficult to achieve for mixtures of light gases having comparable kinetic diameters. Moreover, high permeability, correspondingly high solubility and diffusivity in dense membranes, are crucial aspects for the performance and further practical application of membrane devices. In this frame, the material used as a selective layer is determinant. Therefore, scientists devote immense efforts to the search of optimal gas-sorbent combinations, including thorough study of existing structures and elaboration of new ones with sieving properties. The large effort and time required for preparation and experimental testing of materials impede the advancement of new membranes.

In this study, we propose procedures based on computational calculations and theoretical models that can be used to predict the behaviour of some of the membrane materials of interest for gas separation applications. In particular, we focus on: i) body-centred cubic VNiTi alloys as novel materials for H_2-selective dense membranes and ii) crystalline porous materials that are attractive media for separation of light gases such as H_2, O_2, CO, CO_2, CH_4 and N_2. These two types of materials are treated using different methodologies, adapted to the needs of our research objectives associated to each material.

In the case of dense metal membranes, the long standing-controversy over occupancy of interstitial hydrogen in V-based alloys is addressed. The V-Ni-Ti system is of particular interest here, exhibiting high H_2 permeability and improved mechanical properties relative to pure V. This work intends to gain understanding of hydrogen-metal interactions as function of alloy composition and thereby to optimize these new materials and advance their development as novel membranes for H_2 separation. We use a first-principles approach that gives insights into the sites preference of hydrogen and assesses the role of Ti and Ni substitutional solutes for the hydrogen absorption affinity. The method based on Density Functional Theory requires no experimental input except crystal structure information. Furthermore, it uses no empirical or fitting parameters in contrast to other computational techniques. Hence this approach provides an alternative way to explore new metal alloys for H_2 separation membranes. The applied methodology can be used further in high-throughput calculations to screen various alloy compositions. The hereto-reported results will be used as guidance for tailoring the formulation of VNiTi solid solutions and preparation of low cost[†] dense alloy membranes in the frame of other projects (e.g. European DEMCAMER project).

Further, we explore how single-component inputs can be used to forecast the ideal selectivity towards light gases of crystalline porous materials, used for membrane preparation. Theoretical models for describing gas separation properties of zeotype materials as function of structural characteristics and operation conditions are proposed. The model parameters can be obtained as experimentally as well as computationally. To analyse the extent of validity and limitations of the models, ideal selectivities of few crystalline porous materials are evaluated, including widely used zeolites (NaA, CaA) and a metal organic framework structure (ZIF-8). The results verified that the theoretical expressions could be used for screening series of zeotype materials when reliable single gas adsorption data are available. However, since the models don't take into account all parameters (namely related to the membrane design) and mechanisms involved in gas transport through porous membranes, their predictions should be considered as values referring to an ideal case.

Riassunto

La separazione di correnti gassose mediante processi a membrana rappresenta un'interessante tecnologia che risulta spesso superiore a differenti tecniche tradizionali, sia in termini di consumo energetico che di impatto ambientale. Un fattore chiave che influenza in modo significativo la separazione di gas mediante processi a membrana è appunto la membrana; in particolare le sue proprietà determinano le prestazioni generali del processo. Tra le differenti proprietà di una specifica membrana, la perm-selettività senza altro è la decisiva. Per membrane dense o sub nanoporose, impiegate appunto nella purificazione di correnti gassose, l'alta permeabilità corrisponde ad alta solubilità e diffusività. Queste due caratteristiche sono aspetti cruciali che devono accuratamente ottimizzate per auspicabili applicazioni delle membrane. L'impegno e lo sforzo, in termini di lavoro e tempo, richiesto per la preparazione e la caratterizzazione dei nuovi materiali da impiegare rallenta lo sviluppo di membrane con proprietà innovative. Così, un grande interesse scientifico è stato dedicato alla ricerca delle relazioni tra struttura chimica alla nanoscala e solubilità e diffusione di molecole gassose per trovare ottimali nuovi materiali.

In questo studio, proponiamo, un'analisi computazionale, basata su calcoli quantistici, e due modelli teorici, entrambi utilizzabili per predire alcune proprietà fondamentali di materiali inorganici di interesse impiegati nella preparazioni di membrane. In particolare, abbiamo focalizzato la nostra attenzione su: i) leghe metalliche di VNiTi con struttura cubica a corpo centrato da utilizzare nella preparazione di membrane dense selettive verso l'idrogeno e ii) materiali cristallino-porosi

---

[†] in comparison with membranes that use Pd or its alloys as a core material

promettenti per la separazione di gas leggeri come: H_2, O_2, CO, CO_2, CH_4 e N_2. Le due tipologie sono state studiate utilizzando diverse metodologie computazionali, in base al tipo di materiale ed agli degli obiettivi della ricerca.

I siti d'assorbimento degli atomi d'idrogeni in leghe a base di vanadio sono stati studiati utilizzando un approccio computazionale a principi primi. La lunga controversia che riguarda la disposizione degli atomi d'idrogeno nella cella unitaria di V e delle sue leghe è stata affrontata e investigata. Una volta analizzati i siti in cui gli atomi d'idrogeno sono assorbiti preferenzialmente, il ruolo degli atomi di Ti e di Ni sull'affinità della lega verso l'idrogeno è stato valutato. Il metodo computazionale, basato sulla Teoria del Funzionale della Densità, non richiede informazioni sperimentali ad eccezione dei dati che riguardano le strutture cristalline delle leghe considerate. In aggiunta, l'approccio seguito non utilizza parametri aggiustabili né empirici né teorici in contrasto con altre tecniche computazionali, così può essere considerato un metodo predittivo utile per esplorare nuove leghe metalliche utilizzabili per la separazione d'idrogeno mediante processi a membrana. I dati ottenuti in questa Tesi possono essere utilizzati per l'ottimizzazione di membrane dense a base di leghe di V a basso costo.

In seguito, sono stati proposti due modelli teorici per valutare i fattori di separazione ideale di materiali cristallino-porosi verso gas leggeri. Le equazioni proposte utilizzano come parametri quelli ottenuti dalle isoterme di adsorbimento dei singoli gas. Questi modelli sono stati proposti per predire la selettività di materiali di tipo zeolitico in funzione di parametri strutturali e condizioni operative. I parametri da utilizzare nelle equazioni proposte possono essere ottenuti sia sperimentalmente che mediante tecniche computazionali. Per analizzare il campo di validità e i limiti dei modelli, i fattori di separazioni ideale delle zeoliti, quali NaA, CaA, e del MOF, ZIF-8, sono stati valutati. I risultati hanno mostrato che per i sistemi considerati le equazioni modello sono in buon accordo con i dati sperimentali, in modo specifico, con la parte dei fattori di separazione connessa all'adsorbimento dei gas. Dunque essi possono essere utilizzati per una preliminare selezione di materiali cristallino-porosi se le isoterme d'adsorbimento dei singoli gas sono disponibili.

Resumen

La separación de gases usando membranas es una tecnología atractiva que suele ser superior a otros procedimientos convencionales de separación de gases en términos de consumo de energía e impacto medioambiental. Un factor clave en la separación con membranas es la propia membrana y sus propiedades, las cuales determinan el desarrollo global del proceso. Una característica esencial de las membranas es la permeoselectividad. En el caso de mezclas de gases ligeros con tamaños moleculares similares resulta especialmente difícil alcanzar factores altos de separación. Además, la

alta permeabilidad, junto con la alta solubilidad y difusividad en las membranas densas, son aspectos cruciales para el desarrollo y aplicación práctica de las membranas. Por ello, los científicos están actualmente poniendo todo su empeño en buscar combinaciones óptimas de materiales para membranas, así como también el desarrollo de nuevos materiales. El gran esfuerzo y tiempo que requiere la preparación y las pruebas experimentales de los materiales de membrana impiden la emergencia de nuevas membranas.

En este estudio se proponen procedimientos basados en simulaciones computacionales y modelos teóricos que se pueden utilizar para predecir el comportamiento de algunos materiales de interés para la separación de gas con membranas. En particular, el estudio se centra en: i) aleaciones de VNiTi cúbicas centradas en el cuerpo como nuevo material para membranas metálicas densas selectivas a H_2 y ii) materiales porosos cristalinos atractivos para la separación de gases ligeros como H_2, O_2, CO, CO_2, CH_4 y N_2. Ambos grupos de materiales se tratan aquí usando diferentes metodologías en función de los objetivos de la investigación.

En el caso de membranas metálicas densas, existe una larga controversia sobre la ocupación intersticial del hidrógeno en el vanadio y sus aleaciones. Por esta razón, se presenta un primer enfoque de principios que dan pistas de los posibles huecos preferentes que ocupa el hidrógeno y evalúan el rol de los solutos que sustituyen al Ti y Ni en lo que a la afinidad de absorción del hidrógeno se refiere. El método basado en los cálculos teóricos de densidad funcional no requiere experimentación excepto la información de la estructura cristalina.

A diferencia de otras técnicas computacionales, en este caso no se necesitan parámetros empíricos. Por ello este enfoque proporciona una vía alternativa para investigar nuevas aleaciones de metales para membranas selectivas a H_2. La metodología aplicada se puede usar además a través de otros cálculos para observar varias composiciones de aleaciones. Los resultados que se presentan se usarán como guía de seguimiento para disoluciones sólidas de VNiTi y para la preparación de membranas densas de aleaciones de bajo coste en el marco del proyecto DEMCAMER.

A continuación se explora cómo el estudio de un único componente se puede usar para predecir la selectividad ideal de medios porosos cristalinos para gases ligeros. Se proponen modelos teóricos que describen las propiedades de la separación de gases de materiales tipo zeolita en función de parámetros estructurales y condiciones de operación. Los parámetros del modelo se pueden obtener tanto experimentalmente como computacionalmente. Para analizar la extensión de la validez y las limitaciones del modelo, se evalúan las selectividades ideales de zeolitas (NaA, CaA) y MOFs (ZIF-8) que se usan habitualmente. Los resultados verifican que las expresiones teóricas podrían usarse para seleccionar los mejores materiales porosos cristalinos idóneos para una separación dada cuando se dispone de datos fiables de difusión y adsorción de gases.

Résumé

La séparation de gaz par membrane est une technologie attractive qui est souvent plus performante que d'autres procédés de séparation plus conventionnels, en termes de consommation d'énergie et d'impact environnemental. Un facteur clé pour la séparation membranaire est la membrane elle-même, dont les propriétés déterminent les performances globales du procédé. Une caractéristique essentielle de la membrane est son aptitude à séparer les espèces contenues dans un mélange. Des facteurs de séparation élevés sont particulièrement difficiles à obtenir pour des mélanges de gaz légers ayant des diamètres cinétiques comparables. De plus, des perméabilités élevées, résultat de solubilités et diffusivités élevées des gaz pour les membranes denses, sont des aspects cruciaux pour les performances et donc pour la mise en application des systèmes membranaires. Dans ce contexte, le choix du matériau utilisé comme couche sélective est déterminant. Par conséquent, les scientifiques consacrent d'immenses efforts à la recherche de combinaisons optimales gaz/matériaux sorbants, tant par l'étude approfondie de structures existantes que par l'élaboration de nouveaux matériaux capables de séparer les molécules. Les efforts et le temps requis pour la préparation et l'étude expérimentale des matériaux membranaires limitent les avancées sur le développement de nouvelles membranes.

Dans cette étude, nous proposons des procédures basées sur des calculs informatiques et des modèles théoriques qui peuvent être utilisés pour prévoir le comportement de certains matériaux membranaires d'intérêt pour les applications de séparation de gaz. En particulier, nous nous sommes concentrés sur: i) des alliages VNiTi de structure cubique centrée, considérés comme de nouveaux matériaux pour les membranes denses sélectives à H_2 et ii) sur des matériaux poreux cristallins qui sont des systèmes attractifs pour la séparation de gaz légers tels que H_2, O_2, CO, CO_2, CH_4 et N_2. Les deux groupes de matériaux sont traités en utilisant une méthodologie différente, adaptée aux besoins des recherches associées à ces matériaux.

Dans le cas des membranes métalliques denses, nous nous sommes intéressés à la controverse, connue de longue date, concernant l'occupation de l'hydrogène interstitiel dans les alliages à base de vanadium. Le système V-Ni-Ti est en effet particulièrement intéressant grâce à sa perméabilité élevée pour H_2 et à ses propriétés mécaniques accrues par rapport au vanadium pur. Ce travail cible la compréhension de la structure ces alliages à l'échelle atomique, de façon à les optimiser et à activer la conception et le développement de ces matériaux comme nouvelles membranes pour la séparation de H_2. Notre approche, basées sur les premiers principes, donne un aperçu des sites préférentiels de l'hydrogène et évalue le rôle des solutés de substitution Ti et Ni, sur l'affinité d'absorption de l'hydrogène. La méthode basée sur la théorie de la fonctionnelle de la densité (DFT) ne nécessite aucune donnée expérimentale autre que l'information sur la structure cristalline. En outre, cette méthode n'utilise aucun paramètre empirique ou d'ajustement, contrairement à d'autres techniques de calcul. Ainsi, cette approche est une voie alternative pour

explorer de nouveaux alliages métalliques utilisables comme membranes de séparation de H_2. La méthodologie appliquée pourra être utilisé ensuite dans des calculs à haut débit pour cribler diverses compositions d'alliage. Les résultats reportés ici seront utilisés comme guide pour adapter la formulation des solutions solides VNiTi et préparer des membranes en alliage denses à faible coût (par rapport aux membranes à base de palladium) dans le cadre d'autres projets (e.g. Projet Européen FP7- DEMCAMER).

Dans le cadre de notre étude sur les membranes cristallines microporeuses, nous démontrons comment les données sur un composant unique peuvent être utilisées pour prédire la sélectivité idéale de ces membranes envers les gaz légers. Des modèles théoriques sont ainsi proposés pour décrire les propriétés de séparation de gaz de matériaux de type zéolithiques (« zeotypes ») en fonction de leurs paramètres structuraux et des conditions de fonctionnement. Les paramètres du modèle peuvent être obtenus expérimentalement ainsi que par le calcul. Afin d'analyser le degré de validité et les limites des modèles, les sélectivités idéales de deux membranes zéolithes classiquement étudiées (NaA, CaA) et d'une membrane MOF (ZIF-8) ont été évaluées. Les résultats démontrent que les expressions théoriques peuvent être utilisées pour le criblage de séries de matériaux microporeux cristallins sous réserve que des données fiables sur l'adsorption de gaz purs soient disponibles pour ces matériaux. Cependant, étant donné que les modèles n'intègrent pas tous les paramètres (notamment liés au design des membranes) et mécanismes impliqués dans le transport de gaz à travers ces membranes, les prédictions doivent être considérées comme celles correspondant à un cas idéal.

Acknowledgements

I thank all people who made their contribution to this work in various ways and supported me in the course of my PhD study.

First I would like to express my sincere gratitude to my supervisors, Dr. Giorgio De Luca at ITM-CNR, Dr. Anne Julbe at the IEM-CNRS and Prof. Dr. Joaquin Coronas at INA, for their continuous guidance and assistance. Dr. Giorgio De Luca introduced me to the world of quantum mechanics, sharing his expertise. Dr. Anne Julbe helped me in my research with her motivation, immense knowledge, thoughtful comments and corrections. Prof. Dr. Joaquin Coronas provided insight, materials and facilities from great value for the research.

Special thanks go to Fernando Cacho-Bailo, Dr. Federica Bisigniano and Dr. Martin Drobek, who helped me professionally through their own example. I am also grateful to Cyril Vallicari for the measurements on confined ZIF-8 membranes, to Dr. Izumi Kumakiri and Prof. Dr. Hidetoshi Kita for providing LTA membranes and to Dr. David Farrusseng for the gas sorption data on ZIF-8.

I place on record my sincere thank to Dr. Michael Dolan, Dr. Keith McLennan and Dr. David Viano for their cooperation, helpful discussions and hospitality.

Financial support from EU-EACEA under the EUDIME project is gratefully acknowledged. I thank Prof. Enrico Drioli, Prof. Raffaele Molinari, Prof. Efrem Curcio, Prof. André Ayral and Prof. Reyes Mallada for the coordination of the doctorate program.

I also thank my fellow colleagues and all of my friends who supported me through this journey. Last but not the least, I would like to thank my family for always standing by my side.

Table of Content

List of Figures

List of Tables

List of Abbreviations

A	Zeolite A
AlPO	Alumino-phosphate
bcc	Body-centred cubic
c1	Referring to disposition of H atoms at one face of a unit cell
c2a	Referring to disposition of H atoms at two adjacent faces
c2o	Referring to disposition of H atoms at two opposite faces
CAS	Chemical Abstracts Service
CCDC	Cambridge Crystallographic Data Centre
CHA	Chabazite
DD3R	Decadodecasil 3R
DFT	Density Functional Theory
DTA	Differential thermal analysis
ECP	Electron core potential
FAU	Faujasite
fcc	Face-centred cubic
GC	Gas chromatograph
GGA	Generalized gradient approximation
GT	Gas translation
HOMO	Highest occupied molecular orbital

IUPAC	International Union of Pure and Applied Chemistry	
LDA	Local density approximation	
LSX	Low-silica zeolite X	
LTA	Linde type A	
LUMO	Lowest unoccupied molecular orbital	
MD	Molecular dynamics	
MFI	Mordenite Framework Inverted	
MMM	Mixed matrix membrane	
MOF	Metal organic framework	
MOR	Mordenite	
MW	Molecular weight	g mol^{-1}
NMR	Nuclear magnetic resonance	
O	Octahedral	
PEM	Proton exchange membrane	
PFG	Pulsed-field gradient	
PSA	Pressure swing adsorption	
QM	Quantum mechanics	
QUENS	Quasi-elastic neutron scattering	
RSC	Relativistic small-core effective basis set	
SIM-1	Substituted imidazolate-based MOF	
SOD	Sodalite	
STP	Standard temperature and pressure	
T	Tetrahedral	

TGA	Thermogravimetric analysis
X	Zeolite X (FAU)
XRD	X-Ray Diffraction
Y	Zeolite Y (FAU)
ZIF	Zeolitic imidazolate framework
ZSM-5	Zeolite Socony Mobil–5

List of Symbols

Latin Symbols

a	Lattice parameter	Å
a	Acceleration	m s^{-2}
b	Langmuir coefficient	kPa^{-1}
D	Diffusivity coefficient	m^2 s^{-1}
d	Diameter	Å
E	Energy	eV or kJ/mol
F	External force	kg m s^{-2}
f	Effective length	Å
$\hat{H}$	Hamiltonian operator	
h	Planck's constant	m^2 kg s^{-1}
J	Flux	mol s^{-1} m^{-2}
K	Equilibrium constant	mol kg^{-1} Pa^{-1}
L	Thickness of the selective layer	m
M	Metal atom or metal ion	
m	Mass	kg
n	Integer number	
N	Number of electrons	
P	Pressure	kPa
Q	Isosteric heat of adsorption	kJ mol^{-1}
q	Amount adsorbed gas	mol kg^{-1}
R	Universal gas constant	kJ mol^{-1} K^{-1}
r	Spatial coordinates	
S	Membrane surface area	m^2
s	Electron spin	
T	Temperature	K
V	External potential	
V	Volume adsorbed gas	cm^3 g^{-1}
z	Probability factor	

Greek Symbols

α	Selectivity	
Γ	Thermodynamic correction factor	
δ	Defined as the ratio d_p/d_m	
θ	Loading	
λ	Diffusional (jump) length	
μ	Chemical potential	J mol^{-1}
$\prod$	Permeance	mol m^{-2} s^{-1} Pa^{-1}
ρ	Density	kg m^{-3}
ψ	Wave function	

Indices

2H	Referring to a pair of hydrogen atoms
A	Component A
Ads	Adsorption
B	Component B
Cluster	Referring to the metal cluster
F	Feed
GT	Gas translation
H	Stands for Henry constant
i	Component A or B
j	Permeate or flux
k	k-th electron
KS	Referring to Kohn-Sham equation
m	Molecule
MS	Maxwell-Stefan
n	Valence
P	Permeate
p	Pore
R	Retentate
s	Referring to self-diffusivity
sat	Saturation
xc	Referring to exchange and correlation contribution

Introduction

Summary

English version: This introductory part provides a brief overview of membranes for gas separation applications. Different membrane types and transport mechanisms occurring in the frame of gas separation membrane processes are outlined. Further, criteria for membrane selection are discussed and case studies of high purity hydrogen production and of light gas separations including N_2, O_2, CO_2 and CH_4 are introduced. Next, the scope of this doctorate thesis is highlighted. Lastly, a short outline of the thesis is provided.

Italian version: Questa parte introduttiva fornisce una panoramica sulle membrane impiegate per la separazione di gas. Diversi tipi di membrane e meccanismi di trasporto sono descritti. Inoltre, differenti criteri per la selezione di membrane saranno analizzati, saranno quindi introdotti alcuni aspetti legati alla produzione d'idrogeno con alto grado di purezza e alla separazione di gas leggeri, quali: N_2, O_2, CO_2 e CH_4 mediante materiali cristallino-porosi. Quindi, lo scopo della Tesi viene definito ed evidenziato. Nell'ultima sezione, vengono, infine, presentati alcuni sviluppi e prospettive di questo lavoro.

Spanish version: Esta parte introductoria proporciona una breve visión general sobre las membranas para las aplicaciones de separación de gases. Se presentan de forma independiente diferentes tipos de membranas y mecanismos de transporte que ocurren en los procesos de separación de gases con membranas. También se discuten los criterios para la elección de membranas y se presentan estudios de casos de producción de hidrógeno de alta pureza y separación de gases ligeros como N_2, O_2, CO_2 y CH_4. A continuación, se resume la temática de esta tesis doctoral. Finalmente, se proporciona un breve índice de la tesis.

French version: Cette partie introductive donne un bref aperçu sur les membranes utilisées pour les applications de séparation de gaz. Les différents types de membranes et les mécanismes de transport impliqués dans les procédés membranaires de séparation de gaz sont décrits. Ensuite, nous discutons les critères de sélection des membranes et nous introduisons des études de cas de production d'hydrogène de grande pureté et de séparations de mélanges de gaz légers contenant N_2, O_2, de CO_2 et de CH_4. Finalement, les objectifs de cette thèse de doctorat sont présentés, ainsi qu'une brève description du plan du manuscrit.

Gas separation membranes

Membranes are not a new invention [1]. In fact biological membranes exist since life exists. However, preparation of synthetic membranes and their industrial application are more recent technology. The chemical community through IUPAC gives the following definition of a membrane: "*structure, having lateral dimensions much greater than its thickness, through which mass transfer may occur under a variety of driving forces*" [2]. Compared to conventional separation techniques, membrane processes are usually simpler and more cost effective in terms of operation. They are able to separate mixtures by difference of components permeation through them. The driving forces for gas transport include for example pressure difference, concentration gradient and electrical potential across the membrane [3]. The variety of membranes spans solid and liquid, homogeneous and heterogeneous, isotropic and anisotropic, porous and dense structures. The available membranes nowadays are quite satisfactory in broad range of applications such as haemodialysis, haemofiltration, electrodialysis, microfiltration, ultrafiltration, and water desalination by reverse osmosis [1]. However, in other areas such as gas separation, industrially accepted products have emerged only in the past 35 years, and improvement of membranes, process design and know-how are still required for further expanding industrial applications in this area [1,4].

Membranes used to separate gaseous mixtures could be comprised as of organic (polymeric) as well as of inorganic materials or a combination of both organic and inorganic species (hybrid and composite structures) [5]. Currently, most industrial gas separation processes employ polymeric membranes, due to their good mechanical properties, reproducibility and low price. However, the performance of these membranes rarely exceeds the upper bound predicted by Robeson in the 1990s for the trade-off between permeability and selectivity [6]. Apart from that, polymeric membranes suffer from limited solvent resistance, poor chemical and thermal stability and swelling that alters their separation properties [7]. Inorganic membranes have better resistance to severe conditions and are topic of considerable research interest for separations involving high temperatures or aggressive media. Mixed structures that incorporate both inorganic and organic components are also available. For example, composite membranes consist of two or more distinct materials that could be of different nature, e.g. mixed matrix membranes (MMMs) [8] are composed of a polymeric matrix with homogeneously dispersed inorganic (nano)particles [9]. The nanostructured inorganic particles, that may be zeolites, metal-organic frameworks, or carbon molecular sieves, are used as filler, dispersed in a continuous polymer phase. The selection of suitable inorganic filler and polymer matrix, along with the interaction between the two phases, play a key role for successful implementation of MMMs.

Organic, inorganic and composite membranes can be either porous or dense. The former are characterised by interconnected pores. Here pore sizes and pore size distributions are determining factors for separation processes. Depending on the pore size of the membrane material and on the kinetic diameter of the gases to be separated, transport of species through membranes occurs via specific mechanism or a combination of mechanisms [10]. Three of the main transport mechanisms, as regards porous materials, are shown in Figure 1. Some of the cases, e.g. capillary condensation that is related to 'vapour' flow [11], are omitted. As a further matter, subcases of the hereto-considered mechanisms are recognised, as explained below. In the case of relatively large pores (between 0.1 and 10 μm) the gas components pass freely through the membrane in convective flow mode. Consequently no separation transpires. For smaller pores (less than 0.1 μm), with diameter comparable to the mean free path of gas molecules (the average distance traversed by a molecule between collisions), the permeation flux of each gas component follows Graham's law of diffusion, i.e. it is inversely proportional to the square root of the molecular weight (MW). This transport mechanism is called Knudsen diffusion. A special case of the Knudsen diffusion is the activated Knudsen-type diffusion, also known as gas translational diffusion. It defines the molecular motion in porous solids that is restricted by energy barrier exerted by the porous network [12]. In zeolites, the energy barrier is imposed by windows separating the voids in the crystalline structure [13]. In the case of activated Knudsen-type diffusion, the penetrants retain their gaseous state. Further, if the pore size is small enough (generally less than 20 Å), molecular sieving takes place. Large molecules cannot penetrate the membrane (size exclusion), while molecules with kinetic diameter smaller than the pore size diffuse through the micropores by a mechanism known as surface diffusion. Here, due to the strong interaction with the solid framework, the molecules loose their gaseous entity and move as an adsorbed phase across the internal surface [14]. However, it should be noted that surface diffusion can occur as well in mesopores, provided that gas species adsorb and propagate along the pore walls [15]. Moreover, if the molecular diameter and pore diameter are of comparable size, the term configurational diffusion is also used [13]. Anyhow, often the denomination configurational diffusion is adopted in a more general way to colligate the transport mechanisms occurring in micropores, where diffusion becomes an activated process, i.e. as a colligation term for gas translational and surface diffusion [12,14]. On the other hand dense membranes don't possess any intentional interconnected pores except tiny void spaces that can accommodate only small molecules [16]. Permeation of larger species is hindered. Transport through these membranes is described by the solution-diffusion mechanism (also known as sorption-diffusion mechanism) [17]. The solution-diffusion mechanism will be briefly described in Part I of this work, while the other aforementioned transport mechanisms will be discussed in greater detail in Part II.

In general porous membranes provide high fluxes but low separation factors, while dense structures offer high selectivity but limited flux. The choice between polymeric and inorganic, porous and dense structure is determined by the composition of the gas mixture, the most valuable gas component, the desired level of purification and the conditions of interest (operation parameters). In some cases, as stated previously, hybrid, mixed and composite membranes are employed.

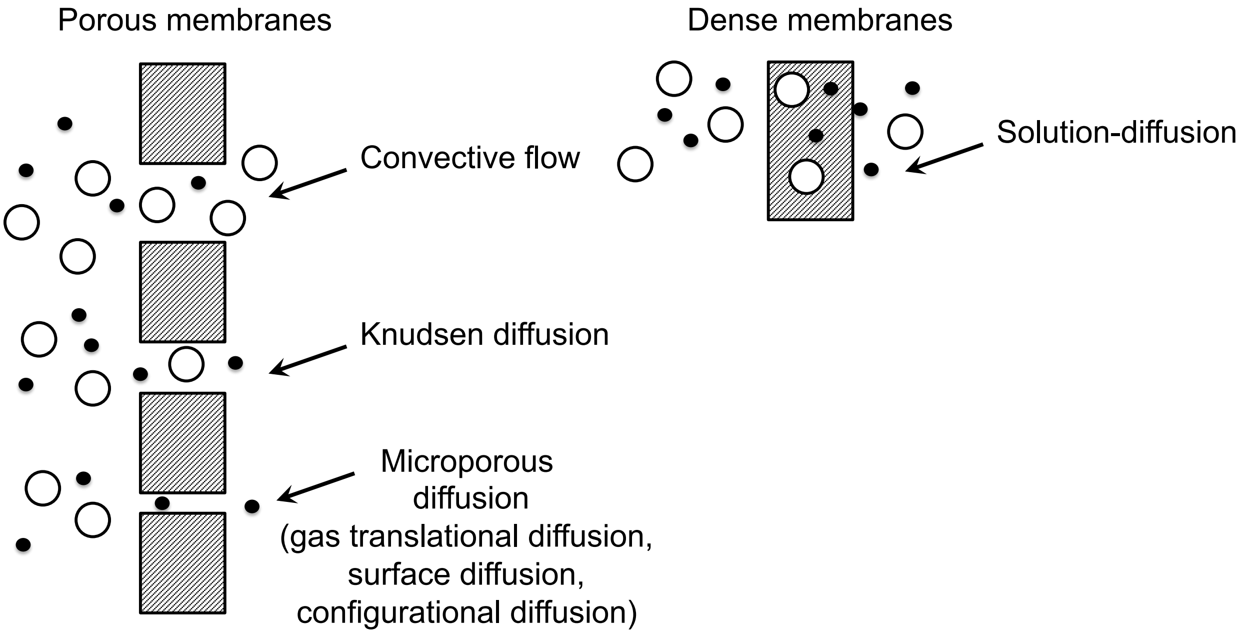

Figure 1: Schematic illustration of gas permeation mechanisms through porous and dense membranes, reproduced from [4] with modifications.

A process that is object of intense scientific attention is the separation of hydrogen from mixed gas streams. Hydrogen is an important chemical feedstock and energy source that has the potential to reduce the dependency on fossil fuels [18]. However, despite that it is the most abundant element in the Universe, on Earth hydrogen occurs mainly in combination with other gases and in organic matter such as plants, coal and petroleum. One way to obtain pure hydrogen is by water splitting via electrolysis but this method remains expensive [19]. Currently, hydrogen production via coal gasification or via steam reforming is more cost-efficient but these methods generate by-products such as CO_2 and CH_4 that need to be further removed. Being more energy efficient than conventional separation techniques such as pressure swing adsorption (PSA) and cryogenic distillation, membrane processes represent a potential pathway for hydrogen purification [17,18].

Table 1 compares five classes of H_2-selective membranes. The list includes both organic (polymers) and inorganic materials (carbon, ceramics and metals). Dense polymeric structures can't compete with the other types of membranes neither in terms of selectivity nor of flux rate. Moreover, polymer membranes operate at low temperatures and hence are not suitable for hydrogen separation under steam reforming reaction conditions or from coal-derived syngas. Due to the high temperature of reforming and gasification steams (between 500 and 800 K) warm- and hot-gas separation techniques are economically beneficial [20]. Porous carbon and microporous membranes are intended to work at high temperatures but still the selectivity is between low and moderate. Utilization of hydrogen as an energy source by deployment of PEM fuel cells requires high purity gas stream. Dense ceramic and dense metal membranes work at temperatures associated with reforming and water-gas-shift reactions and have the advantage of very high (theoretically infinite) H_2 separation factor. Due to their high permeability, the latter are good match for hydrogen production. However, considering that the core material of current dense metal membranes is palladium, they are (and will be more and more) expensive for large-scale applications [21]. Therefore scientists are aimed to identify non-precious metals alternative to Pd for development of H_2 purification membranes.

Table 1: Comparison of different types of H_2-separation membranes [20].

Membrane type **Property**	**Dense Polymer**	**Porous Carbon**	**Microporous Ceramic**	**Dense Metal**	**Dense Ceramic**
Optimum temperature range	<373 K	773-1173 K	473-873 K	573-873 K	873-1173 K
H_2 selectivity	Low	Low	Moderate	Very high	Very high
H_2 flux	Low	Moderate	High	High	Moderate
Transport mechanism in the optimum temperature range	Solution/ Diffusion	Molecular sieving	Molecular sieving	Solution/ Diffusion	Solution/ Diffusion

Other key gas separations are N_2/O_2 and CO_2/CH_4. They are important for both environmental and economical reasons [22]. Metal dense membranes of the type discussed above are not able to separate these pairs since they block the transport of all species larger than atomic hydrogen. Zeolites and MOFs are well known membrane materials for separation of such light gases, due to their uniform porous topology with pore diameters of molecular dimensions [23]. Here, a crucial factor for successful purification is the careful selection of an adequate crystalline porous material between the numerous available structures. Therefore, the relationship between structure and selectivity is a subject of intensive research in this domain. The availability of models able to forecast the selectivity of zeotype materials towards light gases will be of great value as a preliminary step for identification of suitable gas-membrane combinations. The correlations should describe the separation properties in a desired range of conditions (temperature and pressure) [13]. In addition, they should preferably have an analytical form containing relatively few parameters. The availability of a coherent set of data to be used as input into the developed models is also demanded for reliable predictive results. The limited availability and complexity of multicomponent data compel one to search for practical predictive correlations that are based on pure-component data [24]. The theoretical values obtained in this manner could represent a reference point to the scientific community, which is an important aspect, considering that recent research is focused on improving permeation properties and augmenting the selectivity of known crystallite porous structures by various synthesis methods and modifications.

Scope of work

An ongoing challenge in membrane technology is to reduce the price and the material resource dependence of dense metal membranes for H_2 purification, while achieving high selectivity and good membrane stability. The high cost of these membranes is due to the use of Pd, which is the dominant material in this application frame [25]. One obvious way to lower the membranes cost is to reduce the amount of precious material used for membrane preparation. Thus, composite membranes consisting of a thin palladium layer deposited onto a porous substrate are being developed [26]. Another avenue towards preparation of inexpensive dense membranes for H_2 separation is to use non-noble metals with competitive transport properties. Vanadium, often referred to as “super-permeable” metal, is considered relevant and less expensive alternative to Pd. However, pure V is not suitable for H_2-separation membranes due to embrittlement susceptibility. Selective alloying with Ni and Ti is reported to improve the mechanical stability of V [27]. Although many research studies are available on Pd and its alloys, V-based alloys still raise questions that need to be addressed.

Attempting to further the development of non-noble dense metal membranes for H_2 separation we decided to explore the hydrogen-metal interactions in VNiTi alloys using quantum mechanics (QM) calculations in the frame of Density Functional Theory (DFT). In this study, we approached the controversy over the sites preference of interstitial hydrogen within V-based metal lattices. Insight into the hydrogen occupation state provides fundamental information for understanding various properties of the hydrogen–metal system, although previous studies didn't reach agreement on the topic. We also investigated another issue related to the behaviour of absorbed hydrogen that is seldom considered in the past, namely the H-H mutual disposition within the metal matrix. Finally, using the knowledge gained by exploring the preceding research questions, the influence of Ti and Ni solute atoms on the hydrogen occupancy and absorption affinity of the alloy was investigated. This information will be a useful guidance for future experimental studies.

Moreover, in this thesis, we expanded our research on gas separation, considering crystalline porous materials that are suitable to purify not only H_2 but also playing role in other important separations such as N_2/O_2 and CO_2/CH_4. Starting from the first natural zeolite discovered in 1756, many zeotype materials emerged over the years. Nowadays the official list of zeolites frameworks sums to 229 types [28] not taking into account the large number zeolite-like metal organic frameworks (MOFs) that have been synthesized in the last years. With this study we were aimed to facilitate the choice of both zeolites and MOFs as materials for gas separation. Therefore we developed theoretical models for evaluating the ideal gas selectivity of these crystalline porous materials. The model parameters can be obtained either from experimental data or from computational methods, which allows for assessment of various real and hypothetical materials of the type.

Outline of the thesis

This work is divided into two parts. Part I *First-principles study of vanadium based alloys* deals with the study of hydrogen occupation and hydrogen absorption affinity in VNiTi alloys. That part consists of 4 chapters. Chapter 1 *Theoretical background* offers a brief description of metal systems, covering crystallographic structures and underlying concepts for selection of metals and alloys as materials for hydrogen separation membranes. Engineering and economical considerations for the choice of metals are discussed. Further the basic concepts of quantum mechanics and DFT are introduced. Chapter 2 *Methodology* covers the computational procedure and atomic models used in this work, followed by the procedure to evaluate hydrogen binding energies in the target alloys. The outcomes of the conducted study are outlined and analysed in Chapter 3 *Results and discussion*. Chapter 4 *Conclusions* summarises the principal findings from the study of VNiTi alloys and suggests investigation goals for the future.

Part II is devoted to the predictive study of zeotype crystalline porous materials. It includes 4 chapters. Chapter 5 *Theoretical background* focuses on the transport mechanisms of gases in crystalline porous materials. Brief overview of zeolites and metal organic frameworks is given with emphasis on their application as membrane materials for gas separation. Further, the reasoning for using the ideal gas selectivity of crystalline porous materials as a predictive feature for emerging membranes is explained and the capabilities and limitations of the theoretical models to describe gas separation behaviours are outlined. Chapter 6 *Methodology* introduces the predictive models, which have been developed and utilized in the course of this PhD work. Next, the model parameters are discussed in particulars. In order to verify the theoretical results, experimental measurements used to evaluate the ideal selectivity of selected model systems are also reported. The results obtained via the predictive models are reported in Chapter 7. Theoretical results for few model systems towards selected light gases are compared to experimental selectivity values and with the literature. The last chapter outlines the conclusions and implications derived from this study.

Bibliography

[1] H. Strathmann, L. Giorno, E. Drioli, An Introduction to Membrane Science and Technology, 1st Ed., Rende, CS, Italy: Consiglio Nazionale delle Ricerche, 2006.

[2] W.J. Koros, Y.H. Ma, T. Shimidzu, Terminology for membranes and membrane processes (IUPAC Recommendations), Pure and Applied Chemistry, vol. 68, no. 7, 1479-1489, 1996.

[3] P. Pandey, R.S. Chauhan, Membranes for gas separation, Progress in Polymer Science, vol. 26, 853-893, 2001.

[4] R.W. Baker, Membrane technology and applications, 2nd Ed., Chichester, WS, UK: John Wiley and sons, 2004.

[5] Y. Kase, Advanced membrane technology and applications, 1st Ed., N.N. Li, A.G. Fane, W.S. W. Ho, and T. Matsuura (Eds.), Hoboken, NJ, USA: John Wiley & sons, 2008.

[6] L.M. Robeson, Correlation of separation factor versus permeability for polymeric membranes, Journal of Membrane Science, vol. 62, 165-185, 1991.

[7] P.S. Goh, A.F. Ismail, S.M. Sanip, B.C. Ng, M. Aziz, Recent advances of inorganic fillers in mixed matrix membrane for gas separation, Separation and Purification Technology, vol. 81, no. 3, 243–264, 2011.

[8] A. Julbe, Zeolite membranes – synthesis, characterization and application, in: Introduction to zeolite molecular sieves, 3rd Ed., J. Cejka, H. van Bekkum, A. Corma, F. Schüth (Eds.), Elsevier, 2007, 181-219.

[9] T.S. Chung, L.Y. Jiang, Y. Li, S. Kulprathipanja, Mixed matrix membranes (MMMs) comprising organic polymers with dispersed inorganic fillers for gas separation, Progress in Polymer Science, vol. 32, no. 4, 483–507, 2007.

[10] V.N. Burganos, Modeling and simulation of membrane structure and transport properties, in: Comprehensive Membrane Science and Engineering, E. Drioli, L. Giorno (Eds.), Amsterdam, The Netherlands: Elsevier, vol. 1, 29-74, 2010.

[11] A.J. Burggraaf, Transport and separation properties of membranes with gases and vapours, in: Fundamentals of inorganic membrane science and technology, A.J. Burggraaf, L. Cot (Eds.), Amsterdam, The Netherlands: Elsevier, vol. 4, 331-433, 1996

[12] J. Xiao, J. Wei, Diffusion mechanism of hydrocarbons in zeolites – I. Theory, Chemical Engineering Science, vol. 47, no. 5, 1123-1141, 1992.

[13] A.J. Burggraaf, Single gas permeation of thin zeolite (MFI) membranes: theory and analysis of experimental observations, Journal of Membrane Science, vol. 155, 45-65, 1999.

[14] P.F. Lito, S.P. Cardoso, A.E. Rodrigues, C.M. Silva, Kinetic modeling of pure and multicomponent gas permeation through microporous membranes: diffusion mechanisms and influence of isotherm type, separation and purification, Separation & Purification Reviews, vol. 44, 283–307, 2015.

[15] A. Ayral, V. Hulea, J.-P. Joulin, A. Julbe, Céramiques pour l'environnement: filtres, membranes, adsorbants et catalyseurs, Techniques de l'Ingénieur, vol. N4805, 2014.

[16] M.V. Mundschau, Hydrogen separation using dense composite membranes, in: Inorganic membranes for energy and environmental applications, A.C. Bose (Ed.), New York, NY, USA: Springer, 2009.

[17] M.D. Dolan, Non-Pd BCC alloy membranes for industrial hydrogen separation, Journal of Membrane Science, vol. 362, 12-28, 2010.

[18] G.Q. Lu, J.C. Diniz da Costa, M. Duke, S. Giessler, R. Socolow, R.H. Williams, T. Kreutz, Inorganic membranes for hydrogen production and purification: A critical review and perspective, Journal of Colloid and Interface science, vol. 314, 589-603, 2007.

[19] N.A. Al-Mufachi, N.V. Rees, R. Steinberger-Wilkens, Hydrogen selective membranes: a review of palladium-based dense metal membranes, Renewable and Sustainable Energy Reviews, vol. 47, 540-551, 2015.

[20] S. Adhikari, S. Fernando, Hydrogen membrane separation techniques, Industrial & Engineering Chemistry Research, vol. 45, 875-881, 2006.

[21] M. Dolan, G. Song, D. Liang, M.E. Kellam, D. Chandra, J.H. Lamb, Hydrogen transport through $V_{85}Ni_{10}M_5$ alloy membranes, Journal of Membrane Science, vol. 373, 14-19, 2011.

[22] E. Garcia-Perez, J.B Parra, C.O. Ania, A. Garcia-Sanchez, J.M. van Baten, R. Krishna, D. Dubbeldam, S. Calero, A computational study of CO_2, N_2, and CH_4 adsorption in zeolites, Adsorption, vol. 13, 469-476, 2007.

[23] Y. Hasegawa, T. Tanaka, K. Watanabe, B.-H. Jeong, K. Kusakabe, S. Morooka, Separation of CO_2-CH_4 and CO_2-N_2 systems using ion-exchanged FAU-type zeolite membranes with different Si/Al ratios, Korean Journal of Chemical Engineering, vol. 19, no. 2, 309-313, 2002.

[24] S. Sircar, A.L. Myers, Gas Separation by Zeolites, in: Handbook of zeolite science and technology, S.M. Auerbach, K.A. Carrado, P.K. Dutta (Eds.), New York, NY, USA: Marcel Dekker, Inc., 2003.

[25] F. Gallucci, A. Basile, F.I. Hay, Membranes for membrane reactors: preparation, optimization and selection, 1st Ed., F. Gallucci, A. Basile (Eds.), Chichester, WS, UK: John Wiley & sons, 2011.

[26] B. Morreale, J. Ciferno, B. Howard, M. Ciocco J. Marano, O. Iyoha, R. Enick, Gasification and associated degradation mechanisms applicable to dense metal hydrogen membranes, in: Inorganic membranes for energy and environmental applications, 1st Ed., A.C. Bose (Ed.), New York, NY, USA: Springer, 2009.

[27] G. Song, M.D. Dolan, M.E. Kellam, D. Liang, S. Zambelli, V–Ni–Ti multi-phase alloy membranes for hydrogen purification, Journal of Alloys and Compounds, vol. 509, 9322-9328, 2011.

[28] http://www.iza-structure.org/databases/, November 2015.

Part I

First-principles study of vanadium based alloys

Summary

English version: In this part, a first-principles study of hydrogen occupation in VNi and VNiTi alloys is reported and the role of Ni and Ti substituents is anticipated. At first, a general introduction to metals and metal alloys is given. Their structural characteristics and related properties are discussed. Next, some of the fundamental ideas of quantum mechanics and Density Functional Theory, as our method of choice, are explained. Further, the setups of the employed computational procedure are indicated, followed by a description of the adopted atomic models and the procedure to evaluate the binding energies in the alloys of interest. In *Results and discussion*, the H-H configuration within the lattice is discussed. The preference of hydrogen for sites of particular symmetry is analysed. The variation of the binding energy as function of alloy composition is also reported and the correlation of this atomistic scale quantity to macro-scale material properties such as H_2 solubility and diffusivity is discussed. Furthermore, guidelines for tailoring the alloy composition with regard to the hydrogen solubility are proposed. Finally conclusions from the conducted study are made and subsequent multi-scale simulations are suggested.

Italian version: In questa sezione è stato riportato uno studio preliminare, *ab-initio,* sulla disposizione degli atomi d'idrogeno nella cella unitaria delle leghe di VNi e VNiTi. La prima parte è dedicata ad una introduzione sui metalli e sulle leghe metalliche in cui le loro proprietà e caratteristiche strutturali vengono discusse. Di seguito, le equazioni base della meccanica quantistica e della Teoria del Funzionale Densità sono illustrati cosi come il metodo computazionale utilizzato per valutare le energie di legame degli atomi d'idrogeno con i metalli che formano le leghe considerate; una descrizione dei modelli atomici (clusters) adottati sono quindi presentati. Nella sezione "Results and Discussion" (Risultati e discussione), le differenti disposizioni degli atomi d'idrogeni nelle celle unitarie sono discusse, soprattutto, riguardo alle distanze H-H nel lattice metallico. La preferenza dell'idrogeno per siti con particolare simmetria è stata anche analizzata. Una volta stabilito le disposizioni più probabili per gli atomi d'idrogeno, la variazione delle energie di legame in funzione della composizione delle leghe è stata riportata. La correlazione tra le energie di legame (scala atomica) è proprietà macroscopiche, quali la solubilità dell'idrogeno

nei materiali, è stata quindi discussa. Una soddisfacente correlazione a livello qualitativo è stata trovata. Infine, linee guida per l'ottimizzazione della composizione di una lega a base di vanadio, al fine di ottenere una migliore solubilità dell'idrogeno, sono state proposte. La sezione si conclude con delle considerazioni sui limiti dello studio condotto, quindi per validare le conclusioni trovate, con il suggerimento per successivi calcoli periodici.

Spanish version: En esta parte se presentan los primeros principios del estudio de la ocupación del hidrógeno en aleaciones de VNi y VNiTi y se anticipa el papel de los sustituyentes del Ni y Ti. Primeramente se ofrece una introducción general de los metales y las aleaciones, y se discuten sus características estructurales y propiedades relacionadas. A continuación, se explican algunas ideas fundamentales de la mecánica cuántica y de la Teoría Funcional de Densidad, así como el método elegido. Después se indican los procedimientos computacionales empleados y se describen los modelos atómicos adoptados y el procedimiento para evaluar las energías de enlace de las aleaciones de interés. En *Resultados y discusión* se discute la coordinación H-H dentro del entramado. Además, se analizan los huecos preferentes del hidrógeno de una determinada simetría. También se presenta la variación de la energía de enlace en función de la composición de la aleación y se discute la conexión de la escala atómica con las propiedades de macro-escala de material como la solubilidad del H_2 y la difusividad. Además se propone una guía para la adaptación de la composición de la aleación con respecto a la solubilidad del hidrógeno. Finalmente, se extraen las conclusiones del estudio llevado a cabo y se sugieren las subsecuentes simulaciones multiescala.

French version: Cette partie intègre une étude des principes premiers de l'occupation de l'hydrogène dans les alliages VNi et VNiTi et prévoit le rôle des substituants Ni et Ti. Dans un premier temps, une introduction générale sur les métaux et alliages métalliques de métaux est présentée. Leurs caractéristiques structurales et les propriétés associées sont décrites. Nous détaillons ensuite certaines des idées fondamentales de la mécanique quantique et de la Théorie de la Fonctionnelle de Densité, qui est notre méthode de choix. En outre, les constructions de la méthode de calcul employée sont indiquées, suivies d'une description des modèles atomiques adoptés et de la procédure pour évaluer les énergies de liaison dans les alliages d'intérêt. Dans la partie *Résultats et discussion*, la configuration H-H au sein du réseau est discutée. La préférence de l'hydrogène pour les sites présentant une symétrie particulière est analysée. La variation de l'énergie de liaison en fonction de la composition de l'alliage est également présentée et la corrélation de cette quantité à l'échelle atomistique avec les propriétés macroscopiques des matériaux telles que la solubilité et la diffusivité de H_2 est discutée. *In fine*, des lignes directrices sont proposées pour adapter la composition des alliages en fonction de la solubilité requise pour l'hydrogène. Les conclusions sur cette étude s'accompagnent de suggestions de simulations multi-échelles.

1 Theoretical background

1.1 Crystal structure of metals

Metals are typically heavy elements and therefore they tend to be densely packed. Besides, metal bonds are not directional and the greatest stability is expected for those crystallographic arrangements that maximize the coordination number of each atom [1]. Distances between neighbouring metal atoms are usually small in order to lower the bond energy. Consequently, metals crystallize as solids with atoms arranged in a regular manner [2]. In an ideal crystal the arrangement of atoms builds a three-dimensional net (lattice) that can be described by translational vectors. This translational symmetry of metal crystals implies that at a given lattice point the configuration of atoms is identical with that at any other point from the structure. The lattices are classified according their symmetry spatial groups by means of lengths and angles between crystallographic axes. This yields 14 unique Bravais lattices in the three-dimensional crystal system, named after their founder. According to the Bravais classification, the elementary unit cells of majority of metals are with face-centred cubic (fcc) or body-centred cubic (bcc) topology (Figure 2). A fcc unit cell is formed by an atom at each corner of a cube and one atom in the centre of each of its faces [3]. Metals with such crystal structure are for example aluminium, silver, gold, copper, nickel, palladium and platinum. A bcc unit cell features an atom at each corner of the cube and one atom at the centre of the cube. Some of the bcc metals are chromium, iron, molybdenum, niobium, tantalum and vanadium. Fcc and bcc unit cells are characterised by a length, a, which is equal for all faces of the cell and is called lattice parameter. The angles between the faces of these unit cells are all equal to 90°. Some metals such as magnesium, titanium and zinc crystallize in a third type of arrangement with hexagonal closed packed structure (not shown here). It is obvious that there is a connection between the chemical constituent and the crystal structure. In general, elements that belong to the same group of the periodic table crystallize in the same type of structure.

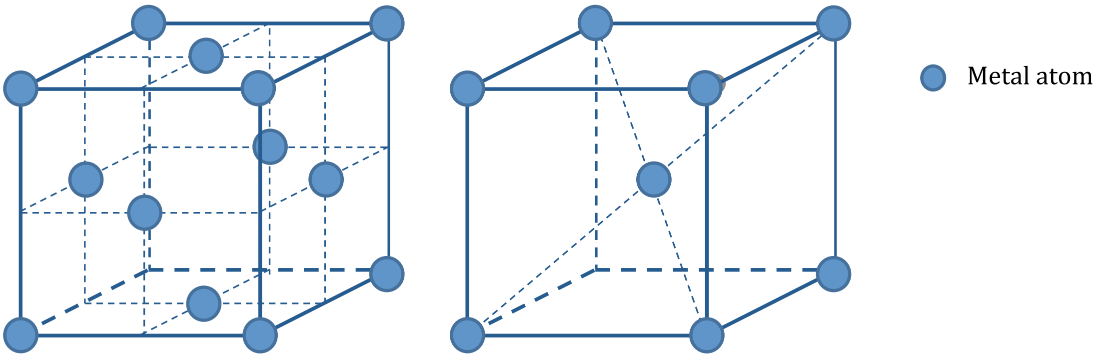

Figure 2: Elementary unit cells of face-centred cubic (left) and body-centred cubic lattice (right).

When different types of metals are mixed together, a metal alloy is built [1]. An alloy can be a solid solution or an intermetallic (multi-phase) alloy. The former consists of a single homogeneous phase with alloying elements distributed over the crystal lattice of the host element. Depending on the size of each element in the mixture, the solid solution that is formed is either substitutional or interstitial (Figure 3). As a general rule, similar in size atoms form substitutional alloys. If one atom type is much smaller then the other, it is trapped in the spaces between the larger atoms. These interatomic spaces are called interstices and thus the alloy is deemed as interstitial. The properties of solid solutions are determined by the chemical composition of the constituents. On the other hand, multiphase alloys consist of a mixture of crystalline solutions with different compositions and symmetry, and their overall properties largely depend on the volume fraction of the distinct phases. Lastly, there are amorphous metals that were not mentioned above because they are novel engineering materials with disordered instead of crystalline structure and belong to the group of alloys. These won't be further discussed in the current study.

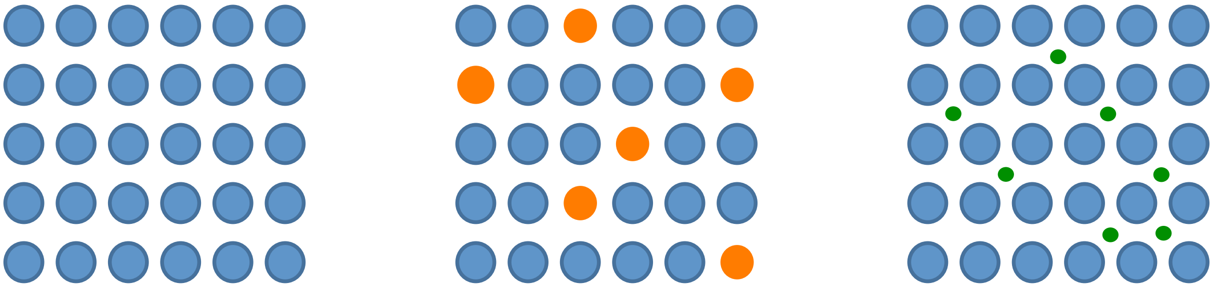

Figure 3: Schematic illustration of pure metal structure (left), substitutional alloy (middle) and interstitial alloy (right).

1.2 Metals and metal alloys for hydrogen separation membranes

Metals and metal alloys are especially attractive materials for H_2-selective dense membranes. A membrane of the type doesn't possess any intentional interconnected pores than small void spaces, i.e. interstices, which can accommodate only atomic hydrogen (1.1 Å diameter) [4]. Consequently hydrogen diffuses across the membrane in dissociated form via series of activated jumps between interstitial sites [5]. All other gases are excluded. This transport mechanism, illustrated schematically in Figure 4, implies the need of a catalyst to govern the dissociation and re-association of hydrogen on the feed and permeate sides of the membrane (steps 2 and 4 in the figure).

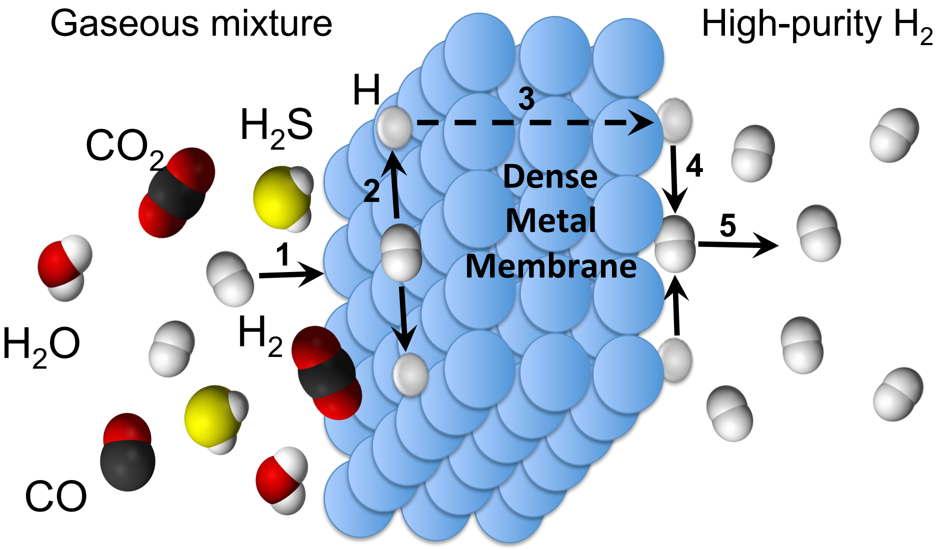

Figure 4: Schematic representation of the multistep H_2 transport mechanism through a dense metal membrane. Step 1: External diffusion; Step 2: Dissociation of H_2 and dissolution of H atoms; Step 3: Internal diffusion; Step 4: Re-association of H atoms and desorption of H_2; Step 5: External diffusion.

The relatively high H_2 solubility and diffusivity combined with catalytic ability established palladium as the dominant material for producing such membranes. However, Pd has certain limitations for widespread application, the emphasis being on the high cost raw materials [6,7] and surface poisoning issues [3]. In an effort to reduce the price and to increase the performance of dense metal membranes, researchers are investigating alternative non-precious elements and novel composite materials. These should replace the core material of the membranes, while the need for Pd is reduced to a thin catalytic layer on the feed and permeate surfaces until a better suitable non-Pd catalyst is developed. Exhibiting high H_2 permeability and being less expensive than Pd, group VB metals (CAS numbering) are promising candidates for H_2-separation applications [6,8,9]. Membranes based on dense foils of vanadium, tantalum or niobium coated with thin Pd-based catalytic and oxidation-protective layer have been patented first in 1967 by Makrides, Wright and Jewett [10]. They have determined that these metals dissolve more hydrogen but have lower diffusion constants than Pd. Later studies state that body-centred cubic (bcc) V, Ta and Nb exhibit both higher hydrogen solubility and diffusivity in comparison with Pd [8]. In any case, the permeability, which according to the solution-diffusion theory is a product of solubility and diffusivity [4], is reportedly always greater for group VB elements compared with palladium [11,12], as shown in Table 2.

Table 2: Hydrogen permeability values of selected metals [11].

Metal	Crystal structure	Hydrogen permeability at 773 K [mol m^{-1} s^{-1} $Pa^{-0.5}$]
Nb	bcc	$1.6 \cdot 10^{-6}$
Ta	bcc	$1.3 \cdot 10^{-7}$
V	bcc	$1.9 \cdot 10^{-7}$
Fe	bcc	$1.8 \cdot 10^{-10}$
Ni	fcc	$7.8 \cdot 10^{-11}$
Pd	fcc	$1.9 \cdot 10^{-8}$
Pt	fcc	$2.0 \cdot 10^{-12}$

The problem associated with such super-permeable metals is that they are prone to brittle failure, i.e. to weakening of the material caused by the H_2 uptake [6]. It is acknowledged that this shortcoming can be reduced through selective alloying. The improved embrittlement resistance of alloys relative to the pure, solute-free metals is attributed to lowered solubility and diffusivity. Consequently the permeability is also decreased. Moreover, alloying can lower the phase transformation temperatures and to inhibit nucleation of brittle hydrides. Thus, it is important to study how alloying influence hydrogen transport through the material and to achieve a good trade-off between mechanical and transport properties [13].

A special case is the system V-Ni-Ti. It is acknowledged that addition of Ni to V decreases the H_2 solubility and therefore reduces the embrittlement susceptibility [14,15]. On the other hand, Ti enhances the solubility of V both by expanding the metal lattice and by forming stable hydrides [4,16,17]. On the negative side, binary VTi alloys are prone to brittle failure. Alloying V with both Ni and Ti results in formation of multi-phase microstructure, containing a primary bcc solid solution and weakly absorbing phases with low volume fraction [9,18]. These NiTi compounds, with crystal structures differing from the parent bcc solid solution, stabilise the overall mechanical stability of the material while the dominant V-rich phase promotes hydrogen permeability [19]. Dissociated hydrogen occupies metal interstices in the bcc lattice and hops between such interstitial sites. The transport properties of VNiTi alloys depend strongly on the ability of the primary phase to accommodate and diffuse hydrogen atoms, i.e. on the sites occupancy. Two distinct absorption sites are available in metal lattices – tetrahedral (T) and octahedral (O) interstices. T and O sites have different concentration and size in a unit cell. In Figure 5 both types of interstitial sites in a body-centred cubic unit cell are illustrated. In particular, in the case of bcc metal, the number of T sites is

24 per unit cell, and the number of O sites totals 18 per unit cell. The number of interstices is lower in the fcc crystal structure and namely 8 T sites and 13 O sites per unit cell. The higher permeability of hydrogen through bcc metals is ascribed namely to the higher amount of available absorption sites. Moreover, in a bcc metal lattice, the size of O interstices (relative to the radius of the metal atoms) is smaller than the size of T interstices, while the opposite is true in fcc metals (Table 3) [8].

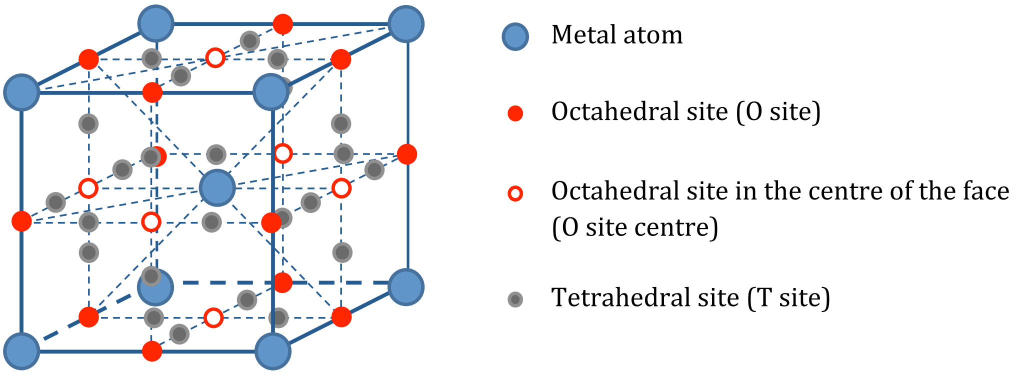

Figure 5: All octahedral (in red colour) and tetrahedral sites (in grey colour) in a bcc unit cell: there is one O site on each of the six bcc cell faces (½, ½, 0) and one on each of the twelve cell edges (½, 0, 0); the T sites are four on each of the six cell faces (½, ¼, 0).

Table 3: Size of T and O sites in bcc and fcc alloys [8].

Structure	Tetrahedral sites	Octahedral sites
	Size of the absorption sites relative to M atom radius	
bcc	0.291	0.155
fcc	0.225	0.411

The sites preference in a given metal is essential for characterisation of H-metal systems as it determines various micro- and macroscopic properties such as phase and mechanical stability, H_2 solubility and diffusivity [20]. Common believe is that in bcc crystal structures H occupies T sites, while O interstices are favoured in fcc metals [21,22,23]. Anyhow, the available studies of vanadium are usually at low temperatures, where phase transitions occur, and they are not conclusive whether H atoms occupy tetrahedral or octahedral sites in the bcc phase [24,25,26,27,28]. When it comes to alloys the question becomes even more controversial. Solute elements alter the volume in the V bcc unit cell and influence the sites energy in the lattice. Better understanding of the H-metal interactions in the V-Ni-Ti system could provide an answer to the aforementioned question and thereby facilitate the design and optimisation of low cost dense membranes for H_2 separation. However, the research on V-based solid solutions is limited and mostly experimental. To advance the knowledge of interactions at atomic scale, employment of special investigation methods such as first-principles computations or diffraction study is required.

1.3 Quantum mechanics and density functional theory

Understanding the properties of materials at fundamental level requires knowledge of the behaviour of atomic and subatomic particles. At such tiny scale the wave-particle duality is observed and Newton's laws that apply in the macroscopic world need to be reconsidered. The science concerned with description of matter at the level of individual atoms is called quantum mechanics (QM). Core equation of QM, analogue to Newton's second law ($F=ma$), is the Schrödinger equation. This equation covers any problem in the electron states of matter including the time. In most cases, however, one is concerned with atoms and molecules without time-dependent interactions [29]. The time-independent, nonrelativistic (in the Born-Oppenheimer approximation) form of the Schrödinger equation is:

$$\hat{H}\psi = E\psi, \tag{1.1}$$

where $\hat{H}$ is the Hamiltonian operator, ψ is the electronic wave function or a set of "eigenstates" and E is the electronic energy "eigenvalue" [30]. The eigenstate ψ_n for any integer n is a solution that has an associated eigenvalue E_n, which satisfies equation (1.1). The lowest energy value is known as the ground state of the electron system. The Hamiltonian is defined in respect to the physical system being described. For a N-electron system it has the form:

$$\hat{H} = \frac{h^2}{2m}\sum_{k=1}^{N}\nabla_k^2 + \sum_{k=1}^{N}V(\boldsymbol{r}_k) + \sum_{k=1}^{N}\sum_{l<k}U(\boldsymbol{r}_k,\boldsymbol{r}_l)\,. \tag{1.2}$$

The first term on the right-hand side defines the kinetic energy of each electron in the system. Here m is the electron mass, h – the Planck constant and ∇^2 – the Laplacian. The kinetic energy of nuclei is excluded due to the Born-Oppenheimer approximation that rests on the fact that nuclei move much slower than electrons, owning to the greater mass of nuclei in comparison to the mass of electrons. Consequently, nuclear kinetic energy can be considered equal to zero and the potential energy due to nuclei is merely a constant. The second term in Eq. (1.2) gives the attractive interaction energy between each electron and the collection of atomic nuclei. The last term describes the electron-electron repulsive interaction. For such system with N electrons, ψ is a function of each of the three spatial coordinates and the spin of each electron, i.e. $\psi = \psi(\mathbf{r}_1, s_1, \mathbf{r}_2, s_2, \ldots, \mathbf{r}_N, s_N)$. This means that for a single N_2 molecule ($N = 14$) ψ is a 56-dimensional function (42 if the spin is neglected). It is proven that the total wave function of a system can be approximated as a product of the individual electron wave functions, which is known as a Hartree product and is given by $\psi = \psi_1(\mathbf{r}, s)\psi_2(\mathbf{r}, s),..., \psi_N(\mathbf{r}, s)$ but this doesn't reduce the number of variables in the mathematical problem.

As we saw in the previous paragraphs, the Schrödinger equation is a many-body problem. It can't be solved analytically when the number of electrons exceeds 3. Therefore, over the past century, several approximated methods (such as the Hartree-Fock method) have been developed in order to find a solution of this fundamental equation. In this frame, the ingenious approximation that Density Functional Theory (DFT) uses in order to solve the Schrödinger equation rests on two theorems proved by Kohn and Hohenberg and on a set of equations derived by Kohn and Sham in the 1960s. The first theorem states that *the external potential $v(\mathbf{r})$ is (to within a constant) a unique functional of $\rho(\mathbf{r})$. Since, in turn $v(\mathbf{r})$ fixes $\hat{H}$, we see that the full many particle ground state is a unique functional of $\rho(\mathbf{r})$* [31]. In other words, the ground-state energy can be expressed as a functional (function of a function) of the electron density, $E = E[\rho(\mathbf{r})]$, given by:

$$E[\rho(\boldsymbol{r})] = \int v(\boldsymbol{r})\rho(\boldsymbol{r})dr + F[\rho(\boldsymbol{r})]. \tag{1.3}$$

The first term on the right-hand side describes the electron-nuclei potential energy, where the expression for the external potential $v(\mathbf{r})$ acting on the electrons due to nuclei of charges Z_α has the form:

$$v(\boldsymbol{r}) = -\sum_{\alpha} \frac{Z_\alpha}{\boldsymbol{r}_\alpha}. \tag{1.4}$$

The second term in Eq. (1.3) accounts for the electron-electron interactions and will be discussed below. From this theorem follows that the properties of a many-particles electron system can be described as a function of three variables – the coordinates of the electron density, $\rho(\mathbf{r})$, instead of 4N variables – the coordinates of each electron that define the wave function, ψ. In this way the 56-dimensional function for N_2 or for any other molecular system is reduced to a problem with 3 dimensions. The second theorem, proven by Kohn and Sham, defines an important property of the functional from the first theorem and namely that the electron density that minimizes the energy of that functional is the true electron density. However, the two scientists remarked: *The major part of the complexities of the many-electron problems is associated with the determination of the universal functional $F[\rho]$.* Although the exact functional was not given by Kohn and Hohenberg, they defined it in a general way as:

$$F[\rho(\boldsymbol{r})] = T_S[\rho(\boldsymbol{r})] + U[\rho(\boldsymbol{r})], \tag{1.5}$$

where $T_S[\rho(\boldsymbol{r})]$ is the kinetic energy of an iso-electronic non-interacting system, and $U[\rho(\boldsymbol{r})]$ is the total electron-electron interactions potential. The latter sums the classical Coulomb repulsion energy and the exchange-correlation energy between electrons:

$$U[\rho(\boldsymbol{r})] = U_{Coul}[\rho(\boldsymbol{r})] + U_{xc}[\rho(\boldsymbol{r})], \tag{1.6}$$

with:

$$U_{xc}[\rho(\boldsymbol{r})] = (T_S[\rho(\boldsymbol{r})] - T[\rho(\boldsymbol{r})]) + (U[\rho(\boldsymbol{r})] - U_{Coul}[\rho(\boldsymbol{r})]). \tag{1.7}$$

The exchange-correlation potential, as described by Eq. (1.7), takes into account the difference between the kinetic energies of a non-interacting system $T_S[\rho(\boldsymbol{r})]$ and of the real interacting system $T[\rho(\boldsymbol{r})]$. Moreover, $U_{xc}[\rho(\boldsymbol{r})]$ describes the non-classical part of the electron-electron interaction energy, expressed as the difference between the total electron-electron repulsion energy and the classical Coulomb electron-electron repulsion energy.

Following from this work, Kohn along with Sham derived a set of equations in which each equation treats only a single electron from the quantum system and depends on three spatial variables [32]. Each equation from this set has the following form:

$$\left[\frac{h^2}{2m}\nabla^2 + V(\boldsymbol{r}) + U_{Coul}(\boldsymbol{r}) + U_{xc}(\boldsymbol{r})\right]\psi_k(\boldsymbol{r}) = \varepsilon_k\psi_k(\boldsymbol{r}). \tag{1.8}$$

The sum of the single-electron wave functions $\psi_k(\mathbf{r})$ defines the electron density:

$$\rho(r) = \sum_{k=1}^{N} |\psi_k(\boldsymbol{r})|^2. \tag{1.9}$$

The one-electron equation (1.8) can be written in a form that resembles the Schrödinger equation (1.1):

$$h_k^{KS}\psi_k(\boldsymbol{r}) = \varepsilon_k\psi_k(\boldsymbol{r}). \tag{1.10}$$

Here, h_k^{KS} is the Kohn-Sham one-electron operator:

$$h_k^{KS} = \frac{h^2}{2m}\nabla^2 + V(\boldsymbol{r}) + U_{Coul}(\boldsymbol{r}) + U_{xc}(\boldsymbol{r}). \tag{1.11}$$

The terms on the right hand side in Eq. (1.11) define, in order, the kinetic energy of a single electron; the Coulomb interaction between one electron and the collection of nuclei; the Hartree potential that describes the classical Coulomb repulsion between the electron being considered and the total electron density defined by all electrons in the system; and finally the exchange-correlation potential of the single electron with the rest of the electrons, which define the electron density.

These Kohn-Sham equations offer a practical computational scheme to find the ground-state energy and the electron density of a many-electron system. The procedure is iterative and follows an algorithm, where a trial electron density $\rho(\mathbf{r})$ is defined and the set of KS equations (Eq. (1.8)) is solved with this arbitrary density to find the single-particle wave functions $\psi_k(\mathbf{r})$. Next, with the obtained $\psi_k(\mathbf{r})$, the electron density is evaluated using Eq. (1.9). The calculated electron density is compared to the initial trial density. If the two densities are equal, then this is the ground-state density and it allows for computing the total energy. If the densities differ, then the trial density is updated and the updated density is used to solve the KS equations. Here we didn't specify how close the two electron densities have to be for considering them equal and in what way the trial density is updated. However, the described method shows that the total energy of the system can be calculated by solving the KS set of equations in an iterative manner.

One of the difficulties towards applying the Density Functional Theory is the exchange-correlation potential that appears in the above equations. Defining U_{xc} is a very difficult task and the true form of this potential is not known. In an effort to find this functional, which existence is proven by the first theorem of Hohenberg and Kohn, many approximated exchange-correlation functionals have been developed over the years, allowing for application of DFT in QM calculations. The two most used approximations are the local density approximation (LDA) and the generalized gradient approximation (GGA). These are implemented in standard software packages. Choosing a functional is an important part of the work when performing DFT calculations.

Another crucial part is the choice of a basis set, i.e. of set of atomic orbitals, used to describe each molecular orbital of the quantum system, which in turn describe the electron density of the system, according to Eq. (1.9). Atomic orbitals are proportional to the exp(-r). They are called Slater-type orbitals (STO). However, this kind of functions makes the mathematical problem too complex. Instead, Gaussian type orbitals (GTO) are mathematically easer to treat but, due to their proportionality to $\exp(-r^2)$, they do not exhibit the same trend of a Slater-type atomic orbital. Consequently, linear combinations of GTOs are used in order to increase their reliability as basis functions. A single Gaussian function is also known as primitive function. The number of primitive functions used in a linear combination increases the accuracy of the calculation but, at the same time, the computational time increases. If an atomic orbital is represented by only one primitive function, it is called single-ζ. If more primitives are used to describe one atomic orbital, the modeling accuracy is improved. In this case the atomic orbital is called multiple-ζ. Higher accuracy is achieved also if the primitives are partitioned into more functions. Here, an example is given with the 6-311G basis sets, which have been used in this work. The name of this basis set is self-explanatory. The digit 6 before the dash indicates the number of primitive functions that are used in a linear combination for the core atomic orbitals. The three digits after the dash (311) show that the basis functions, which are used to approximate the valence atomic orbitals, are three. Each basis function is composed by a different number of primitive functions, expressed by the value of the corresponding digit. The first one is represented by 3 functions (3 is the first digit after the dash). The second one is composed by a single function (denoted by the second digit after the dash). The third is also expressed by a single function (last digit). All functions are Gaussian-type, which is indicated by the letter G at the end of the name of this basis set. Furthermore, some specific basis functions such as polarization and/or diffusion can be added to increase the reliability for the investigation of some particular atomic systems.

In conclusion of this part, it should be noted that a large number of DFT studies proved that this theory is able to accurately describe the total energy of various atoms and molecules. In principle, it can be used for all elements from the periodic table. In the following chapters, DFT calculations are applied to VNi and VNiTi alloys to gain information on the absorption sites preference by hydrogen atoms and the corresponding binding energies as function of alloy composition.

2 Methodology

2.1 Computational procedure

Northwest Computational Chemistry Package (NWChem) [33] was used for the total energy DFT simulations in this work. Preliminary calculations were carried out on HP Z210 CMT Workstation and in the course of work CINECA supercomputers have been utilised to achieve satisfactory calculation efficiency. All calculations in this study were performed for closed-shell systems, i.e. each molecular orbital is occupied by two electrons with the opposite spin. The convergence tolerance was $2.7 \cdot 10^{-5}$ eV for the energy and $5.4 \cdot 10^{-4}$ eV for the root mean square of the electron density. Tests using different functionals (such as the gradient-corrected BLYP and B3LYP) and basis sets (Stuttgart RSC 1997 ECP and LANL2DZ for metal atoms; 6-311G** and 6-311G for hydrogen) were carried out to set up a computational procedure that provides an acceptable trade-off between accuracy and computational time. Some of the results are summarized in Table 4. Sufficiently converged results were not obtained with the gradient corrected functional BLYP. Therefore the hybrid Becke, 3-parameter, Lee-Yang-Parr (B3LYP) generalized gradient approximation (GGA) functional was chosen to describe the electron exchange correlation [34]. A comparison between two basis sets – LANL2DZ and Stuttgart RSC 1997, applied for the transition metals, showed that with the latter convergence is reached in less expense of computational time. As a result, initial calculations to identify the disposition of a pair of hydrogen atoms in the binary alloy $V_{84.2}Ni_{15.8}$ have been performed with the Gaussian-type basis sets Stuttgart RSC 1997 ECP and 6-311G** without a level shift. The electron core potential, Stuttgart RSC 1997 ECP, was employed to describe the core electrons of V, Ni and Ti. In all subsequent calculations the same electron core potential and basis set were used to describe the atomic orbitals of metal atoms, while the 6-311G basis set have been employed for the hydrogen atoms. Besides, a level shift was included to improve convergence of the calculations. In particular, level-shifting of 30 eV was applied to the diagonal elements of the unoccupied block of the Fock-matrix when the gap between the highest occupied and the lowest unoccupied orbitals (HOMO-LUMO gap) is less than 5.4 eV.

Table 4: Comparison of different functionals and basis sets in respect to the computational time for reaching convergence. The calculations were carried out for a 19-atomic VNi cluster with two embedded H atoms at tetrahedral interstices.

Functional	Basis set	Iterations to converge	Time/processor [s]
B3LYP	Stuttgart RSC 1997	400	83,034.1
B3LYP	LANL2DZ	899	102,732.6
BLYP	Stuttgart RSC 1997	Not converging	
BLYP	LANL2DZ	Not converging	

2.2 Atomic models

In the current study, bcc VNi (used as a benchmark material) and VNiTi alloys of different composition were represented adopting cluster models of the lattice structure. From computational time considerations it is important to use clusters with a limited number of atoms without compromising the accurate description of the target material. On the other hand, in order to investigate various alloy compositions, the number of atoms in the generated clusters should be high enough to enable variation of the metal ratio. Taking both considerations into account, supercells consisting of 19 metal atoms (3 bcc unit cells), shown in Figure 6, have been used to perform the herein-reported DFT calculations.

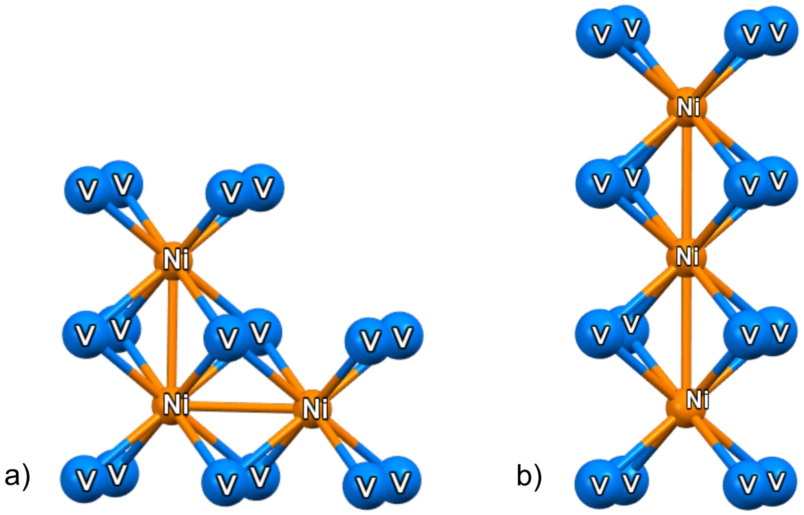

Figure 6: Clusters (supercells) used for different H-H dispositions (See Section 2.3) a) the $V_{84.2}Ni_{15.8}$ cluster for c2a disposition; b) the $V_{84.2}Ni_{15.8}$ cluster for c1 and c2o dispositions.

In principle, lattice parameters of metal alloys can be estimated by the Vegard's law, which states that a property value of an alloy can be determined from a linear interpolation of the property values of its constituent elements [35]. Accordingly the lattice constant of a binary alloy with the general chemical formula $A_{(1-x)}B_x$ is calculated by:

$$a_{A(1-x)Bx} = (1-x) \cdot a_A + x \cdot a_B. \tag{2.1}$$

Despite of that, it has been established that the properties of most solid solutions are not accurately predicted by this empirical rule [36]. For example, in case of obedience to Vegard's law, the lattice parameter of a binary alloy consisting of 85 at.% V (a_V= 3.04 Å) and 15 at.% Ni (a_{Ni} = 3.52 Å) should be 3.1120 Å. However, the reported in the literature experimental value for the alloy $V_{85}Ni_{15}$ is 3.0093 ± 0.0003 Å [18]. Therefore, it can be expected that prediction of the lattice constants of ternary alloys in such average manner will result in significant deviation from the real values. Lattice parameters can be evaluated also via QM calculations but these require considerable computational time.

In this study, the cluster compositions were chosen to be as close as possible to already experimentally investigated alloys [18], which have been used as a physical reference to the conducted theoretical study. This strategy allowed saving of computational resources by adopting experimental lattice parameters of the real solid solutions for the corresponding cluster models, as given in Table 5. In the case of VNiTi, the primary bcc phase (referred to as "phase composition") was considered. It is worth noting that the nominal composition of the experimental ternary alloys is different from the composition of the primary phase, due to formation of weakly absorbing compounds (see Introduction). For example V alloyed with Ni and Ti in the atomic ratio of 75:15:10 respectively, results in multi-phase microstructure. The predominant V-rich phase (94.7 % volume fraction) has a bcc crystal topology (space group Im-3m, Number 229) and composition equal to $V_{83.4}Ni_{7.8}Ti_{8.8}$, as reported in [18]. Two other phases are formed – a simple cubic phase (space group Pm-3m, Number 221) with composition $V_{12.9}Ni_{42.0}Ti_{45.1}$ and a face-centred cubic phase (space group Fd-3m, Number 227) with composition $V_{15.5}Ni_{54.4}Ti_{30.1}$. Nonetheless, the total volume fraction of these two phases is less than 5.5 % and they were not taken into account in the current study.

Table 5: Experimental alloy compositions [18] and corresponding cluster compositions.

Nominal Composition	**Phase Composition**	**Cluster Composition**	**№ Atoms in Cluster**			**$a^{\dagger}$ [Å]**
			№ V	**№ Ni**	**№ Ti**	
$V_{85}Ni_{15}$	$V_{85}Ni_{15}$	$V_{84.2}Ni_{15.8}$	16	3	0	3.0093
$V_{75}Ni_{15}Ti_{10}$	$V_{83.4}Ni_{7.8}Ti_{8.8}$	$V_{84.2}Ni_{5.3}Ti_{10.5}$	16	1	2	3.0331
$V_{80}Ni_{15}Ti_{5}$	$V_{81.9}Ni_{14.0}Ti_{4.1}$	$V_{84.2}Ni_{10.5}Ti_{5.3}$	16	2	1	3.0085
$V_{55}Ni_{15}Ti_{30}$	$V_{63.8}Ni_{6.9}Ti_{29.3}$	$V_{63.1}Ni_{5.3}Ti_{31.6}$	12	1	6	3.0998

$^{\dagger}a$ is the lattice parameter of the bcc phase

All clusters were constructed using a pre- and post-processing program for displaying MOLecular DENsity – Molden. The software allows for building of molecular structures via the incorporated Z-matrix editor and supports a number of output formats. Moreover, Molden reads outputs from various *ab initio* packages including NWChem. In addition, the Mercury program by the Cambridge Crystallographic Data Centre (CCDC) has been used as a visualization tool due to the flexible display settings for three-dimensional structures.

2.3 Hydrogen occupation

All calculations, involving interstitial hydrogen, were carried out considering a pair of H atoms (representing a dissociated hydrogen molecule) embedded in the generated 19-atomic metal clusters, which modelled the crystal lattice of the target alloys. This corresponds to 1.1 at.% hydrogen. Using two H atoms has sense in respect of the employed cluster approach as it promotes the symmetry of the atomic models. Furthermore, information not only on H-metal interactions but also on H-H coordination within the lattice is obtained.

The preference of a pair of hydrogen atoms for specific absorption sites as function of alloy composition was described through the binding energy (E_b) expressed as the difference between the total energy of the metal cluster with embedded hydrogen ($E_{2H/Cluster}$) and the energies of the cluster without interstitial hydrogen ($E_{Cluster}$) and of a non-interacting hydrogen molecule (E_{H2}):

$$E_b = E_{2H/Cluster} - E_{Cluster} - E_{H2}. \tag{2.2}$$

With this definition, negative energies represent binding states that are energetically preferred relative to gaseous hydrogen.

At the first stage of the research, the favourable dispositions of an individual H atom towards another H atom within the V-based lattice have been explored. The binding energy in six non-equivalent T positions in the binary $V_{84.2}Ni_{15.8}$ cluster were calculated. Three possible configurations were identified:

- Both H atoms occupying interstitial sites at the same face of the bcc unit cell – configuration 1 (denoted as c1);
- The pair of H atoms occupying sites at adjacent faces of the unit cell – configuration 2 adjacent (denoted as c2a);
- The pair of H atoms occupying sites at opposite faces of the unit cell – configuration 2 opposite (denoted as c2o).

For each of these configurations two non-equivalent cases have been considered– a small spatial distance and a large spatial distance between the two H atoms. Consequently, the number of the investigated non-equivalent tetrahedral configurations in the $V_{84.2}Ni_{15.8}$ alloy is six in total (Figure 7). Many cases are a repetition of one of these six dispositions, i.e. they are equivalent because the environment around the pair of H atoms (in terms of type of neighbouring nuclei and distances between both H-H and H-metal atoms) is identical. As a consequence, the external potential, defined in Section 1.3 (Eq. 1.4), is identical for these configurations and their total energy is the same. However, it must be noted that not all non-equivalent dispositions of the hydrogen occupation were studied in this work. Only a finite number of dispositions were examined in order to understand and identify trends in the hydrogen arrangement and absorption affinity in the target V-based alloys.

Further, E_b in a range of non-equivalent octahedral positions, identified in the same manner as the non-equivalent T sites (without considering the configuration c2a), were calculated for a ternary cluster model with composition $V_{84.2}Ni_{10.5}Ti_{5.3}$ These positions are shown in Figure A 1 in Appendix.

Finally the sites preference of a pair of H atoms in alloys with different compositions was explored. Here, a binary $V_{84.2}Ni_{15.8}$ alloy and three ternary VNiTi alloys with different metal atomic ratio (as reported in Table 5) have been investigated. In these DFT calculations, for reasons explained in Chapter 3, only the c2o H-H coordination was considered. It has to be noted that the symmetry of the generated cluster with composition $V_{63.1}Ni_{5.3}Ti_{31.6}$ provides two types of T and O absorption sites – near a Ti solute atom and away from it. Both cases were taken into account.

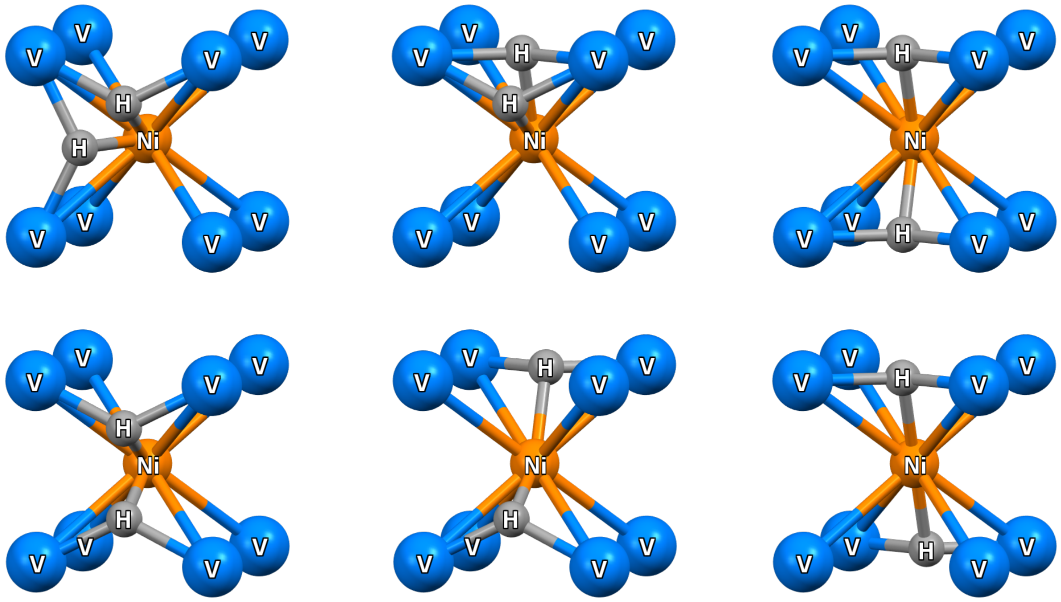

Figure 7: The investigated non-equivalent H tetrahedral configurations of a pair of H atoms a VNi unit cell: left – c1, middle – c2a, right – c2o; top – small H-H distance, bottom – large H-H distance.

3 Results and discussion

The binding energy of two H atoms embedded in the six investigated non-equivalent tetrahedral configurations (c1, c2o and c2a with small and large H-H distance) in the $V_{84.2}Ni_{15.8}$ clusters (illustrated in Figure 6), showed that interstitial H atoms prefer to occupy positions away from one another. The results, summarized in Table 6, indicated that the favourable hydrogen dispositions are when the pair of H atoms sits at the adjacent faces and at the opposite faces of a bcc unit cell with large H-H distances. Simultaneous occupation of two absorption sites at one face of the unit cell is excluded. This means that H atoms are unlikely to cluster in the bulk metal. E_b for the tetrahedral configuration c2o-large is higher (-0.03 eV) than for c2a-large (-0.36 eV). However, from symmetry considerations (i.e. each H atom must have equal chemical environment), the total energy calculations of the c2a dispositions were performed with a different cluster than the supercell employed for c1 and c2o configurations. The former cluster has lower symmetry in comparison to the latter, resulting in slow convergence of the calculations. Moreover, modelling different metal compositions using this cluster cause additional asymmetry. Therefore the second favourable disposition, c2o, was used further in this study.

Table 6: Binding energies of a pair of H atoms in non-equivalent tetrahedral positions in the V84.2Ni15.8 cluster model.

Cluster	**H configuration**	**H-H distance [Å]**	***E_b* [eV]**
$V_{84.2}Ni_{15.8}$	T c1-small	1.0645	1.14
	T c1-large	1.5051	0.35
	T c2a-small	1.0636	0.65
	T c2a-large	3.1922	-0.36
	T c2o-small	3.0093	0.14
	T c2o-large	3.3647	-0.03

The DFT calculations on octahedral hydrogen occupation in the ternary alloy $V_{84.2}Ni_{10.5}Ti_{5.3}$ confirmed the expected preference of two H atoms to occupy interstices with a large spatial distance, as shown in Table 7 and Figure 8.

Table 7: Binding energies of a pair of H atoms in non-equivalent octahedral positions and in the favourable tetrahedral configuration in the $V_{84.2}Ni_{10.5}Ti_{5.3}$ cluster model.

Cluster	**H position**	**Distance H-H [Å]**	***E_b* [eV]**
$V_{84.2}Ni_{10.5}Ti_{5.3}$	O centre	3.0085	2.92
	O c1-small	2.1273	0.06
	O c1-large	3.0085	0.41
	O c2o-small	3.0085	0.56
	O c2o-large	4.2547	-0.07
	T c2o-small	3.0085	0.26
	T c2o-large	3.3636	-0.18

The distance between the H atoms embedded in the octahedral sites in the configurations c1 with large H-H distance and c2o with small H-H distance, is equal (3.0085 Å). However, the chemical environment around the H atoms in these two configurations is not the same and therefore there is a slight deviation between their binding energy values (E_b = 0.41 eV for c1-large, E_b= 0.56 eV for c2o-small). Yet, although a pair of H atoms embedded in the O sites centre and also in T c2o-small sites are spatially separated from each other again by 3.0085 Å, the difference between the binding energy in these sites is considerable (E_b = 2.92 eV for c1-large, E_b= 0.26 eV for c2o-small). This difference in E_b, despite the equal H-H spatial separation, is due to the different site symmetry (T, O and O centre are absorption sites of different type as explained in 1.2). This confirms that sites preference doesn't depend only on the geometry of the system but it's a more complex phenomenon. Hence, the observation that two H atoms preferentially take positions away from one another is applicable when considering interstices of identical symmetry, i.e. considering T and O sites separately. However, electron configuration has higher impact than geometrical factors. In fact, even if the distance between H atoms with O coordination of type c2o is larger than the H-H distance in T sites with the same coordination, T occupation is energetically preferred in $V_{84.2}Ni_{10.5}Ti_{5.3}$.

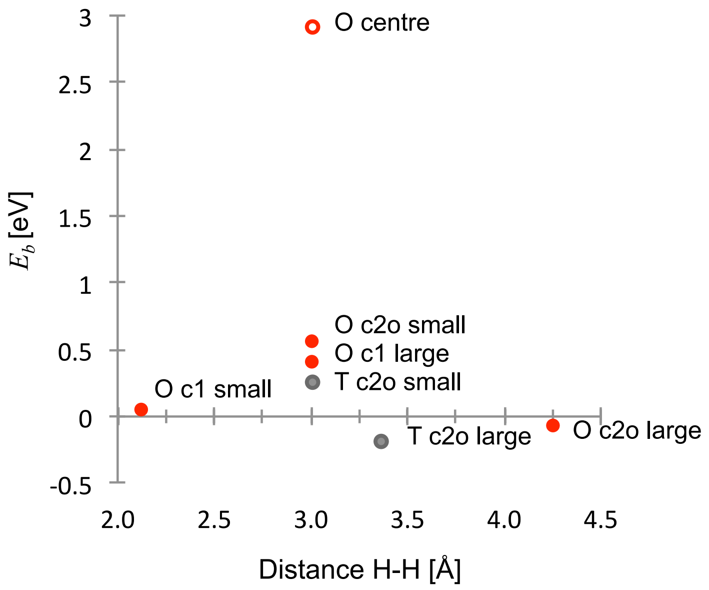

Figure 8: Binding energies of a pair of hydrogen atoms in $V_{84.2}Ni_{10.5}Ti_{5.3}$ in respect of the H-H distance.

Exploiting the obtained results for the preferred H-H configuration in the V-based metal lattice, it was important to explore if T sites are always favoured over O sites in VNi(Ti) bcc solid solutions with different phase composition. The quantum mechanics calculations on tetrahedral and octahedral occupancy in four such alloys with varied metal atomic ratios, gave difference between the lowest and the highest E_b in T and O sites usually less than 2 eV (Figure 9). The largest calculated energy difference (3.1 eV) is between the binding energies related to T sites and the O sites in the centre of the face for the $V_{84.2}Ni_{10.5}Ti_{5.3}$ alloy. These results suggest that, despite of the prevailing view for tetrahedral occupancy in bcc vanadium, both T and O sites are responsible for the H uptake in VNiTi alloys. Surprisingly the interstitial absorption sites with lowest hydrogen binding energy are different for each of the modelled alloys, indicating that sites occupancy depends significantly on the presence of solute atoms. Consequently macroscopic properties such as H_2 solubility are influenced. Calculations on the E_b in clusters with varied Ni:Ti ratio, while keeping the concentration of vanadium constant, showed stabilisation of H atoms with higher Ti content at the expense of Ni. This theoretical observation is in agreement with the literature [4,6,14,37]. Moreover, if the amount of V is decreased at the expense of Ti, i.e. the Ti concentration increases beyond certain limit, without changing the concentration of Ni, the hydrogen affinity of the alloy decreases ($V_{63.1}Ni_{5.3}Ti_{31.6}$).

The calculated binding energy can be correlated to the ability of the alloy to dissolve hydrogen [28]. If we assume that the contribution of the vibrations and entropy variation are similar for each of the investigated metal alloys, then we can establish a relationship between the nanoscale property

E_b and the macroscale property solubility. Among the solid solutions screened heretofore, two alloys had sites with negative E_b values. A positive binding energy implies that the equilibrium between gas and absorbed phase is shifted towards the gaseous phase, thus high pressure is needed for dissolving gaseous hydrogen in the given interstitial site. Within the investigated compositional range $V_{84.2}Ni_{5.3}Ti_{10.5}$ exhibited the lowest E_b (at T site), i.e. the highest H solubility. Probably due to size effects (Ti has a larger atomic radius than V [38]) further increase of the amount of substitutional Ti up to about 30 at.% (the composition $V_{63.1}Ni_{5.3}Ti_{31.6}$), by simultaneous decrease of the V concentration, lowered the absorption affinity of the solid solution in comparison with the alloy with 10.5 at.% Ti. Hence there is a maximum value for the optimal concentration of Ti solutes in V-based alloys, which corresponds to the highest solubility value. This concentration appears to be between 10 at.% and 30 at.% Ti. The lowered solubility of the $V_{63.1}Ni_{5.3}Ti_{31.6}$ alloy might be attributed to the reduced V content in the primary phase with about 20 at.% in comparison to the other two ternary alloys. In summary, in order to achieve stabilisation of hydrogen atoms and to augment the solubility of the alloy, the concentration of vanadium should remain high, while varying the ratio between Ti and Ni. However, more alloy compositions have to be considered in order to validate this theoretical finding.

If the binding energy can be related to the ability of the alloy to dissolve hydrogen, the correlation of E_b with the rate of movement of H atoms within the crystal lattice (diffusion coefficient) is not straightforward. However, both diffusion and solubility are important as each of these transport properties contributes to the permeability. The current view about transport of hydrogen in a metal lattice is that it hops from O site to T site and vice versa. Even if the equilibrium occupancy in a given metal or alloy is tetrahedral, without indications of stable octahedral occupation, hydrogen hops from T to T sites via O interstices [39]. Direct jumps from O to O or from T to T sites are not thermodynamically feasible. To predict the diffusivity properties of the alloys of interest, the rate of thermally activated jumps has to be evaluated. This can be done by calculating vibrational frequencies of H atoms in the absorption sites and the jump activation energies, which are defined as the difference between the energies of H atoms in interstitial sites and in transition states. Such calculations haven’t been performed in this study. However, analysing of the experimental lattice parameters of the hereto-investigated alloys, we can assume that the diffusivity of $V_{84.2}Ni_{10.5}Ti_{5.3}$ (a = 3.0085 Å) is higher than the diffusivity of $V_{84.2}Ni_{5.3}Ti_{10.5}$ (a = 3.0331 Å) and $V_{63.1}Ni_{5.3}Ti_{31.6}$ (a = 3.0998 Å). This prediction is based on the fact that a larger lattice parameter leads to an increase in the distance between interstitial sites and thus to a larger hopping distance for the absorbed hydrogen atoms [4,40]. As a result hydrogen diffuses with greater difficulty in alloys with larger lattice constants in comparison to alloys with smaller lattice constants. The obtained results can be used as guidelines for tailoring materials for H_2-selective membranes.

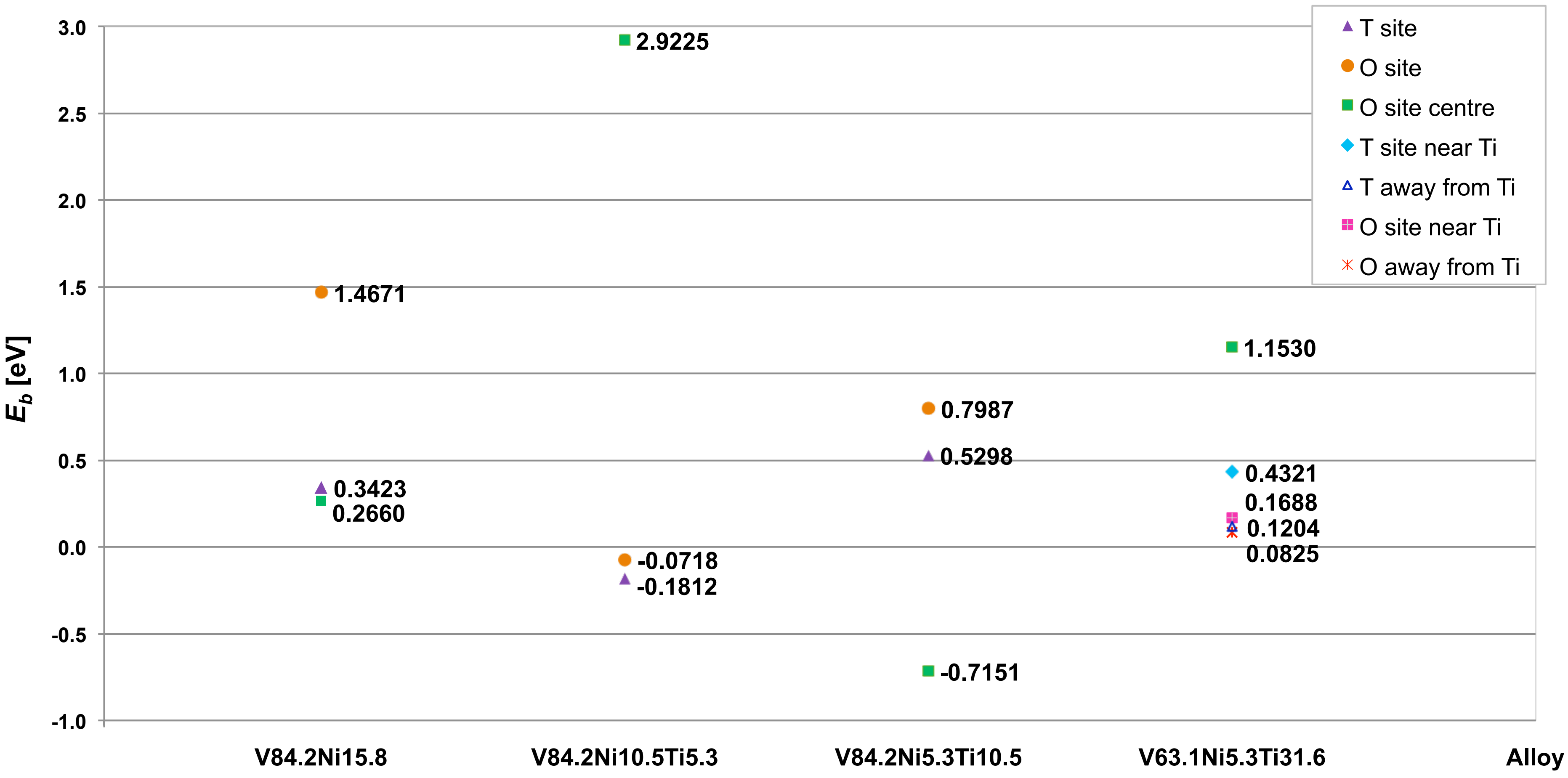

Figure 9: Hydrogen binding energies (E_b) for a pair of H atoms placed in the T and O sites in four alloy formulations: $V_{84.2}Ni_{15.8}$ (a = 3.0093 Å), $V_{84.2}Ni_{10.5}Ti_{5.3}$ (a = 3.0085 Å), $V_{84.2}Ni_{5.3}Ti_{10.5}$ (a = 3.0331 Å) and $V_{63.1}Ni_{5.3}Ti_{31.6}$ (a = 3.0998 Å).

4 Conclusions

VNiTi alloy membranes are promising candidates for H_2 separation applications, and an understanding of the H_2 absorption affinity in V-based alloys in terms of occupancy and energetics is important for their development. The hereto-reported DFT study aims to inform the design and optimisation of non-Pd membranes in that regard. The results indicate that H atoms prefer to stay away from one another within the metal lattice of VNi-based alloys, taking positions with a large H-H spatial separation. Notwithstanding, the preference for a large spatial distance is valid when considering sites of identical symmetry but not when trying to determine if tetrahedral or octahedral occupation is favoured. When both T and O sites are considered simultaneously, one of these symmetries is energetically favoured for a given VNiTi composition and this is not necessarily the site that provides larger H-H distances. The preference of hydrogen for either tetrahedral or octahedral interstices in the investigated V-based solid solutions changes in respect of the V:Ni:Ti ratio, i.e. the sites occupancy depends on the alloy composition.

The results from this DFT study show that in order to achieve stabilisation of hydrogen and thus higher hydrogen solubility of the bcc alloys, the vanadium concentration should be kept high enough (over 80 at.%), while the concentration of titanium should be not less than 10 at.%. Among the hereto-investigated metal systems $V_{84.2}Ni_{5.3}Ti_{10.5}$ is the alloy with the lowest binding energy. Hence, if lattice vibrations and entropy are similar for the tested metal alloys, $V_{84.2}Ni_{5.3}Ti_{10.5}$ should exhibit the highest hydrogen solubility.

Neutron diffraction experiments are able to provide important information for validation of the results obtained by this first-principles approach. In addition to the hereto-performed DFT calculations using spatially localized functions, plane wave computations with periodic boundary conditions would improve the accuracy of the *ab initio* representation of the H-metal system.

The presented DFT approach can be used as an explanatory and predictive methodology, complementary to experimental approaches that are limited by economical and time factors, especially in terms of evaluating multiple materials. Expanding the work to other VNi-based alloys, exploring other substituents than Ti, can provide important information on metal alloys as candidate materials for preparing H_2 separation membranes.

Bibliography

[1] W. Pfeiler, Alloy physics, 1st Ed., W. Pfeiler (Ed.), Weinheim, Germany: Wiley-VCH, 2007.

[2] A. Kiejna, K.F. Wojciechowski, Metal Surface Electron Physics, 1st Ed., Oxford, UK: Elsevier Science, 1996.

[3] N.A. Al-Mufachi, N.V. Rees, R. Steinberger-Wilkens, Hydrogen selective membranes: a review of palladium-based dense metal membranes, Renewable and Sustainable Energy Reviews, vol. 47, 540-551, 2015.

[4] M.V. Mundschau, Hydrogen separation using dense composite membranes, in: Inorganic membranes for energy and environmental applications, A.C. Bose (Ed.), New York, NY, USA: Springer, 2009.

[5] S. Kang, S. Hao, D.S. Sholl, Using First-principles Models to Advance Development of Metal Membranes for High Temperature Hydrogen Purification, in: Inorganic, Polymeric and Composite Membranes. Structure, Function and Other Correlations, S.T. Oyama, S.M. Stagg-Williams (Eds.), Amsterdam, The Netherlands: Elsevier, 2011, 309-332.

[6] M. Dolan, G. Song, D. Liang, M. E. Kellam, D. Chandra, J. H. Lamb, Hydrogen transport through V85Ni10M5 alloy membranes, Journal of Membrane Science, vol. 373, 14-19, 2011.

[7] E. Ozdogan, J. Wilcox, Investigation of H_2 and H_2S adsorption on niobium-and copper-doped palladium surfaces, The Journal of Physical Chemistry B, vol. 114, no. 40, 12851-12858, 2010.

[8] M.D. Dolan, Non-Pd BCC alloy membranes for industrial hydrogen separation, Journal of Membrane Science, vol. 362, 12-28, 2010.

[9] P. Jiang, Y. Yu, G. Song, D. Liang, M. Kallem, M. Dolan, Effect of heat treatment on microstructure, hardness and rollability of $V_{55}Ti_{30}Ni_{15}$ alloy membranes, Materials and Design, vol. 63, 136-141, 2014.

[10] A.C. Makrides, M.A. Wright, D.N. Jewett, Separation of Hydrogen by Permeation, 3,350,846, Nov 7, 1967.

[11] S.A. Steward, Review of hydrogen isotope permeability through metals, US National Laboratory, UCRL-53441 1983.

[12] M.V. Mundschau, X. Xie, C.R. Evenson, Superpermeable hydrogen transport membranes, in Nonporous inorganic membranes, M.V. Mundschau A.F. Sammells (Eds.), Weinheim, Germany: Wiley-VCH, 107-138.

[13] K. Lee, M. Yuan, J. Wilcox, Understanding deviations in hydrogen solubility predictions in transition metals through first-principles calculations, The Journal of Physical Chemistry C, vol. 119, no. 34, 19642-19653, 2015.

[14] C. Nishimura, M. Komaki, M. Amano, Hydrogen permeation characteristics of vanadium-nickel alloys, Materials Transactions, vol. 32, no. 5, 501-507, 1991.

[15] M.D. Dolan, K.G. McLennan, J.D. Way, Diffusion of atomic hydrogen through V-Ni alloy membranes under nondilute conditions, Journal of Physical Chemistry C, vol. 116, 1512-1518, 2012.

[16] M.D. Dolan, G. Song, K.G. McLennan, M.E. Kellam, D. Liang, The effect of Ti on the microstructure, hydrogen absorption and diffusivity of V-Ni alloy membranes, Journal of Membrane Science, vol. 415-416, 320-327, 2012.

[17] M.D. Dolan, K.G. McLennan, G. Song, D. Liang, M.E. Kellam, The effect of Ti on hydrogen absorption and diffusivity in V–Ti–Al alloy membranes, Journal of Membrane Science, vol. 446, 405–409, 2013.

[18] G. Song, M.D. Dolan, M.E. Kellam, D. Liang, S. Zambelli, V–Ni–Ti multi-phase alloy membranes for hydrogen purification, Journal of Alloys and Compounds, vol. 509, 9322-9328, 2011.

[19] M.D. Dolan, M.A. Kochanek, Ch.N. Munnings, K.G. McLennan, Hydride phase equilibria in V-Ti-Ni alloy membranes, Journal of Alloys and Compounds, vol. 622, 276-281, 2015.

[20] A. Machida, H. Saitoh, H. Sugimoto, T. Hattori, A. Sano-Furukawa, N. Endo, Y. Katayama, R. Iizuka, T. Sato, M. Matsuo, S. Orimo, K. Aoki, Site occupancy of interstitial deuterium atoms in face-centred cubic iron, Nature Communications, vol. 5, 2014.

[21] J. Hauck, Structural Relations between Vanadium, Niobium, Tantalum Hydrides and Deuterides, Acta Crystallographica, vol. A34, 389-399, 1978.

[22] H. Wipf, Diffusion of hydrogen in metals, in: Hydrogen in metals III, Topics in applied physics, H. Wipf (Ed.), Berlin, Germany: Springer, 1997, vol. 73, 51–91.

[23] A.L. Companion, F. Liu, D.P. Onwood, On the location of a hydrogen atom in body-centred cubic 3d transition metal lattices, Journal of the Less-Common Metals, vol. 107, 131-138, 1985.

[24] W.R. Gray, D.G. Westlake, S.T. Ockers, Electrical resistivity of V-H alloys, Metallurgical Transactions, vol. 1, 1361-1364, May 1970.

[25] J. Wanagels, S.L. Sass, B.W. Batterman, The ordering of hydrogen in β-Vanadium Hydride, Physica Status Solidi (a), vol. 10, no. 1, 49-57, 1972.

[26] H. Asano, M. Hirabayashi, Low-temperature phase transition near V_3H_2, Physica Status Solidi (a), vol. 16, no. 1, 69-72, 1973.

[27] M.I. Darby, M.N. Read, Energy of hydrogen in B.C.C. transition metals, Journal of the Less-Common Metals, vol. 91, 209-215, 1983.

[28] S. Aboud, J. Wilcox, A density functional theory study of the charge state of hydrogen in metal hydrides, The Journal of Physical Chemistry C, vol. 114, no. 24, 10978-10985, 2010.

[29] R.G. Parr, W. Yang, Density-Functional Theory of atoms and molecules, J.B. Goodnough, J. Halpern, J.S. Rowlinson R. Breslow (Eds.), Oxford University Press, 1989.

[30] D.S. Sholl, J. Steckel, Density Functional Theory: A practical introduction. Hoboken, NJ, USA: John Wiley & sons, 2009.

[31] P. Hohenberg, W. Kohn, Inhomogeneous electron gas, Physical Review, vol. 136, no. 3B, 864-871, Nov. 1964.

[32] W. Kohn, L.J. Sham, Self-consistent equations including exchange and correlation effects, Physical Review, vol. 140, no. 4A, 1133-1138, Nov. 1965.

[33] M. Valiev, E.J. Bylaska, N. Govind, K. Kowalski, T.P. Straatsma, H.J.J. van Dam, D. Wang, J. Nieplocha, E. Apra, T.L. Windus, W.A. de Jong, NWChem: a comprehensive and scalable open-source solution for large scale molecular simulations, Computer Physics Communications, no. 181, 1477–1489, 2010.

[34] A.D. Becke, Density-functional thermochemistry. III. The role of exact exchange, Journal of Chemical Physics, vol. 98, 5648-5652, 1993.

[35] L. Vegard, Die Konstitution der Mischkristalle und die Raumfüllung der Atome, Zeitschrift für Physik, vol. 5, no. 1, 17-26, 1921.

[36] S.T. Murphy, A. Chroneos, C. Jiang, U. Schwingenschlögl, R.W. Grimes, Deviations from Vegard’s law in ternary III-V alloys, Physical Review B, vol. 82, 0732011-0732014, 2010.

[37] Y.-S. Lee, C. Ouyang, J.-Y. Suh, E. Fleury, Y. Whan Cho, J.-H. Shim, Role of alloying elements in vanadium-based binary alloy membranes for hydrogen separation, Journal of Membrane Science, vol. 423-424, 332–341, 2012.

[38] O.N. Senkov, D.B. Miracle, Effect of the atomic size distribution on glass forming ability of amorphous metallic alloys, Materials Research Bulletin, vol. 36, 2183-2198, 2001.

[39] K.G. McLennan, E. MacA. Gray, J.F. Dobson, Deuterium occupation of tetrahedral sites in palladium, Physical Review B, vol. 78, no. 014104, 1-8, 2008.

[40] J. Völkl, G. Alefeld, Diffusion of hydrogen in metals, in Hydrogen in metals, G. Alefeld, J. Völkl, (Eds.), Berlin, Germany: Springer-Verlag, 1978, vol. 28, 321-348.

Part II

Predictive models for the ideal selectivity of crystalline porous materials

Summary

English version: In this part of the thesis, predictive models for the ideal selectivity of crystalline porous materials towards light gases are developed and analysed. In the first chapter, an overview of zeolites and MOFs, discussing their structural features and some applications, is given. The second chapter of this part introduces the derivation of analytical equations for evaluating the ideal selectivity of zeotype membrane materials as a function of single-component sorption data and operation conditions. The model parameters are further discussed and their values, used to predict the selectivity of chosen zeotype adsorbents, are summarised. Moreover, experimental measurements for validation of the theoretical results are described. In the last chapter, the theoretical and the experimental ideal selectivities of zeotype materials are compared and analysed.

Italian version: In questa sezione della tesi, sono stati sviluppati ed analizzati modelli predittivi per ottenere i fattori di separazioni ideali di materiali cristallino-porosi verso gas a basso peso molecolare. Una panoramica delle zeoliti e dei MOF con un'analisi sulle loro caratteristiche strutturali ed alcune loro applicazioni è presentata nel successivo capitolo. Il secondo capitolo presenta, invece, la derivazione delle equazioni di lavoro (equazioni modello) per la stima dei fattori di separazioni ideali di materiali di tipo zeolitico in funzione di parametri, quali quelli ottenibili dalle isoterme d'adsorbimento di un singolo gas, e dalle condizioni operative. I parametri del modello sono discussi insieme ai valori usati per predire la selettività. Quindi le misure sperimentali usate per la validazione dei risultati teorici sono state presentate ed analizzate. Nell'ultimo capitolo, infine, i valori teorici e sperimentali delle selettività ideali sono confrontati e discussi.

Spanish version: En esta parte de la tesis se analizan y desarrollan modelos predictivos para la selectividad ideal de materiales cristalinos porosos con gases ligeros. En el siguiente capítulo se da

una visión general de las zeolitas y los MOFs, discutiendo sus características estructurales y algunas sus aplicaciones principales. El segundo capítulo de esta parte presenta la derivatización de ecuaciones analíticas para la evaluación de la selectividad ideal de materiales zeolíticos en función de parámetros fácilmente obtenibles. Se discuten los parámetros usados en los modelos y se resumen los valores aplicados para predecir la selectividad de las zeolitas adsorbentes utilizadas. Además, se describen las medidas experimentales para la validación de los resultados teóricos. En el último capítulo se analizan y comparan la selectividades ideal-teórica y experimental de los materiales zeolíticos con los que se ha trabajado.

French version: Dans cette partie de la thèse, des modèles prédictifs de la sélectivité idéale des matériaux poreux cristallins envers les gaz légers sont développés et analysés. Le premier chapitre présente une vue d'ensemble sur les zéolithes et les MOFs, en discutant leurs caractéristiques structurales et quelques applications. Le deuxième chapitre présente la construction des équations analytiques utilisées pour évaluer la sélectivité idéale des matériaux zéolithiques en fonction des données de sorption de gaz purs et des conditions opératoires. Les paramètres du modèle sont ensuite discutés et les valeurs utilisées pour prédire la sélectivité des adsorbants zéolithiques sélectionnés sont résumées. En outre les mesures expérimentales permettant de valider les résultats théoriques sont décrites. Le dernier chapitre permet de comparer et d'analyser les sélectivités idéales théoriques et expérimentales des membranes zéolithiques.

5 Theoretical background

5.1 Transport mechanisms in microporous crystalline materials

The capability of crystalline porous membranes to separate light gases depends strongly on the material's framework and pore sizes. However, it is worth noting that neither the porous framework nor the molecules are rigid structures [1]. In fact, the probability of electron density distribution in atoms reaches zero at infinity. In any case, approximated values for the atom size can be given because the electron density falls off rapidly in short distance from the nucleus. Furthermore, describing a molecule as a sphere with a particular diameter is an accepted oversimplification. The kinetic diameter of a molecule (d_m) is a reflection of its smallest effective dimension. Nonetheless, di- and multi-atomic molecules possess rather cylindrical shape characterised by a second dimension except the kinetic diameter and this is the effective length (f_m). The vibration of the crystalline lattice and possible distortions of both molecule and porous material when they are in contact make it even more difficult to define a precise diameter of either of them. Regardless the above-mentioned facts, the ratio of the approximated pore diameter (d_p) over the kinetic molecular diameter of the permeating gases ($\delta = d_p/d_m$) is commonly used as characteristic descriptor for predicting the separation behaviour of porous media towards particular gases. Below is discussed the characterisation of transport mechanisms proposed by A.J. Burggraaf [2] but other authors, among whom J. Xiao and J. Wei, give similar classifications [1]. Logically if $\delta << 1.0$, i.e. if d_p is much smaller than d_m, the molecule experiences strong repulsive force from the porous network and it is excluded due to size sieving. If d_p and d_m are of comparable size, $\delta \approx 1.0$, the mechanism is deemed as configurational diffusion. Here, following from the previous discussion, if the porous channels and windows are slightly smaller than the molecular diameter, the molecule still might enter the material. This is especially valid for metal organic frameworks, due to the relatively high flexibility of the network, compared to zeolites. It should be remarked that in the case of configurational diffusion, a molecule is not bonded as strongly as by solution-diffusion mechanism that occurs when atoms enter interstitial sites in a solid solution, e.g. in the case of hydrogen absorption in dense metal membranes (See Part I). In the frame of the classification provided by Burggraaf, in the range $1.0 \leq \delta \leq 1.24$ the term surface diffusion is established. Maxwell-Stefan (MS) model is claimed to accurately describe both configurational and surface diffusion [2]. This model is reportedly not suitable for cases where gas translational (GT) diffusion ($1.24 \leq \delta \leq 3.0$) is the controlling transport mechanism. Instead, GT regime is covered by the activated Knudsen model, in which gas molecules are considered to move between cages in a translational mode by overcoming obstructions formed by the small channels connecting adjacent sorption sites. Here, the diffusional activation energy is considered to be the difference between the potential energy of a molecule residing in the channel and one residing at the intersection of the crystalline framework. It should be remarked that Burggraaf use the term configurational diffusion for ratios between the pore size and the molecular size that are smaller than the ratios where surface diffusion occurs, i.e. *δ(configurational diffusion)* < *δ(surface diffusion)* < *δ(gas translational diffusion)*. In contrast, Xiao and Wei use the term configurational diffusion to colligate the terms surface diffusion (that actually in their work appears under the name solid vibration model) and gas translational diffusion. Due to this contradiction in the terminology, in this thesis the denomination configurational diffusion is avoided and the expressions surface and gas translational diffusion are used.

The well-defined framework of zeolites and MOFs, characterised by the microporous topology with pore openings of uniform dimensions, preconditions the suitability of theoretical models such as the Maxwell-Stefan *ansatz* and the activated Knudsen formulation to describe the transport properties of gas molecules inside these materials. In contrast, processes in amorphous materials are more difficult to model. In this thesis we are interested in separation of gases with molecular diameter in the range 2.5 Å – 4 Å, and therefore in small-pore crystalline solids that are able to discriminate among such gaseous molecules and to separate desirable components. Thus, according to the classification discussed above, for gas molecules able to be adsorbed, surface diffusion with the corresponding MS model can describe well the transport mechanism of the target sorbate-sorbent systems.

The Maxwell-Stefan formulation was developed independently by James Clerk Maxwell in 1866 [3] and by Josef Stefan in 1871 [4]. The driving force for molecular movement in this phenomenological model is the chemical potential [5]. Components moving with different velocities exert a drag on each other, equal to the difference between their velocities divided by a proportionality factor, which is defined as the binary MS diffusivity. Therefore this approach is commonly applied for multicomponent systems pointing to the fundamentally multicomponent nature of diffusion. However, it has been shown in the past that the formulation can be reduced to describe single-component diffusion in zeotype materials, without contradicting the multicomponent concept of diffusion [6]. In fact, even when considering a single-gas flux through a zeolite or MOF layer, we are treating a multicomponent system comprised of the diffusing gas and the crystalline porous material. Yet, the Maxwell-Stefan *ansatz* defines diffusive fluxes by balancing forces so that the total diffusive flux vanishes. A fixed adsorbent cannot satisfy the condition to balance the flux of the permeating component. Considering vacant adsorption sites as diffusing pseudo-species circumvents this issue. The concept is based on the realization that whenever a molecule jumps, a vacancy makes a counter jump. The adsorption at vacancies can be considered as a kind of friction against the movement of the diffusing component. Equations for single-component diffusion through porous materials in accord with the vacancy-based Maxwell-Stefan approach can be found in the literature [7]. However, they are mostly used to theoretically correlate diffusion coefficients such as Fickian transport diffusivity and Maxwell-Stefan surface diffusivity. Practical applications of such simple models to describe the permeation behavior of zeolite-guest systems are not well explored. Thus, in this study, we focused on the separation properties of zeolite layers adopting the aforementioned phenomenology. In particular, we developed two models for evaluating the gas selectivity of crystalline porous materials under different assumptions for the diffusivity dependency on loading. The derivation of the models is shown in details in section 6.1. Additionally, the activated Knudsen model, which is considered as suitable for prediction of the transport and separation properties of zeolites and MOFs with larger pores or/and at high temperature, is discussed.

5.2 Zeolites and MOFs

Zeolites are crystalline inorganic (aluminosilicate) materials with open microporous structures. Their frameworks are based commonly on TO_4 tetrahedrons with T being a silicon or aluminium atom. Typically the composition of a zeolite can be expressed with the general chemical formula $M_{x/n}[(AlO_2)_x(SiO_2)_y]zH_2O$, where M is a metal cation, that counterbalances the charge of the framework when an Al^{3+}-ion replaces a Si^{4+}-ion, and *n* is the valence of the cation [8]. All Al and Si atoms are surrounded by oxygen atoms in the tetrahedrons and are not exposed to the surface. Hence, the oxygen atoms and the cations form the surface. Water is removed from the structure by heating. Aluminium rich zeolites (e.g. zeolites A and X) have Si/Al ratios approaching 1, but always higher than 1. This is explained by the Löwenstein's avoidance rule that permits only Si-O-Al and Si-O-Si linkages. Al-O-Al linkages are proven to be instable [9]. The cations that maintain structural charge balance are not part of the framework. They are loosely held and therefore exchangeable. Pure silica synthetic forms also exist, e.g. decadodecasil 3R (DD3R) and silicalite-1. The absence of aluminium implies that the network is free of extra-framework cations.

Zeolites can be classified in groups according to the number of oxygen atoms that form a pore [10]. Sodalite (SOD) is characterised by extra-small pore framework with apertures of 6-membered oxygen rings. Sodalite cages are constructive bricks of most of the zeolites and it is also used for fabrication of membranes [11]. Small pore zeolites possess 8-oxygen-ring openings, e.g. CHA, LTA, DDR [12]. Intermediate pore zeolites, such as MFI and MEL, have 10-oxygen atoms around each pore opening. The zeolites with 12-oxygen-rings are defined as large pore frameworks, e.g. FAU, MOR. Extra-large topologies have pores delimited by 14 or more oxygen atoms (e.g. $AlPO_4$-8). Zeolite materials are used as powders, thin films or membranes and find various applications in catalysis, sorption, ion exchange and separation processes due to their capability for molecular recognition at nanoscale [13]. Membranes employing these materials are chemically and mechanically robust and can be used over a wide range of operation conditions [14]. In many light gas separations they outperform polymeric membranes in terms of selectivity and permeance. Therefore many research efforts are devoted to develop and analyse zeolite membranes [15].

One of the extensively studied aluminosilicates is zeolite A, which is also named Linde type A. It is abbreviated as LTA after the three-letter codes established by the IUPAC Commission on Zeolite Nomenclature. The three-dimensional LTA-type framework consists of sodalite cages arranged in a cubic manner, resulting in 8-oxygen-ring pore openings, as illustrated in Figure 10. The sodalite cages are linked between each other through double 4 oxygen-rings. The Si/Al atomic ratio of the framework is usually equal to 1 but can be also higher than 1.

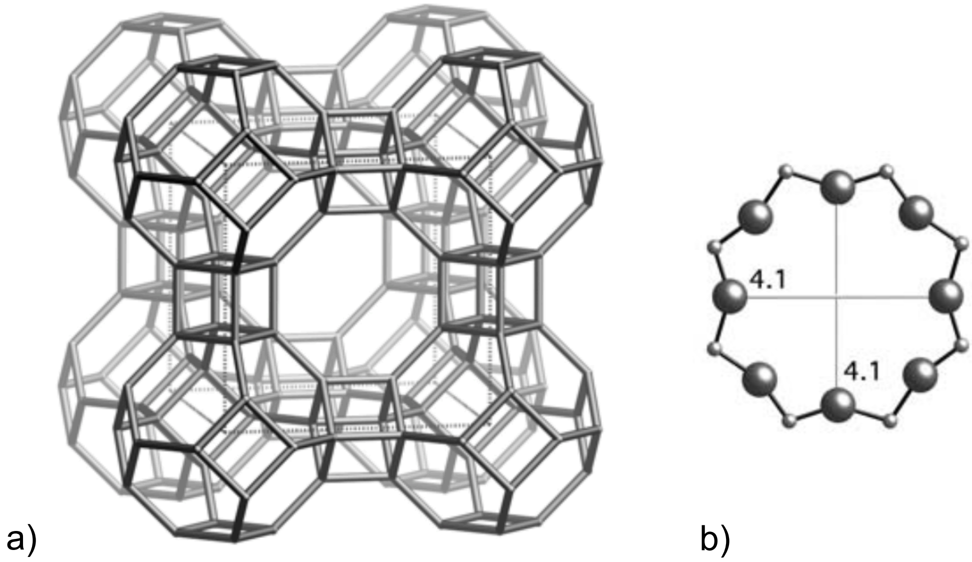

Figure 10: Schematic representation of a) a LTA unit cell; b) a 8-oxygen-ring forming the pore entrance of LTA. *Images from* [16].

The exchangeable cations in LTA, which serve to offset the $(AlO_2)^-$ groups, are the adsorption sites for gas molecules. They sit near the centres of the 6-membered oxygen ring of the sodalite building block and all of them are accessible to gas molecules. LTA is known in few different forms according to type of extra-framework cations in a unit cell and the respective diameter of the pores. The most common representatives are 3A (the potassium form K-LTA with nominal diameter of 3.0 Å), 4A (the sodium form Na-LTA with pore diameter of 3.9 Å, reported usually with its nominal diameter of 4 Å) and 5A (the calcium form Ca-LTA with measured pore size of 4.3 Å and nominal diameter equal to 5 Å) [8]. Structural properties of these molecular sieves are summarized in Table 8. The only commercialised membrane type is Na-LTA (or shortly NaA) with the first commercial unit realised on the market in 1999 by Mitsui Engineering & Shipbuilding Co. Ltd [17]. Being nitrogen-selective, in contrast to the chiefly oxygen-selective polymeric and carbon membranes [18], Linde type A zeolites are of interest for production of oxygen-enriched air. Reportedly NaA has a great potential also for removal of H_2O from Fischer-Tropsch product streams containing CO, H_2 and CH_4 in order to inhibit the oxidation (caused by water) of the catalyst and to promote the reaction rate. Such light gas separations are governed by the interaction of gas molecules with the charge-compensating cations. However, the only realized industrial application of LTA membranes is for organics dehydration. A few years ago, ITQ-29, a pure silica form (or sometimes germanosilicate) of zeolite A, was discovered [19].

Table 8: Nomenclature and structural properties of the most common Linde type A zeolites.

Type	3A	4A	5A
Other names	KA, K-LTA	NaA, Na-LTA	CaA, Ca-LTA
Chemical formula†	$K_{7.2}Na_{4.8}[(AlO_2)_{12}(SiO_2)_{12}]$	$Na_{12}[(AlO_2)_{12}(SiO_2)_{12}]$	$Ca_{4.5}Na_3[(AlO_2)_{12}(SiO_2)_{12}]$
Channel system	3-dimensional		
Unit cell	Cubic (space group Fm-3c)		
Nominal pore size [Å]	3	4	5
Measured pore size [Å]	3.3 [8]	3.9 [8] – 4.1 [16]	4.3 [8]

†The chemical formula is shown as reported in Ref. [20] without the water content.

Another well-known zeolite structure is faujasite (FAU), shown in Figure 11. With the 12-membered ring pore openings, FAU-type zeolites belong to the large pore frameworks. Depending on the Si/Al ratio, synthetic faujasite-type zeolites are divided into two classes – X and Y. The silicon-to-aluminium atomic ratio in X is between 1 and 1.5, while in Y it is between 1.5 and 3 [21]. Zeolite X is called low-silica X (LSX) when this ratio is 1.

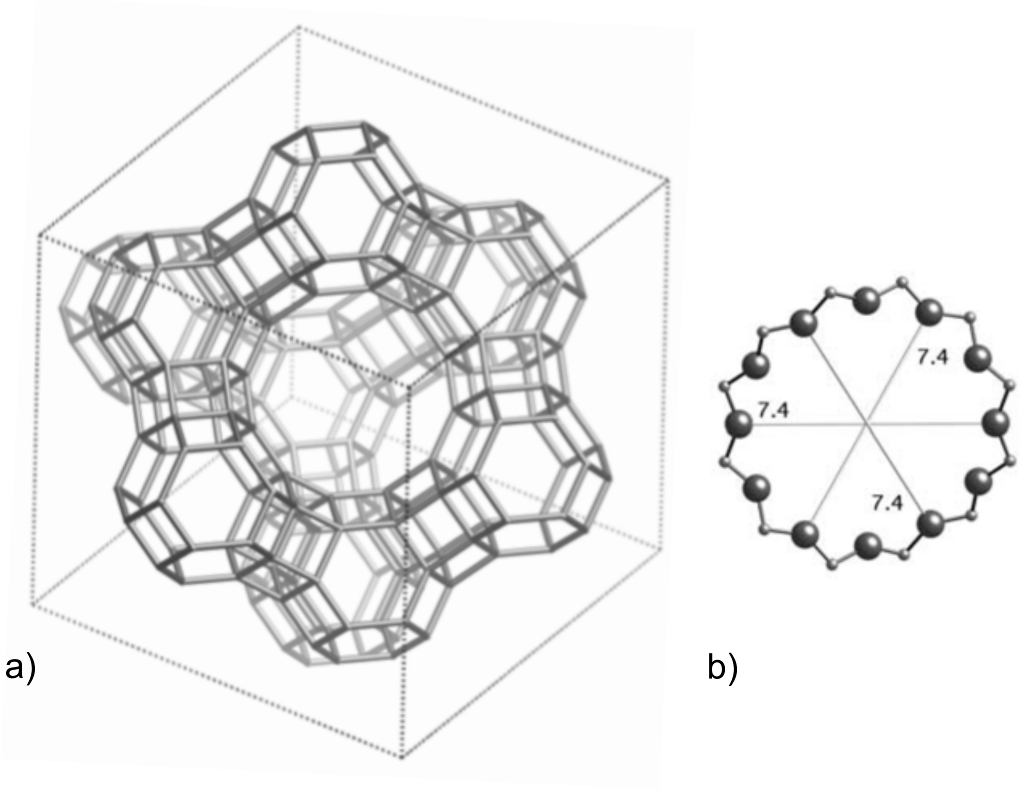

Figure 11: Schematic representation of a) a FAU unit cell; b) a 12 oxygen-ring forming the pore of FAU. *Images from* [16].

As in the case of zeolite A, the extra-framework cations compensating the charge for each Al atom are commonly monovalent (e.g. K^+, Na^+ Li^+) or divalent (such as Ca^{2+}, Mg^{2+}, Ba^{2+}), where the valence determines their number. The formula of a typical NaX unit cell is $Na_{86}[(AlO_2)_{86}(SiO_2)_{106}]$, and of CaX it is $Ca_{40}Na_6[(AlO_2)_{86}(SiO_2)_{106}]$ [22]. In contrast to LTA, in FAU not all cations are accessible adsorption sites. Cations in supercages (at sites II and III) are accessible for gas molecules, while these at positions in hexagonal prisms and cubooctahedrons (sites I, I' and II') are considered to be inaccessible [23]. Sites I (I'), II (II') and III are indicated in Figure 12. It is reported that when the content of sodium ions in FAU zeolite is low, all cations are located in hidden sites, yielding a very low adsorption affinity [24]. Therefore high aluminium content, and thus higher cation number and charge density, is desired for enhanced adsorption selectivity. On the contrary, structures with higher Si/Al ratio are proven to be more stable in high temperatures and to chemical leaching. The access window diameters also depend on the exchangeable ions and for NaX the aperture of the largest channels is approximately 7.4 Å, and for CaX this value is increased to 10 Å [25].

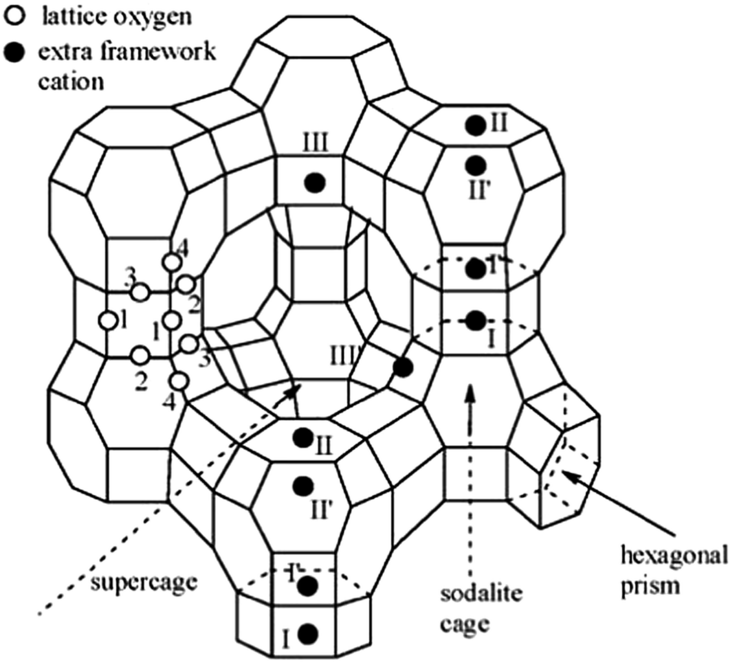

Figure 12: Positions of the potential charge-compensating cations in a FAU supercage. *Image from RSC Adv* [26].

Often considered as similar or complementary to zeolites are the metal-organic framework materials. They possess hybrid porous structure with organic part, namely organic linkers, coordinating the metal ions. MOFs attracted a great deal of attention in the last years due to their very high specific surface areas and tuneable pore sizes [27]. Zeolitic imidazolate frameworks (ZIFs) are a subgroup of MOFs. The materials of this class consist of tetrahedral clusters of MN_4 with M = Co, Cu, Zn, etc., linked by simple imidazolate ligands [28].

Due to their exceptionally high thermal, chemical and moisture stability, ZIF-8 is one of the most extensively studied materials from this subgroup [29]. Its chemical formula is $C_8H_{12}N_4Zn$ but the notation $Zn(MeIM)_2$, where MeIM stands for methylimidazolate, is common. The pore limiting diameter of ZIF-8 is 3.4 Å, which is less than the kinetic diameter of CH_4, but owning to the framework's flexibility [30], the window of the framework allows CO_2, N_2, and CH_4 to diffuse into the pores.

Both classes of crystalline materials discussed here, zeolites and MOFs, are able to separate molecules by the effect of competitive adsorption, differences in diffusion kinetics and/or molecular sieving [31]. Thus, understanding the separation mechanism of such membrane materials is not a trivial matter.

5.3 Capabilities and limitations of predictive models

It is necessary to remark that the hereto-proposed models are suited to provide information on the ideal separation behaviour of crystalline porous materials used for gas selective membranes. Since single-gas data inputs are utilized, competitional permeation of molecules when in mixture is not taken into account. Mixture selectivities often differ significantly from the ideal values and implications for the transport mechanism and for the gas-gas and gas-adsorbent interactions can be extracted from the deviation. For example a CO_2 molecule has a larger molecular diameter and molecular weight compared to N_2. The Knudsen separation factor for CO_2 versus N_2 equals 0.78. However, reversed CO_2/N_2 selectivities are reported for a range of crystalline porous materials (as DDR [32], LTA [32], FAU [33,34,35], ZIF-8 [36,37] and SIM-1 [27], to list some of them) with higher mixture selectivity values compared to the ideal selectivities. This indicates preferential adsorption of CO_2 and reduced diffusion of N_2, i.e. N_2 kinetics are slowed down in the presence of CO_2.

Moreover, the experimental results obtained with membranes made of a given material depend on the synthesis processes and measuring techniques/conditions. A simple example is NaA zeolite used as membrane material. Different synthesis method applied to prepare NaA membranes can lead to H_2 permeance values in a wide range, e.g. from $0.64 \cdot 10^{-8}$ [38] to $213 \cdot 10^{-8}$ mol m^{-2} s^{-1} Pa^{-1} [39]. However, the H_2/N_2 separation factors reported in these two cases are 4.6 for the former and 5.6 for the latter, indicating that material selectivity is comparable. And while these selectivity values agree rather well, it is not uncommon for scientific documents to claim that membranes based on the same core material exhibit selectivities within a wide margin. These differences are an indication for the great research efforts towards development of better performing, reproducible, defect-free materials [40]. In this frame, theoretical selectivity values set a needed benchmark that can provide guidelines for design and optimisation of crystalline porous membrane materials, including selection of filler materials for MMMs. In any case, quantitative modelling of the selectivity of membranes requires many factors to be taken into account and often each membrane configuration must be investigated separately, e.g. it is a difficult task with hard to impossible transferability to other cases.

6 Methodology

6.1 Model development

The transport equation describing the flux of components through a material vary in respect of the diffusion mechanism, which in turn, in the case of porous media, depends on the ratio between the size of the limiting pores and the molecular diameter. Zeolites and MOFs belong to the group of crystalline porous materials with diffusion mechanism mainly dominated by surface diffusion, described by the Maxwell-Stefan model and in some cases (high temperature, large pore molecular sieve and small nonpolar gas molecules) by gas translational diffusion and its equivalent activated Knudsen diffusion, as underlined in Section 5.1.

According to the MS model as developed for diffusion in zeolite-guest systems, the flux of a component *i* through the membrane per unit cross-sectional area is defined as [41]:

$$J_{MS,i} = -\rho q_{sat,i} D_{MS,i} \left(\frac{\theta_{i,j}}{RT} \nabla \mu_i \right). \tag{6.1}$$

In this equation ρ is the bulk density of the material and $D_{MS,i}$ is the single-component Maxell-Stefan diffusivity that reflects interactions between the adsorbed species and the vacancy adsorption sites (in fact if a molecule jumps a vacancy makes a counterjump). θ is the fractional occupancy (loading), defined as $\theta = q/q_{sat} \leq 1$, where q is the number of adsorbed molecules and $q_{sat,i}$ is the maximum sorption capacity of component *i* (saturation limit). The gradient of the chemical potential over the thickness of the sieving material, $\nabla\mu_i$, divided to the universal gas constant *R* and the temperature T can be expressed as:

$$\frac{1}{RT} \nabla \mu_i = \frac{1}{\theta_{i,j}} \Gamma \nabla \theta_{i,j}, \tag{6.2}$$

where Γ is a thermodynamic correction factor that converts the chemical potential gradient into a gradient of the occupancy. By insertion of Eq. (6.1) into Eq. (6.2), the following expression is obtained for a mono-dimensional system (the differential operator is transformed into a single derivative):

$$J_{MS,i} = -\rho q_{sat,i} D_{MS,i} \Gamma \frac{d\theta_{i,j}}{dx}, \tag{6.3}$$

with the thermodynamic correction defined as:

$$\Gamma \equiv \theta_{i,j} \frac{\partial ln P_{i,j}}{\partial \theta_{i,j}}. \tag{6.4}$$

Two common approaches are reported in the literature for the loading dependency of single-component diffusion in zeolites [1]. The first one is for concentration-independent diffusivity [2,5,42]. This assumption is reportedly true for gas-adsorbent systems with relatively weak confinement [6]. The second approach correlates the diffusion rate of molecules from site to site within the framework with the probability to find a vacant site for a jump [1,2]. Following this approach, different relationships for correcting the diffusion coefficient, $D_{MS,i}$, for its dependency on the loading, have been proposed [43]. One of these is given by $D_{MS}(\theta) = D_{MS}(0)(1 - \theta)$, with $D_{MS}(0)$ being the diffusion coefficient at zero loading or self-diffusivity.

Firstly, we take into consideration the assumption that the single-component Maxwell-Stefan diffusivity is independent on the loading:

$$D_{MS,i} \neq f(\theta_{i,j}). \tag{6.5}$$

In this case, one can also write $D_{MS}(\theta) = D_{MS}(0)$. Integration of Eq. (6.3) is performed between the feed (x = 0) and the permeate side (x = L) of the adsorbent (see also Figure B 1 in Appendix B):

$$\int_0^L \frac{J_{MS,i}}{dx} = -\rho q_{sat,i} D_{MS,i}(0) \int_{\theta_F}^{\theta_P} \Gamma d\theta_{i,j}. \tag{6.6}$$

Then, a model that describes the relationship between the occupancy and the pressure for pure components is employed. The applicability and limitations of the Langmuirian description of adsorption in zeolite have been discussed in the past and although many authors propose different isotherm equations such as Toth, Freundlich, Langmuir-Freundlich, Unilan, Radke-Prausnitz, Mathews-Weber, Volmer and so on [44], the Langmuir-type isotherm is frequently adopted in adsorption studies due to its simplicity and thermodynamic consistency [5]. The use of the Langmuir isotherm implies that the permeant concentrations at the feed and the permeate side are close to equilibrium. Reportedly, more complicated adsorption models not only require evaluation of more parameters but also imply a higher uncertainty of the determined parameter values [45].

Substitution of the expression for the thermodynamic correction factor, Γ (Eq. (6.4)), in the integral (Eq. (6.6)), yields:

$$J_{MS,i} = -\frac{\rho}{L} q_{sat,i} D_{MS,i}(0) \int_{\theta_F}^{\theta_P} \theta_{i,j} \frac{\partial ln P_{i,j}}{\partial \theta_{i,j}} d\theta_{i,j}. \tag{6.7}$$

Langmuir-type isotherm is used to transform further the function under the integral. The well-known relationship that describes Langmuir monolayer adsorption is:

$$\frac{q_i}{q_{sat,i}} = \theta_{i,j} = \frac{b_i P_{i,j}}{1 + b_i P_{i,j}}. \tag{6.8}$$

Here b_i is the adsorption equilibrium constant. It indicates the adsorption strength of a molecule onto a surface [46]. Simple transformation to express the pressure as function of θ results in:

$$P_{i,j} = \frac{\theta_{i,j}}{1 - \theta_{i,j}} \frac{1}{b_i} \tag{6.9}$$

Since in Eq. (6.7) the differential of the logarithm of pressure is needed, after simple algebra, $\partial lnP_{i,j}$ is expressed:

$$lnP_{i,j} = ln\theta_{i,j} - \ln\left(1 - \theta_{i,j}\right) - lnb_i \Rightarrow \partial lnP_{i,j} = \frac{1}{\theta_{i,j}\left(1 - \theta_{i,j}\right)} d\theta_{i,j} \tag{6.10}$$

Replacing the expression for $\partial lnP_{i,j}$ in Eq. (6.7), gives:

$$J_{MS,i} = -\frac{\rho}{L} q_{sat,i} D_{MS,i}(0) \int_{\theta_F}^{\theta_P} \theta_{i,j} \frac{1}{\theta_{i,j}\left(1 - \theta_{i,j}\right)} \frac{d\theta_{i,j}}{\partial\theta_{i,j}} d\theta_{i,j}. \tag{6.11}$$

In the next series of equations (6.12 – 6.14), Eq. (6.11) is transformed by crossing off the items that are repeated in the numerator and denominator and integrating in the interval $[\theta_F, \theta_P]$:

$$J_{MS,i} = \frac{\rho}{L} q_{sat,i} D_{MS,i}(0) \int_{\theta_F}^{\theta_P} -\frac{1}{\left(1 - \theta_{i,j}\right)} d\theta_{i,j}, \tag{6.12}$$

$$J_{MS,i} = \frac{\rho}{L} q_{sat,i} D_{MS,i}(0) \left[\ln\left(1 - \theta_{i,j}\right)\right]_{\theta_F}^{\theta_P}, \tag{6.13}$$

$$J_{MS,i} = \frac{\rho}{L} q_{sat,i} D_{MS,i}(0) ln \frac{1 - \theta_{i,P}}{1 - \theta_{i,F}}. \tag{6.14}$$

Expressing the loading from the Langmuir-type isotherm (Eq. (6.8)) yields:

$$J_{MS,i} = \frac{\rho}{L} q_{sat,i} D_{MS,i}(0) ln \frac{1 - \dfrac{b_i P_{i,P}}{1 + b_i P_{i,P}}}{1 - \dfrac{b_i P_{i,F}}{1 + b_i P_{i,F}}}, \tag{6.15}$$

which finally gives:

$$J_{MS,i} = \frac{\rho}{L} q_{sat,i} D_{MS,i}(0) ln \frac{1 + b_i P_{i,F}}{1 + b_i P_{i,P}}. \tag{6.16}$$

The ideal gas separation factor (α^*), also called permselectivity, is defined as ratio of single-component permeances assuming equal conditions for the gas fluxes:

$$\alpha^*_{A,B} = \frac{\Pi_A}{\Pi_B}. \tag{6.17}$$

The permeance of a gas is defined as the single-component flux divided to the pressure difference between feed and permeate side:

$$\Pi_i = \frac{J_i}{\Delta P_i} \tag{6.18}$$

Insertion of the transport equation derived above (Eq. (6.16)) into the expression for the ideal selectivity, i.e. Eq. (6.17), yields:

$$\alpha^*_{A,B} = \frac{\Delta P_B}{\Delta P_A} \frac{\frac{\rho}{L} q_{sat,A} D_{MS,A}(0) ln \frac{1 + b_A P_{A,F}}{1 + b_A P_{A,P}}}{\frac{\rho}{L} q_{sat,B} D_{MS,B}(0) ln \frac{1 + b_B P_{B,F}}{1 + b_B P_{B,P}}}. \tag{6.19}$$

By convention, the stronger adsorbed component is chosen to be component A whereas letter B indicates the weaker adsorbed molecule. The bulk density and the thickness of the selective layer of the membrane coincide and therefore can be crossed off. Considering ΔP_i equal for both single gases, the selectivity boils down to the ratio between single-component fluxes:

$$\alpha^*_{A,B} = \frac{D_{MS,A}(0)}{D_{MS,B}(0)} \frac{q_{sat,A}}{q_{sat,A}} \frac{ln \frac{1 + b_A P_{A,F}}{1 + b_A P_{A,P}}}{ln \frac{1 + b_B P_{B,F}}{1 + b_B P_{B,P}}}. \tag{6.20}$$

In the following, the work equation (6.20) is referred to as model (*1*) and it expresses the ideal separation factor under the assumption that D_{MS} are independent on the loading. Looking at model (*1*), it is instructive to consider both the adsorption selectivity (α_{Ads}) and the diffusion selectivity (α_{Diff}) in order to understand the underlying features contributing to the permselectivity of materials. In fact, it is important to emphasize that the form of model (*1*) allows for distinguishing between these factors. The first term on the right-hand side in Eq. (6.20) is the ratio between the diffusion coefficients at zero loading of the two components and it has the meaning of α_{Diff}. The term after the ratio $D_{MS,A}/D_{MS,B}$ defines α_{Ads}.

As stated above, the Maxwell-Stefan diffusivity can also exhibit a loading dependence, given by:

$$D_{MS,i}(\theta) = D_{MS,i}(0)\left(1 - \theta_{i,j}\right). \tag{6.21}$$

Here $D_{MS,i}(0)$ is the diffusivity at zero coverage and it is often equated to the self-diffusivity $D_{S,i}$ of a single component. Expressing $D_{MS,i}(\theta)$ through Eq. (6.21) in Eq. (6.3) results in:

$$J_{MS,i} = -\rho q_{sat,i}\left[D_{MS,i}(0)\left(1 - \theta_{i,j}\right)\right]\Gamma \frac{d\theta_{i,j}}{dx}. \tag{6.22}$$

In this case, the integration procedure is performed as:

$$\int_0^L J_{MS,i} dx = -\rho q_{sat,i} D_{MS,i}(0) \int_{\theta_F}^{\theta_P} \left[\Gamma - \theta_{i,j}\Gamma\right] d\theta_{i,j}. \tag{6.23}$$

In the following set of equations (6.24–6.29), Eq. (6.23) is transformed and the definite integral over the interval with limits $x = 0$, $\theta = \theta_F$ and $x = L$, $\theta = \theta_P$ is found:

$$\int_0^L J_{MS,i} dx = -\rho q_{sat,i} D_{MS,i}(0) \left[\int_{\theta_F}^{\theta_P} \Gamma d\theta_{i,j} - \int_{\theta_F}^{\theta_P} \theta_{i,j}\Gamma d\theta_{i,j}\right], \tag{6.24}$$

Using the general expression for the thermodynamic correction factor, Eq. (6.4) in Eq. (6.24), yields:

$$\int_0^L J_{MS,i}dx = -\rho q_{sat,i}D_{MS,i}(0)\left[\int_{\theta_F}^{\theta_P}\theta_{i,j}\frac{\partial lnP_{i,j}}{\partial\theta_{i,j}}d\theta_{i,j} - \int_{\theta_F}^{\theta_P}\theta_{i,j}\theta_{i,j}\frac{\partial lnP_{i,j}}{\partial\theta_{i,j}}d\theta_{i,j}\right]. \tag{6.25}$$

Employing the Langmuir-type function to relate the pressure to the loading (Eqs. (6.9) and (6.10), gives:

$$\int_0^L J_{MS,i}dx = -\rho q_{sat,i}D_{MS,i}(0)\left[\int_{\theta_F}^{\theta_P}\frac{1}{\left(1-\theta_{i,j}\right)}d\theta_{i,j} - \int_{\theta_F}^{\theta_P}\theta_{i,j}\frac{1}{\left(1-\theta_{i,j}\right)}d\theta_{i,j}\right], \tag{6.26}$$

$$\int_0^L J_{MS,i}dx = -\rho q_{sat,i}D_{MS,i}(0)\int_{\theta_F}^{\theta_P}\left(\frac{1}{\left(1-\theta_{i,j}\right)} - \theta_{i,j}\frac{1}{\left(1-\theta_{i,j}\right)}\right)d\theta_{i,j}, \tag{6.27}$$

$$\int_0^L J_{MS,i}dx = -\rho q_{sat,i}D_{MS,i}(0)\int_{\theta_F}^{\theta_P}d\theta_{i,j}, \tag{6.28}$$

$$J_{MS,i}L = \rho q_{sat,i}D_{MS,i}(0)(\theta_F - \theta_P). \tag{6.29}$$

Finally, as in model (*1*), the fractional occupancy is described via a Langmuir-type isotherm, resulting in a transport equation in the form:

$$J_{MS,i} = \frac{\rho}{L}q_{sat,i}D_{MS,i}(0)\left(\frac{b_iP_{i,F}}{1+b_iP_{i,F}} - \frac{b_iP_{i,P}}{1+b_iP_{i,P}}\right). \tag{6.30}$$

Insertion of Eq. (6.30) in the expression for the ideal selectivity (Eq. (6.17)), combined with the definition of permeance (Eq. (6.18)), yields:

$$\alpha_{A,B}^* = \frac{\Delta P_B}{\Delta P_A}\frac{\frac{\rho}{L}q_{sat,A}D_{MS,A}(0)\left(\frac{b_AP_{A,F}}{1+b_AP_{A,F}} - \frac{b_AP_{A,P}}{1+b_AP_{A,P}}\right)}{\frac{\rho}{L}q_{sat,B}D_{MS,B}(0)\left(\frac{b_BP_{B,F}}{1+b_BP_{B,F}} - \frac{b_BP_{B,P}}{1+b_BP_{B,P}}\right)}. \tag{6.31}$$

Making the same arrangements as for model (*1*) and namely that component *A* is the stronger adsorbed component in respect to component *B* and that *ΔP*$_i$ is equal for *i* = *A* and *i* = *B*, the model assuming that *D*$_{MS}$ are loading dependent takes the form:

$$\alpha_{A,B}^* = \frac{D_{MS,A}(0)}{D_{MS,B}(0)}\frac{q_{sat,A}}{q_{sat,A}}\frac{\left(\frac{b_AP_{A,F}}{1+b_AP_{A,F}} - \frac{b_AP_{A,P}}{1+b_AP_{A,P}}\right)}{\left(\frac{b_BP_{B,F}}{1+b_BP_{B,F}} - \frac{b_BP_{B,P}}{1+b_BP_{B,P}}\right)}. \tag{6.32}$$

The work equation (6.32) is named here model (*2*) and just as model (*1*), it can be divided into two parts, corresponding to the two factors that dictate the permselectivity of a given porous material towards gases A and B. The ratio of the diffusivities expresses the diffusion behaviours, while the ratio of the saturation limits together with the term that incorporates equilibrium constants provides description of the adsorption selectivity. Thus, each of the contributions to the permeability can be separately manipulated. This doctorate work focuses on the adsorption separation factor.

The temperature dependence of the selectivity is taken into account in both models via the temperature dependent equilibrium constants. The dependence of the Langmuir parameters on the temperature is described via the Van't Hoff equation:

$$\frac{dlnb_i}{d\frac{1}{T}} = \frac{Q_{Ads,i}}{R}, \tag{6.33}$$

where $Q_{Ads,i}$ is the heat of adsorption.

It is worth noting that the hereto-derived models are based on assumptions that are appropriate for limited systems, i.e. for sorbate-sorbent systems, where surface diffusion occurs. For zeolites and MOFs with larger ratios between pore and molecule size, gas translational diffusion mechanism dominates the mass transport through the membrane material. In this case, the activated Knudsen model is considered to be more suitable to predict the ideal separation factor towards light gases. This model describes the GT flux of a component in respect of its molecular weight (M_i) and the activation energy for diffusion ($E_{D,i}$). The flux of a single-component is described by [47]:

$$J_{GT,i} = \frac{\lambda_i}{z}\sqrt{\frac{8RT}{\pi M_i}}e^{-\frac{E_{D,i}}{RT}}\frac{dp_{i,j}}{dx}, \tag{6.34}$$

where λ_i is the diffusional (jump) length and it is often related to the distance between adjacent adsorption sites [1]. The factor z is called probability factor and it's inverse in Eq. (6.34) ensures that only those molecules moving in the direction under consideration, x, contribute to the diffusive flow. Integration across a membrane of thickness L is performed as follows:

$$\int_0^L J_{GT,i}dx = \frac{\lambda_i}{z}\sqrt{\frac{8RT}{\pi M_i}}e^{-\frac{E_{D,i}}{RT}}\int_{P_F}^{P_P} dp_{i,j}, \tag{6.35}$$

$$J_{GT,i} = \frac{\lambda_i}{zL}\sqrt{\frac{8RT}{\pi M_i}}e^{-\frac{E_{D,i}}{RT}}\left(P_{i,P} - P_{i,F}\right). \tag{6.36}$$

Hence, using Eqs. (6.17) – (6.18) and Eq. (6.36), one can define the ideal separation factor of a zeotype material, in the case of gas translational diffusion:

$$\alpha^*_{A,B} = \frac{\Delta P_B}{\Delta P_A} \frac{\frac{\lambda_A}{zL}\sqrt{\frac{8RT}{\pi M_A}}\, e^{-\frac{E_{D,A}}{RT}}\left(P_{A,P} - P_{A,F}\right)}{\frac{\lambda_B}{zL}\sqrt{\frac{8RT}{\pi M_B}}\, e^{-\frac{E_{D,B}}{RT}}\left(P_{B,P} - P_{B,F}\right)}. \tag{6.37}$$

Realizing that λ_i depends on the crystalline material, consequently $\lambda_A = \lambda_B$, and assuming identical experimental conditions for the fluxes of components A and B, the model is reduced to:

$$\alpha^*_{A,B} = \sqrt{\frac{M_B}{M_A}}\, \frac{e^{-\frac{E_{D,A}}{RT}}}{e^{-\frac{E_{D,B}}{RT}}}. \tag{6.38}$$

This model denoted as model (*3*) has just two parameters M_i and $E_{D,i}$. The activation energy, $E_{D,i}$, is given by the difference between the potential energy of a molecule that resides on the pore walls and one that is desorbed from the internal surface into the gaseous phase in the pore system. This energy is function of the molecular and pore diameters. Considering a given porous material, $E_{D,i}$ increases with increasing molecular size [2]. However, this simple model (*3*) has an obvious downside, which is the lack of explicit correlation to other operation conditions than the exponential dependence on temperature.

In Table 9, a list of light gases is given, with their kinetic diameters and effective lengths in Angstroms and the molecular weights in g mol^{-1}. The values are taken from the literature. However, these values vary in different references and rather should be taken as orientation.

Table 9: Kinetic diameter, effective length and molecular weight of some light gases.

Gas	d_m [Å]	f_m [Å]	MW [g mol^{-1}]
Helium (He)	2.28 [41]	2.28 [41]	4
Argon (Ar)	3.42 [41]	3.42 [41]	39.94
Hydrogen (H_2)	2.8 [41]	2.8 [41]	2.02
Oxygen (O_2)	3.03 [41]	4.29 [41]	32
Nitrogen (N_2)	3.32 [41]	4.42 [41]	28.02
Carbon oxide (CO)	3.03 [41]	4.02 [41]	28.01
Carbon dioxide (CO_2)	3.03 [41]	5.35 [41]	44.10
Methane (CH_4) †	3.72 [41]; 3.99 [48];	3.72 [41]; 3.99 [48]	16.04

†The underlined dimension is used as a reference for the values reported in Table 10.

The molecular diameters listed in Table 9 were used to calculate approximate values for the ratio (δ) of the pore size of selected crystalline porous materials to the molecular size of the corresponding gases. Here again, the pore diameter of the zeolites and ZIF-8 metal organic framework can vary in different information sources. The δ values are shown in Table 10, where red colour is used to mark the factor δ when it is less than 1.0. This value indicates strong repulsion potential of the molecule from the pore. Values between 1.0 and 1.24 are marked in green and correspond to surface diffusion mechanism (described by the Maxwell-Stefan formulation). Lastly values in the interval 1.25 and 3.0 are indicated in blue and for these gas-zeolite pairs gas translational diffusion is considered to be the valid transport mechanism.

Table 10: Ratios of the pore size of some crystalline porous material to the molecular diameters of various gases: red color – $\delta < 1$; green color – δ = 1-1.24 (MS); blue color – δ = 1.25-3.0 (GT).

Material	d_p [Å]	$\delta = d_p/d_m$							
		He	**Ar**	**H_2**	**O_2**	**N_2**	**CO**	**CO_2**	**CH_4**
SOD	2.8 [49]	1.23	0.82	1	0.92	0.84	0.92	0.92	0.75
CHA	3.8 [49]	1.67	1.11	1.36	1.25	1.14	1.25	1.25	1.02
LTA	4.1 [8]	1.79	1.20	1.46	1.35	1.23	1.35	1.35	1.10
DDR	4.4 [49]	1.93	1.29	1.57	1.45	1.33	1.45	1.45	1.18
MFI, ZSM-5	5.6 [49]	2.46	1.64	2	1.85	1.69	1.85	1.85	1.51
FAU	7.4 [49]	3.25	2.16	2.64	2.44	2.23	2.44	2.44	1.99
ZIF-8	3.4 [37]	1.49	0.99	1.21	1.12	1.02	1.12	1.12	0.91

These values indicate that, if the classification given by Burggraaf [2] is considered, many gas separations should be modeled using the simple model *(3)*. Nevertheless, a look at the literature shows that equations based on the Maxwell-Stefan formulation are widely used to describe the transport properties of gas-zeolite systems with $\delta \geq 1.24$. An example is the application of Maxwell-Stefan equations for description of multicomponent permeation of light gases across MFI membranes [5,50,51]. The transport of gaseous molecules trough MFI can be described as a combination of surface and GT diffusion, where the contribution of the latter is important for elevated temperatures [47]. In fact, the transition between surface diffusion based permeation and gas translational mechanism is not sharp. According to Xiao and Wei [1] it depends on zeotype, molecular shape and temperature. In the presence of extra-framework cations, as in the case of LTA and FAU zeolites, predominant mechanism is surface diffusion, due to the strong attractive field of these cations that acts on the gas molecules.

Moreover, as briefly mentioned in Section 5.2, separation of gases in porous media is affected by three factors [25]:

- Size or steric exclusion, where large molecules cannot enter the pores;
- Thermodynamic selectivity, where some components are preferentially adsorbed over others;
- Kinetic selectivity, where certain molecules enter and diffuse through the pores faster than others.

Thus, giving too much importance to the geometrical factor alone is a naïve concept.

6.2 Model parameters

The models (*1*) and (*2*) for evaluation of the ideal selectivity of crystalline porous materials, as derived in section 6.1, employ single-component parameters: saturation limit, Langmuir coefficient, isosteric heat of adsorption and Maxwell-Stefan single-component diffusivity. Moreover, they correlate the separation factor with the operation conditions such as pressure and temperature. The aforementioned model parameters can be obtained as experimentally as well as by using computational methods, e.g. molecular dynamics or quantum mechanics calculations. Evaluation of the parameters is beyond the scope of this thesis. Thus, in order to implement the developed models, we used values for these parameters mainly from the literature.

Nonetheless, it is worth noting that in many cases the three model parameters describing the adsorption of gases in crystalline solids can be obtained from adsorption isotherms, which in turn can be measured experimentally (e.g. via volumetric or gravimetric methods) or computed (via Grand Canonical Monte Carlo simulations for example). Specifically, the saturation limit q_{sat} can be approximated from the plateau of the Langmuir isotherm. The Langmuir constant b_i can be evaluated using the relationship:

$$b_i = \frac{K_H}{q_{sat}}, \tag{6.39}$$

where K_H is the Henry constant and q_{sat} is the saturation limit.

Lastly, the isosteric heat of adsorption, i.e. the molar enthalpy of adsorption at fixed surface coverage, can be determined, for the case of zero coverage limit, from isotherms measured at different temperatures, applying the Clausius-Clapeyron equation [52]:

$$Q_{Ads} = R\frac{\partial lnP}{\partial(1/T)}. \tag{6.40}$$

A plot of lnp against $1/T$ gives a straight line with slope of Q_{Ads}/R. Although the obtained Q_{Ads} value is temperature dependent, it is widely accepted that the variation of the enthalpy of adsorption is small enough in a given temperature range, so that the isosteric heat and heat of adsorption are assumed equal [46,52].

In contrast to adsorption, diffusion data is somehow more controversial. Diffusion coefficients can be measured experimentally using macroscopic methods such as chromatography and frequency response method or microscopic techniques such as pulsed-field gradient NMR (PFG-NMR) or quasi-elastic neutron scattering (QUENS) [53]. Some systems show satisfactory agreement between different types of measurement but other systems show large difference between the diffusivity values [54]. The discrepancies are ascribed to the defect structure of real zeolite crystals. An idea about the difficulties associated with evaluation of diffusion coefficients can be obtained having a look at the titles of articles on the topic, such as "Measurement of Diffusion in Zeolites – A Never Ending Challenge?" by J. Kärger (2003) [55], and "Diffusion in zeolites – a continuing saga" by D.M. Ruthven (2010) [54]. Diffusivities can be also computed using molecular dynamics simulations but again the results differ in respect to the adopted force field and the utilized approach (equilibrium or non-equilibrium MD, assumption of flexible or rigid framework etc.).

Here, we firstly explored the N_2/O_2 adsorption selectivity of LTA zeolite. The separation process is governed by the interactions of the gas molecules with the exchangeable cations that are part of the zeolite framework [23]. Preferential adsorption of nitrogen over oxygen is due to the stronger quadrupolar moment of N_2 ($1.52 \cdot 10^{26}$ esu[‡] cm^2, in comparison with this of O_2, being $0.39 \cdot 10^{26}$ esu cm^2 [25]), which interact with the electric field gradient, associated with the cations. Therefore, the number, charge density and accessibility of the extra-framework cations are important factors for the selectivity of the material. This fact led to many research studies that are focused on altering the separation properties of Linde type A zeolite by ion exchange. On the other hand, N_2 molecules are slightly larger, which is leading to kinetic selectivity in favor of O_2 [56]. G.V. Baron et al. (1993) studied adsorption equilibria of light gases on LTA zeolite [57]. In this work, Henry constants (K_H), heats of adsorption and micropore diffusivities on dehydrated samples of NaA and CaA were determined by a chromatographic method. G. De Luca et al. (2002) also report the adsorption properties of CaA towards oxygen and nitrogen, obtained by means of Density Functional Theory calculations [52]. Since saturation loadings were not reported in neither of these studies, and converting Henry's constants to Langmuir parameters requires the q_{sat}, the values should be treated with caution. We exploited the provided adsorption data for N_2 and O_2 in these two works, transforming the equilibrium constant via saturation loadings from the literature. In reference [25] the oxygen and nitrogen saturation capacities on LTA are reported equal to 1.41 mol/kg for both gases. This value corresponds to full occupation of all adsorption sites available in the framework. The identical saturation capacities of these two gases on the target material have been confirmed

---

[‡] electrostatic unit of charge

by P.M. Mathias et al. [58]. The sorption parameters used for evaluation of α^{*}_{Ads} of NaA via models *(1)* and *(2)* are shown in Table 11, while these concerning CaA are summarized in Table 12.

Table 11: Model parameters for N_2 and O_2 on NaA zeolite at 298 K.

Zeolite	Gas	q_{sat} [25] [mol kg^{-1}]	K_H [10^{-6} mol kg^{-1} Pa^{-1}]	b_i [10^{-3} kPa^{-1}]	Q_{Ads} [kJ mol^{-1}]
NaA [57]	N_2	1.41	2.53	1.79	18.1
	O_2	1.41	0.82	0.58	12.5

Table 12: Model parameters for N_2 and O_2 on CaA zeolite at 298 K.

Zeolite	Gas	q_{sat} [25] [mol kg^{-1}]	K_H [10^{-6} mol kg^{-1} Pa^{-1}]	b_i [10^{-3} kPa^{-1}]	Q_{Ads} [kJ mol^{-1}]
CaA [52]	N_2	1.41	10.4	7.38	30.54
	O_2	1.41	1.7	1.21	18.83
CaA [57]	N_2	1.41	9.24	6.55	28.0
	O_2	1.41	1.57	1.11	20.8

Furthermore, the micropore self-diffusivities at 298 K, reported by G.V. Baron et al., were used to analyze the effect of the diffusivity on the permselectivity. The values are $0.014 \cdot 10^{-12}$ m^2/s for N_2 and $0.24 \cdot 10^{-12}$ m^2/s for O_2 in NaA, and $1.5 \cdot 10^{-12}$ m^2/s for N_2 and $5.0 \cdot 10^{-12}$ m^2/s for O_2 in CaA.

Further, since in recent years metal organic frameworks stole the spotlight from zeolites, we tested how the predictive models perform, when used to predict the selectivity of one MOF material (ZIF-8). Henry's constant values and saturation limits for CO_2 and CH_4 were deduced from experimental pure-component adsorption isotherms, given in Figure 13. The equilibrium data fit a type-I isotherm corresponding to Langmuir model, which is in agreement with the assumptions made to obtain the proposed selectivity equations. The isotherms of both gases are considered to be close to saturation. The isosteric heats of adsorption were taken from the literature [59]. The sorption parameters are given in Table 13.

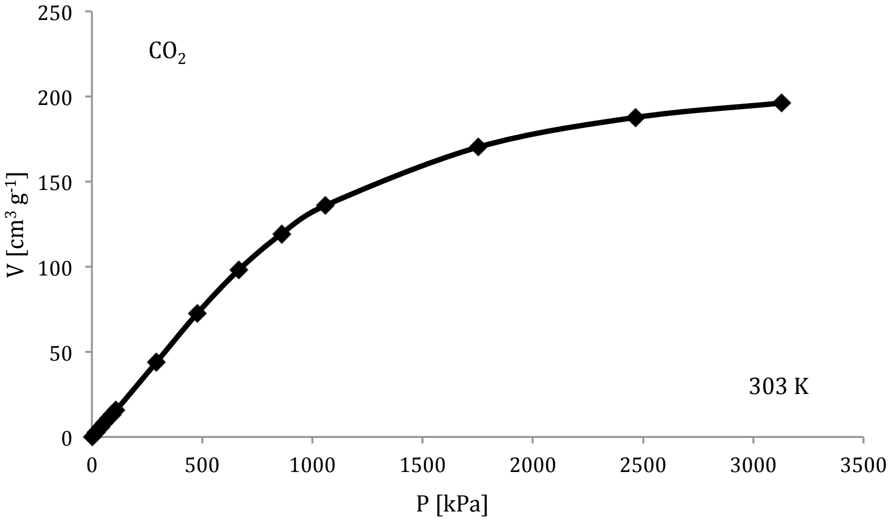

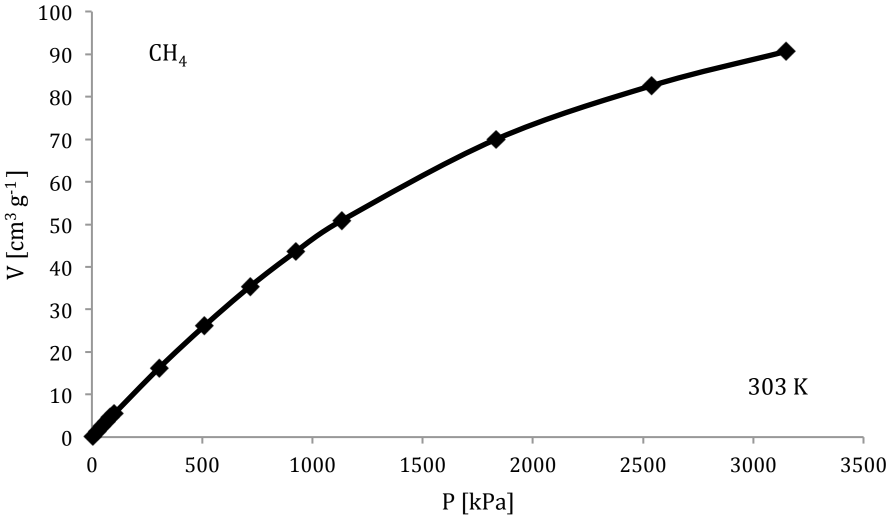

Figure 13: Adsorption isotherms of a) pure CO_2 and b) pure CH_4 on ZIF-8 at 303 K. *Data provided by David Farrusseng (IRCELyon).*

Table 13: Model parameters for CO_2 and CH_4 on ZIF-8 at 303 K.

Material	Gas	q_{sat} [mol kg^{-1}]	K_H [10^{-6} mol kg^{-1} Pa^{-1}]	b_i [10^{-4} kPa^{-1}]	Q_{Ads} [59] [kJ mol^{-1}]
ZIF-8	CO_2	8.76	6.26	7.15	15.93
	CH_4	4.05	2.52	6.22	12.44

6.3 Selectivity measurements

In order to validate the predictive capabilities of the developed models, we evaluated experimentally the ideal selectivity of tubular NaA and ion-exchanged CaA membranes and compared the results with the theoretical values.

Two tubular NaA membranes on porous α-alumina support, provided by the Graduate School of Science and Engineering at Yamaguchi University (Japan), were tested. The preparation of the original 4A membranes by hydrothermal synthesis is described in reference [60]. Further CaA zeolite membranes were modified by ion exchange of the NaA membranes. In order to establish the conditions for ion exchange, we preliminary tested the procedure using 4A zeolite powder. The initial $CaCl_2$ solution and the mother liquor after ion exchange were analysed by EDTA titration. The NaA and CaA powder samples were characterized by X-ray diffraction (XRD) to confirm that the crystal structure corresponds to LTA zeolite. Moreover, termogravimetric analysis (TGA) was carried out for each of the Linde A types (NaA and CaA) in order to monitor the mass loss due to water removal as function of temperature and to establish a proper pre-treatment procedure for the membranes prior permeation testing. The ion exchange test procedure, the titration experiment, the XRD patterns and the TGA curves can be found in Appendix B. The results from the ion exchange test showed that 68 % ion exchange was achieved. Thus, adapting the same procedure, each 4A membrane was immersed in 0.25 M aqueous solution of $CaCl_2$ at 50 °C for 3 hours, then thoroughly washed with distilled water and dried at 100 °C.

The single gas permeations of nitrogen and oxygen through the NaA and the CaA membranes were measured to determine the ideal N_2/O_2 selectivity. Preliminary the testing membrane was outgassed under vacuum at 200 °C overnight to remove any adsorbed impurities. Temperatures over 200 °C were not applied due to the different thermal expansion of the support and the zeolite layer, which can cause a membrane failure in terms of pore collapsing and cracks. For the permeation experiments the membrane was sealed with O-rings in a stainless-steel module and the module was placed in a gas chromatographic oven. The experimental setup is illustrated in Figure 14. Pre-treatment and activation of the membrane were carried out with He flow at 130 °C between 4 and 8 hours prior new experimental series. Regeneration between gas changes was operated by simultaneous purging with He stream and heating at 130 °C for at least 2 hours. The permeation experiments were conducted at 35 °C. The testing gas was fed to the outer-surface (zeolite layer side) of the membrane at 50 cm^3(STP)/min. Counter-current argon sweep gas stream of 80 cm^3(STP)/min was employed to maintain a total pressure drop of 10.5 kPa. The permeate composition was analysed using MicroGC Agilent 3000A gas chromatograph. Equilibration of the single-component permeation through the tested membranes took up to 15 hours.

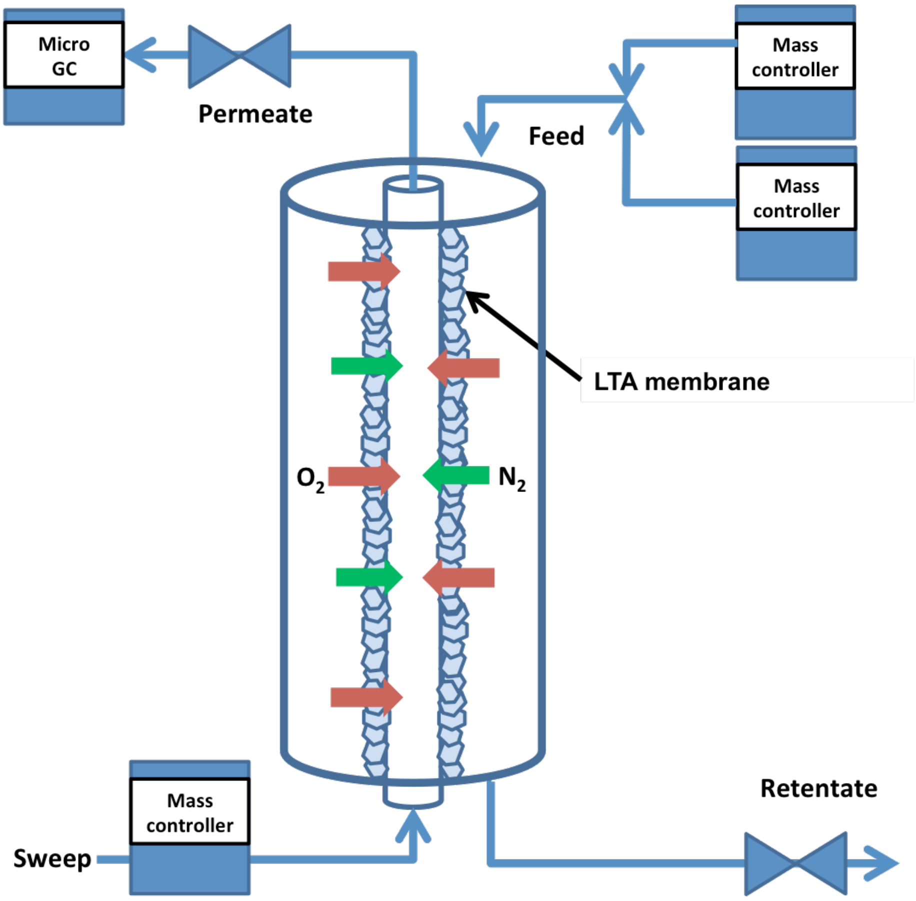

Figure 14: Schematic illustration of the equipment used for single-gas permeance measurements of LTA membranes. *Illustration courtesy of Fernando Cacho*.

Permeance values were calculated in mol m^{-2} s^{-1} Pa^{-1} according the following equation:

$$\Pi_i = \frac{q_{P,i}}{S\Delta P_{i,MLOG}}, \tag{6.41}$$

where the logarithmic mean partial pressure is defined as:

$$\Delta P_{i,MLOG} = \frac{P_{i,R} - (P_{i,R} - P_{i,P}x_{i,P})}{ln\left(\frac{P_R}{P_{R-}P_{i,P}x_{i,P}}\right)}. \tag{6.42}$$

The N_2 and O_2 permeance curves obtained with the two NaA membranes and their ion-exchanged equivalents are shown in Figure 15 to Figure 18. Ideal selectivities were calculated as the ratio of the equilibrated permeance values.

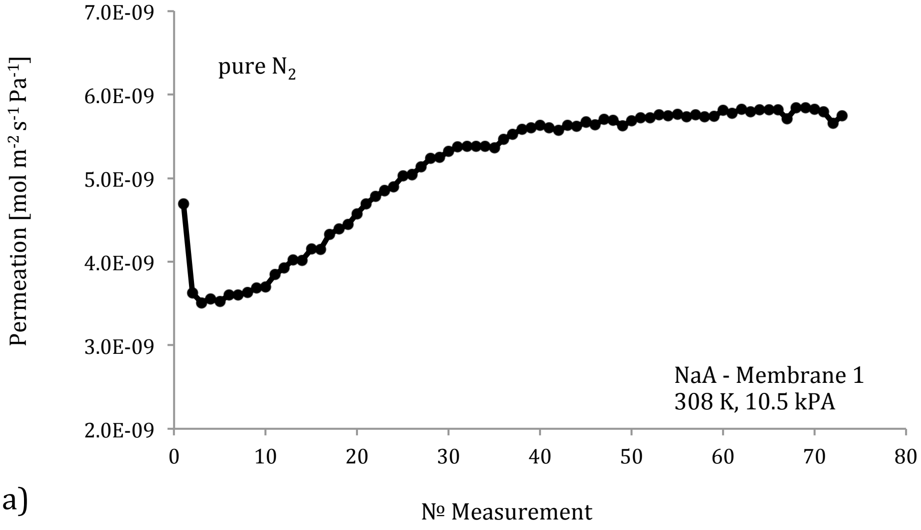

a)

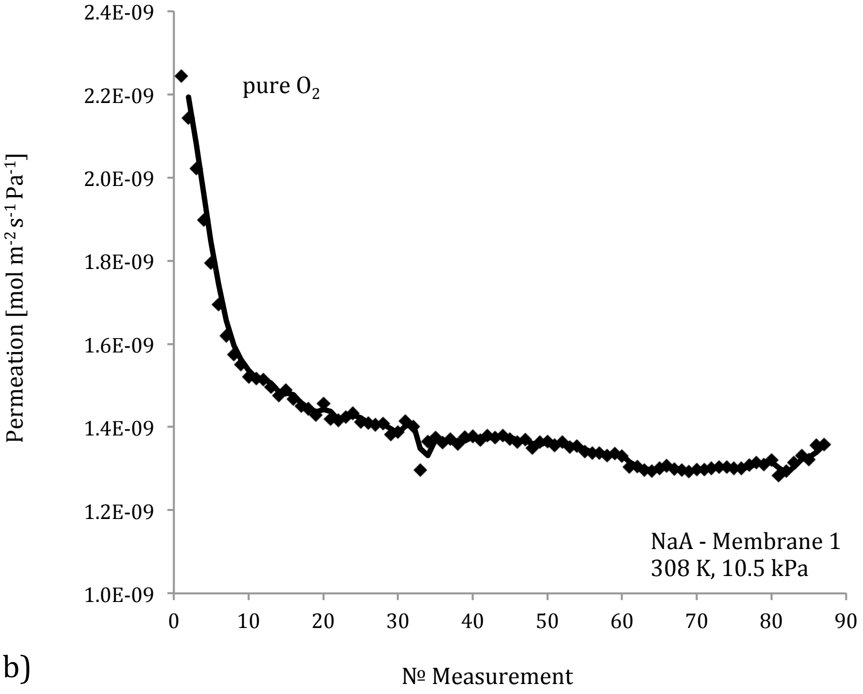

b)

Figure 15: Single gas permeances of a) N_2 and b) O_2 through NaA – Membrane 1 at 308 K and 10.5 kPa pressure drop. The x-axis corresponds to the GC measurements of the permeate composition that were recorded over time with steps between 4 min to 15 min.

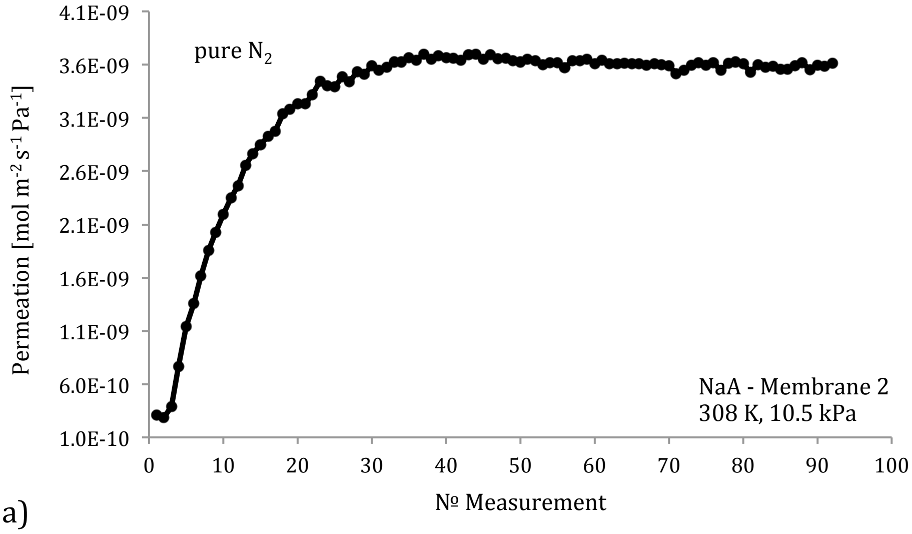

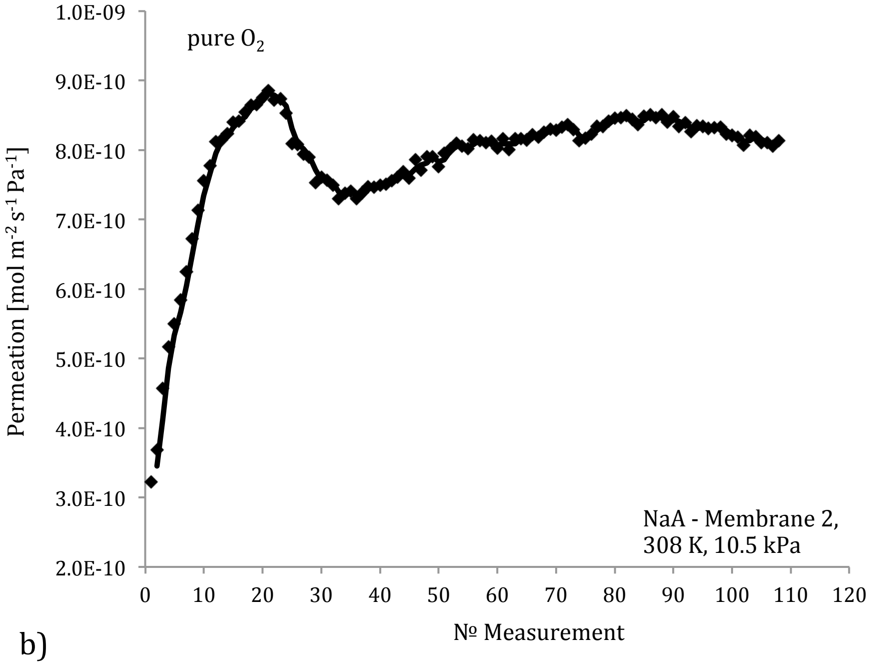

Figure 16: Single gas permeances of a) N_2 and b) O_2 through NaA – Membrane 2 at 308 K and 10.5 kPa pressure drop. The x-axis corresponds to the GC measurements of the permeate composition that were recorded over time with steps between 4 min to 15 min.

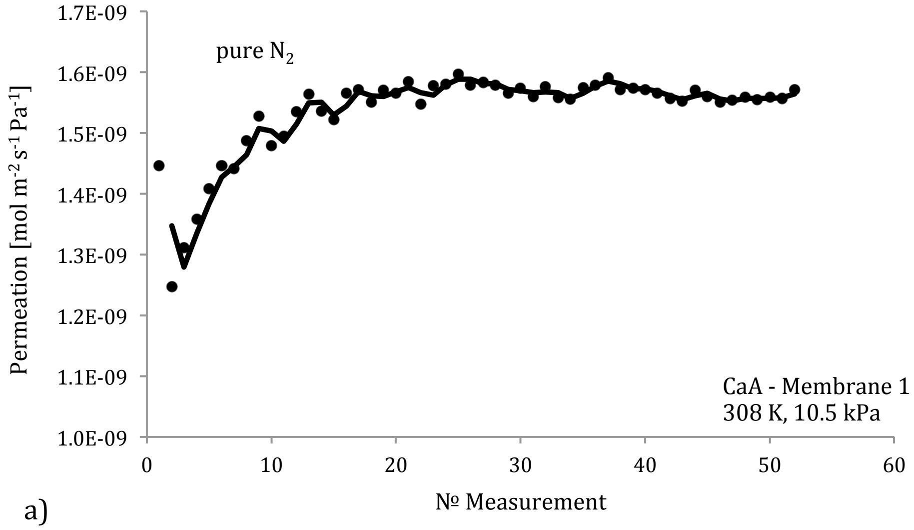

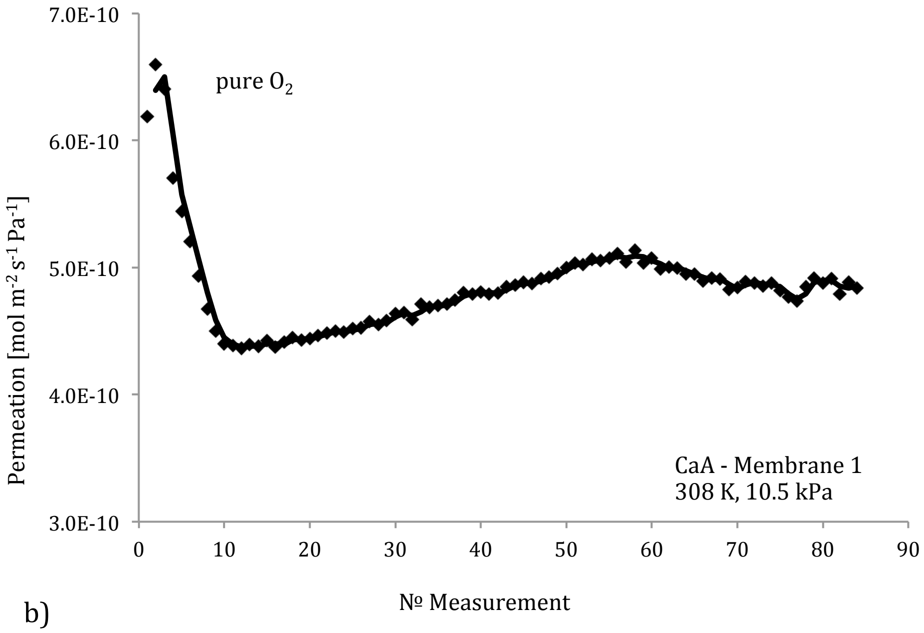

Figure 17: Single gas permeances of a) N_2 and b) O_2 through CaA – Membrane 1 at 308 K and 10.5 kPa pressure drop. The x-axis corresponds to the GC measurements of the permeate composition that were recorded over time with steps between 4 min to 15 min.

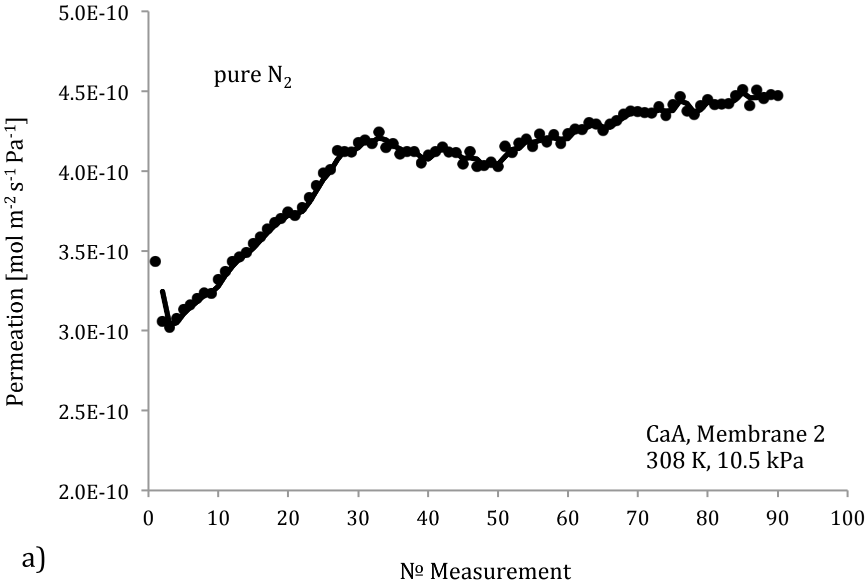

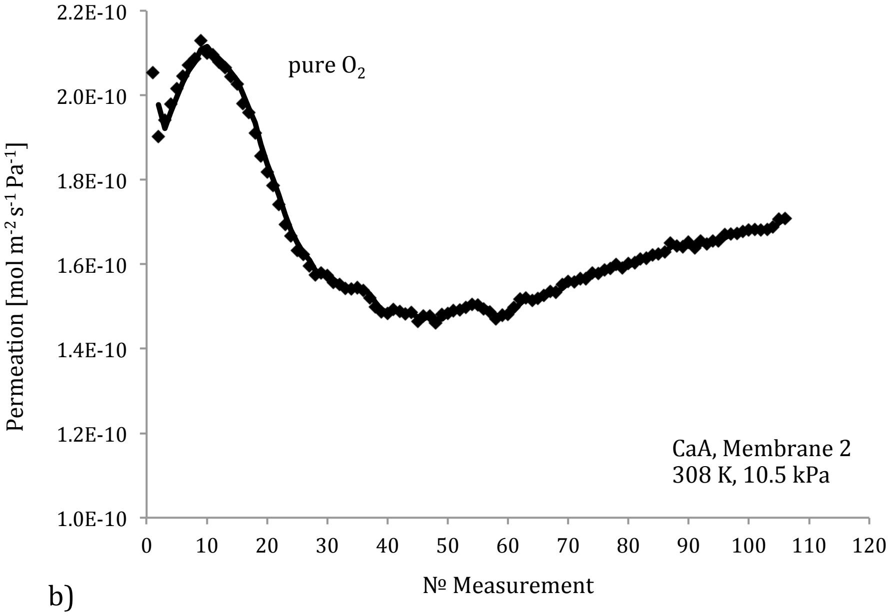

Figure 18: Single gas permeances of a) N_2 and b) O_2 through CaA – Membrane 2 at 308 K and 10.5 kPa pressure drop. The x-axis corresponds to the GC measurements of the permeate composition that were recorded over time with steps between 4 min to 15 min.

Further, experimental ideal selectivities of infiltrated ZIF-8 membranes were evaluated from the single-gas permeances. In the utilized membranes, the ZIF-8 material is fully confined within the macropores of the ceramic tubular support. The preparation and characterization of the synthetized membranes is reported in reference [62]. The single-gas permeances were measured by a bubble flowmeter connected to the atmosphere. Regeneration treatment in vacuum was carried out for 30 min when changing the testing gases. The experiments were conducted at three different temperatures (20 °C, 47 °C and 77 °C) and transmembrane pressure in the range 50-200 kPa (Figure 19 – Figure 21).

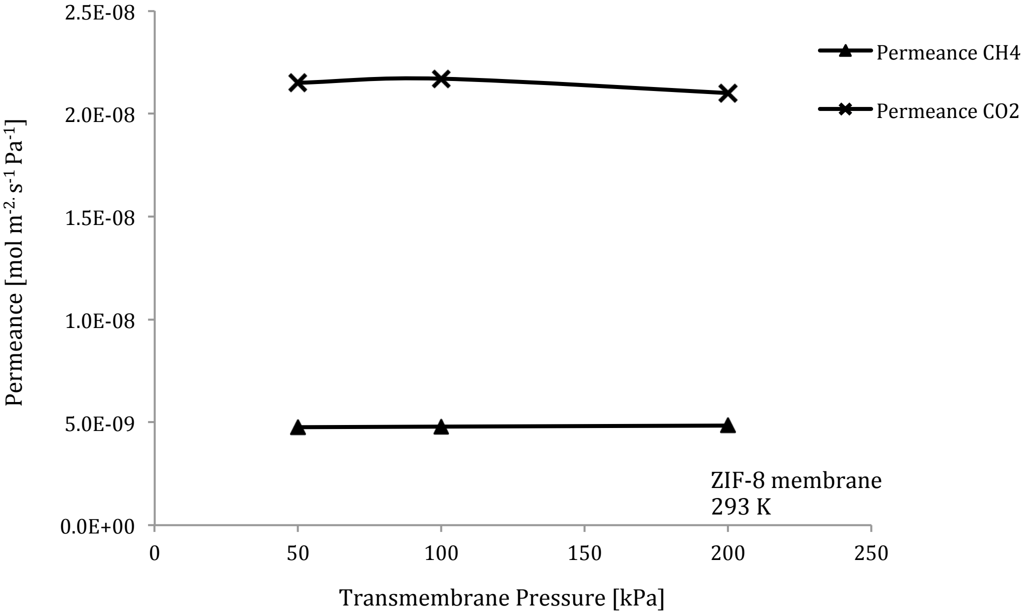

Figure 19: Permeance of pure CH_4 and pure CO_2 through ZIF-8 confined membrane at 293 K and pressure drop in the range 50 – 200 kPa.

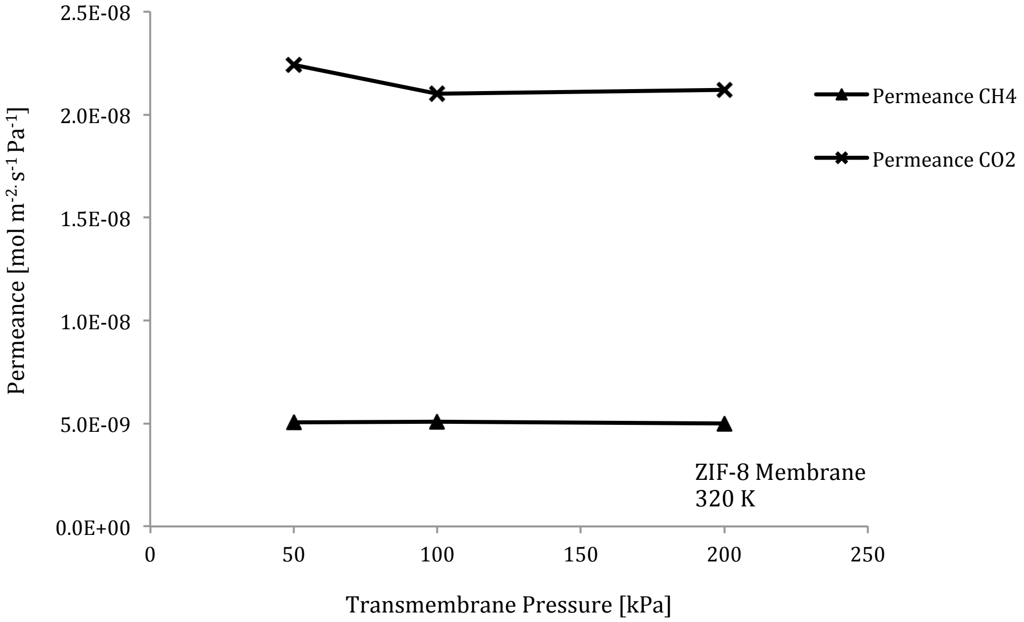

Figure 20: Permeance of pure CH_4 and pure CO_2 through ZIF-8 confined membrane at 320 K and pressure drop in the range 50 – 200 kPa.

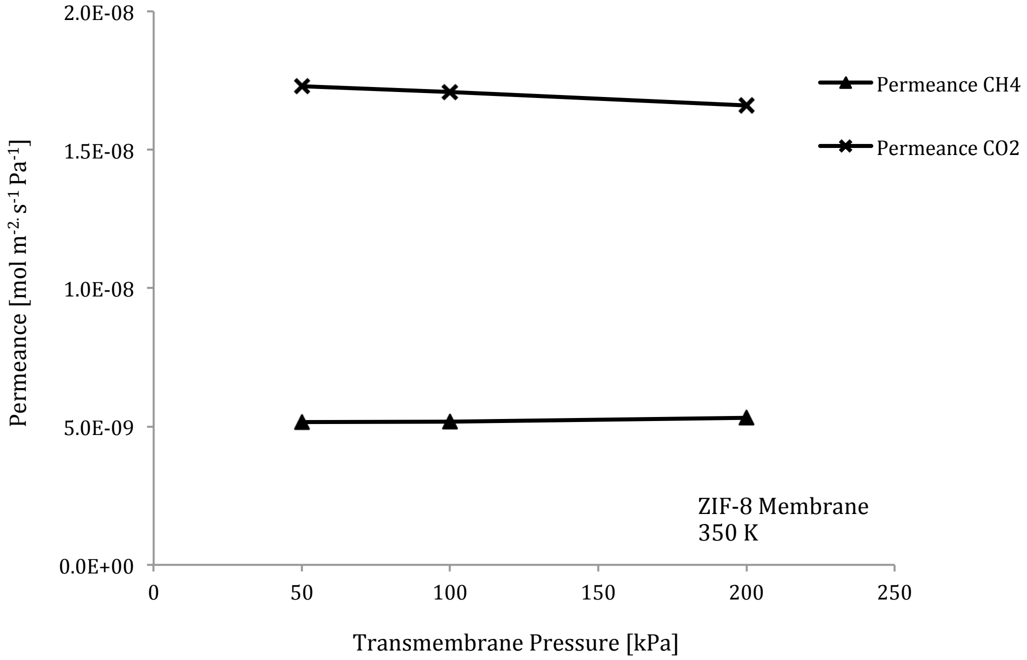

Figure 21: Permeance of pure CH_4 and pure CO_2 through ZIF-8 confined membrane at 350 K and pressure drop in the range 50 – 200 kPa.

7 Results and discussion

The N_2/O_2 selectivity of NaA zeolite as function of temperature was predicted according models (*1*) and (*2*), using the equilibrium data reported in [57] (see Table 11), as shown in Figure 22. The pressure drop, chosen to implement the model is 10.5 kPa with 134.5 kPa feed pressure and 124.0 kPa permeate pressure. The adsorption selectivity, evaluated via the model that assumes diffusivity independence on the loading, decreases continuously with increasing temperature. On the other hand, the model derived under the assumption that $D_{MS}(\theta) = D_{MS}(0)(1 - \theta)$, predicts a maximum of the curve α^*_{Ads} versus T. Moreover, the former model forecasts higher values of α^*_{Ads} in respect to the latter model.

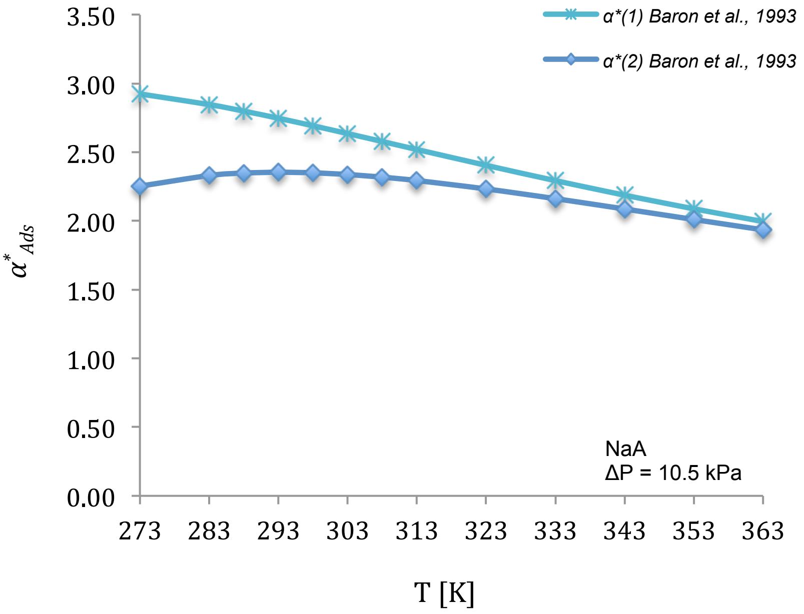

Figure 22: Adsorption selectivity of NaA modelled as function of temperature at ΔP = 10.5 kPa. $\alpha^*(1)$ and $\alpha^*(2)$ stand for the values obtained by model (*1*) and (*2*) respectively.

Furthermore, the adsorption selectivity of NaA for N_2 over O_2 was predicted as function of feed pressure, permeate pressure and temperature, using models (*1*) and (*2*). The results, obtained by variation of the feed pressure in the interval 124.5-194.5 kPa and constant permeate pressure (P_P = 124 kPa), are given in Figure 23, Table 14 and Table 15. They indicate that increasing feed pressure and respectively augmenting pressure drop lowers the selectivity. The predicted values for variation of the permeate pressure in the interval 124-194 kPa by constant feed pressure (P_F = 194.5 kPa), are shown in Figure 24, Table 16 and Table 17. In this case, with increasing permeate pressure, the pressure drop diminishes and the selectivity also decreases. The change in the selectivity with variation of the feed and permeate pressures is more strongly pronounced at low temperatures.

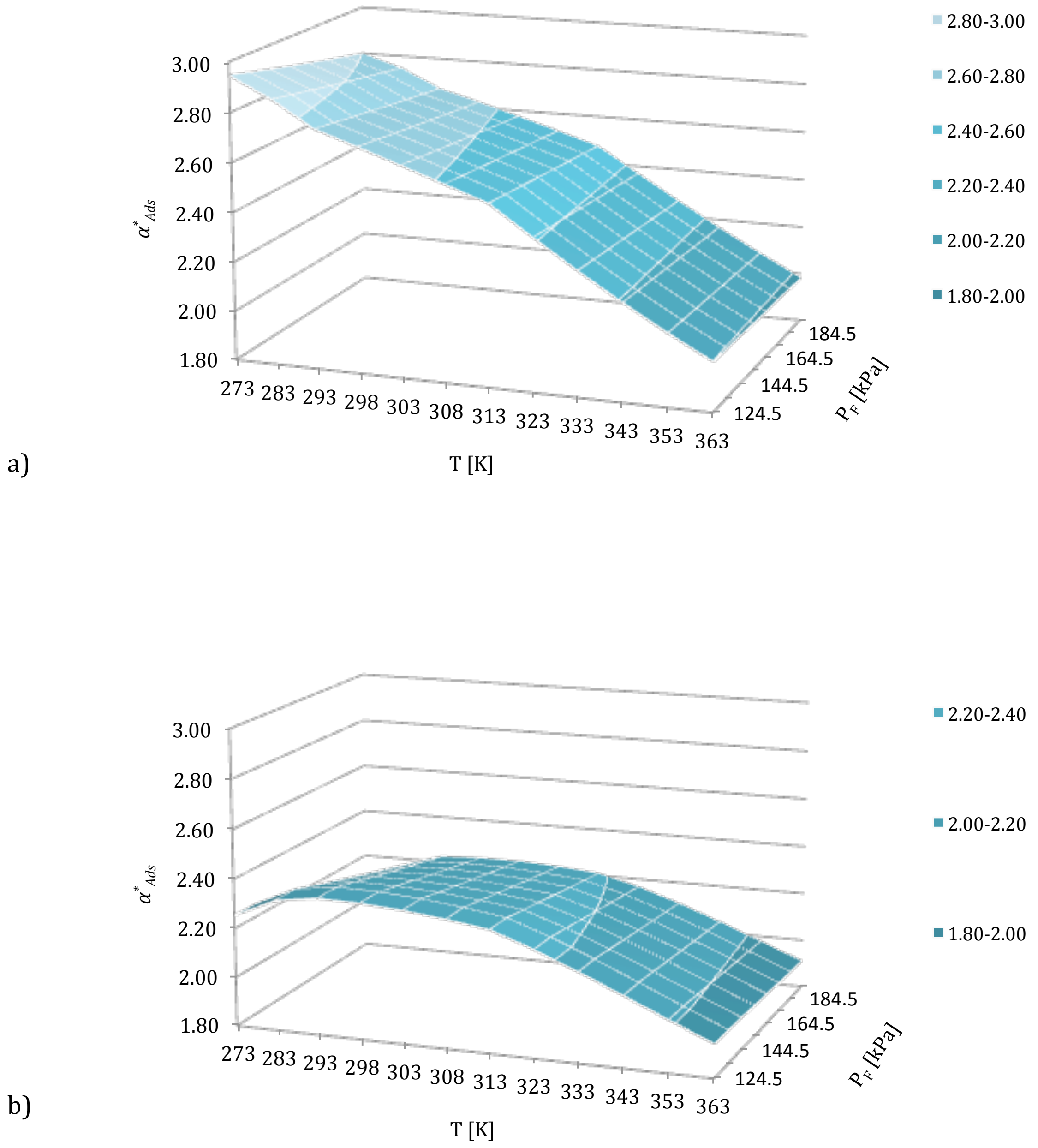

Figure 23: Adsorption selectivity of NaA calculated by a) model (*1*) and b) model (*2*) as function of temperature and pressure. Feed pressure is varied, while permeate pressure is constant (P_P = 124 kPa).

Table 14: Values for the predicted adsorption selectivity of NaA, calculated by model (*1*), as function of temperature and pressure. Feed pressure is varied, while permeate pressure is constant (P_P = 124 kPa).

T [K]	P_F [kPa]							
	124.5	134.5	144.5	154.5	164.5	174.5	184.5	194.5
273	2.95	2.92	2.90	2.88	2.86	2.84	2.82	2.80
283	2.87	2.85	2.83	2.81	2.80	2.78	2.76	2.75
293	2.76	2.75	2.73	2.72	2.71	2.69	2.68	2.67
298	2.71	2.69	2.68	2.67	2.66	2.65	2.63	2.62
303	2.65	2.64	2.63	2.62	2.60	2.59	2.58	2.58
308	2.59	2.58	2.57	2.56	2.55	2.54	2.53	2.52
313	2.53	2.52	2.51	2.50	2.50	2.49	2.48	2.47
323	2.41	2.41	2.40	2.39	2.39	2.38	2.37	2.37
333	2.30	2.29	2.29	2.28	2.28	2.27	2.27	2.27
343	2.19	2.19	2.18	2.18	2.18	2.17	2.17	2.17
353	2.09	2.09	2.09	2.08	2.08	2.08	2.07	2.07
363	2.00	2.00	1.99	1.99	1.99	1.99	1.98	1.98

Table 15: Values for the predicted adsorption selectivity of NaA, calculated by model (*2*), as function of temperature and pressure. Feed pressure is varied, while permeate pressure is constant (P_P = 124 kPa).

T [K]	P_F [kPa]							
	124.5	134.5	144.5	154.5	164.5	174.5	184.5	194.5
273	2.25	2.25	2.22	2.19	2.15	2.12	2.10	2.07
283	2.33	2.33	2.30	2.27	2.25	2.22	2.20	2.17
293	2.35	2.35	2.33	2.31	2.29	2.26	2.24	2.22
298	2.35	2.35	2.33	2.31	2.29	2.27	2.25	2.23
303	2.34	2.34	2.32	2.30	2.28	2.27	2.25	2.23
308	2.32	2.32	2.30	2.29	2.27	2.25	2.24	2.22
313	2.29	2.29	2.28	2.26	2.25	2.24	2.22	2.21
323	2.23	2.23	2.22	2.21	2.20	2.19	2.18	2.17
333	2.16	2.16	2.15	2.14	2.14	2.13	2.12	2.11
343	2.09	2.09	2.08	2.07	2.07	2.06	2.05	2.05
353	2.01	2.01	2.01	2.00	1.99	1.99	1.98	1.98
363	1.94	1.94	1.93	1.93	1.92	1.92	1.91	1.91

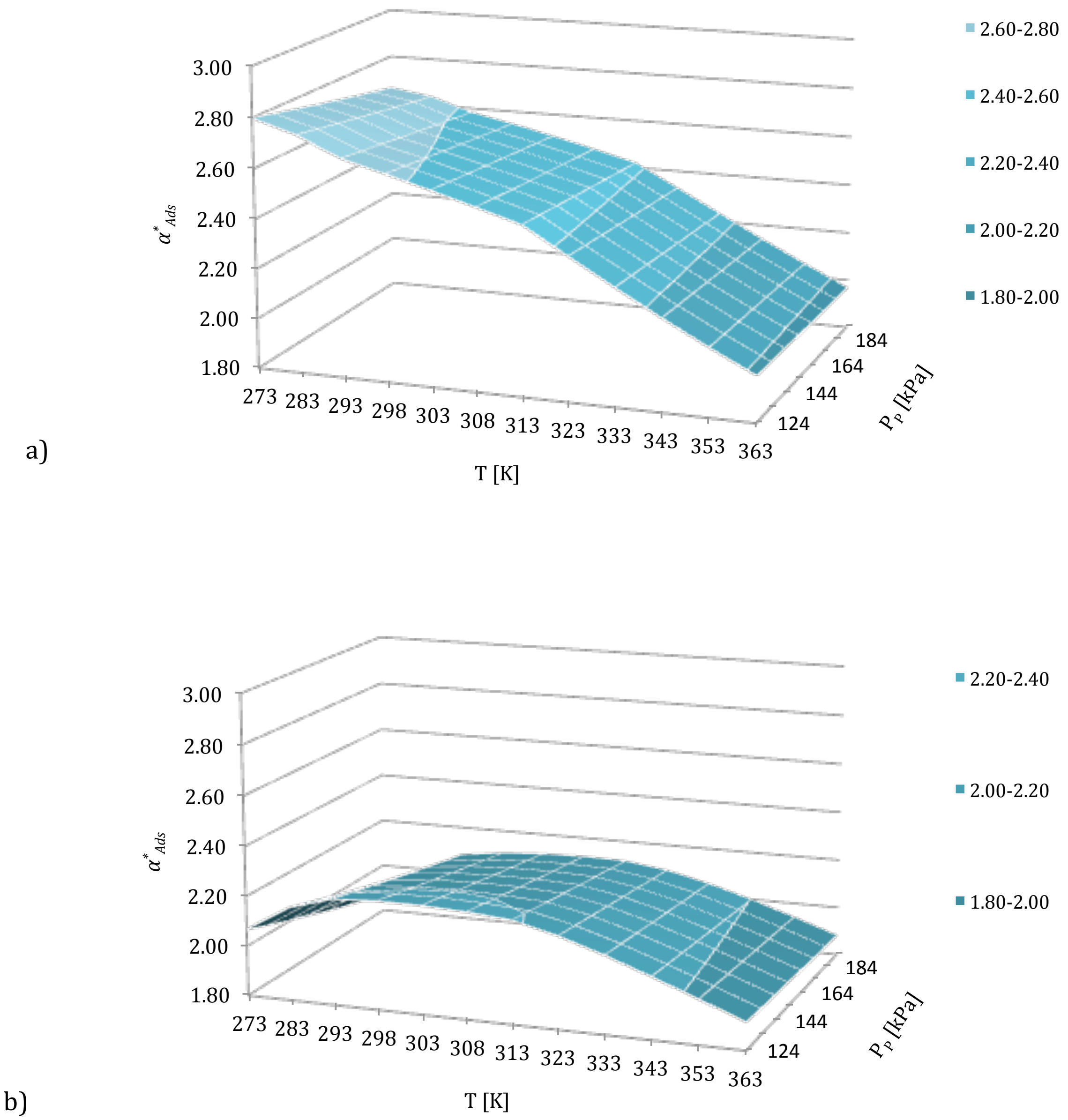

Figure 24: Adsorption selectivity of NaA calculated by a) model (*1*) and b) model (*2*) as function of temperature and pressure. Feed pressure is constant (P_F = 194.5 kPa) and permeate pressure is varied.

Table 16: Values for the predicted adsorption selectivity of NaA, calculated by model (*1*), as function of temperature and pressure. Feed pressure is constant (P_F = 194.5 kPa) and permeate pressure is varied.

T [K]	P_P [kPa]							
	124	134	144	154	164	174	184	194
273	2.80	2.78	2.76	2.74	2.72	2.70	2.68	2.66
283	2.75	2.73	2.71	2.70	2.68	2.67	2.65	2.64
293	2.67	2.66	2.64	2.63	2.62	2.61	2.59	2.58
298	2.62	2.61	2.60	2.59	2.58	2.57	2.56	2.55
303	2.58	2.56	2.55	2.54	2.54	2.53	2.52	2.51
308	2.52	2.52	2.51	2.50	2.49	2.48	2.47	2.46
313	2.47	2.47	2.46	2.45	2.44	2.43	2.43	2.42
323	2.37	2.36	2.36	2.35	2.34	2.34	2.33	2.33
333	2.27	2.26	2.26	2.25	2.25	2.24	2.24	2.23
343	2.17	2.16	2.16	2.16	2.15	2.15	2.14	2.14
353	2.07	2.07	2.07	2.06	2.06	2.06	2.05	2.05
363	1.98	1.98	1.98	1.98	1.97	1.97	1.97	1.97

Table 17: Values for the predicted adsorption selectivity of NaA, calculated by model (*2*), as function of temperature and pressure. Feed pressure is constant (P_F = 194.5 kPa) and permeate pressure is varied.

T [K]	P_P [kPa]							
	124	134	144	154	164	174	184	194
273	2.07	2.04	2.00	1.98	1.95	1.92	1.89	1.87
283	2.17	2.15	2.12	2.09	2.07	2.04	2.02	2.00
293	2.22	2.20	2.18	2.16	2.14	2.12	2.10	2.08
298	2.23	2.21	2.19	2.17	2.15	2.14	2.12	2.10
303	2.23	2.21	2.20	2.18	2.16	2.15	2.13	2.11
308	2.22	2.21	2.19	2.18	2.16	2.15	2.13	2.12
313	2.21	2.20	2.18	2.17	2.15	2.14	2.13	2.12
323	2.17	2.16	2.14	2.13	2.12	2.11	2.10	2.09
333	2.11	2.10	2.09	2.08	2.08	2.07	2.06	2.05
343	2.05	2.04	2.03	2.03	2.02	2.01	2.01	2.00
353	1.98	1.97	1.97	1.96	1.96	1.95	1.95	1.94
363	1.91	1.91	1.90	1.90	1.89	1.89	1.88	1.88

The N_2/O_2 adsorption selectivity of the Ca-form of LTA zeolite has been also predicted. This time the model parameters (summarized in Table 12) were extracted from two independent literature sources – experimental [57] and theoretical study [52]. Initially the pressure difference was kept equal to the value used for NaA simulations (10.5 kPa) and α^*_{Ads} as function of temperature was predicted via models (*1*) and (*2*). The correlation selectivity-versus-temperature is plotted in Figure 25. Here, the maximum of the curve, which was previously observed for NaA according model (*2*), was obtained with both analytical formulae. One explanation for the observed maximum could be the difference in the isosteric heats of adsorption of the two gases. The value of Q_{st} is higher for N_2 in comparison to O_2. This adsorption parameter determines the temperature dependency of the equilibrium constant, b_i. As a consequence the rate of change of b_i with the temperature is different for nitrogen and oxygen.

Another observation that can be drawn from Figure 25 is that the difference between the selectivity values predicted by the two models is quite large at low temperatures and almost vanishes at high temperatures. Moreover, the curves obtained with theoretical (DFT) and experimental model parameters don't coincide. In fact, the values predicted by use of the adsorption parameters reported from the DFT calculations and from the chromatographic study are similar at low temperatures but at high temperatures there are strong deviations. As further matter, the results obtained with model (*2*) and the experimental parameters did show less pronounced maximum.

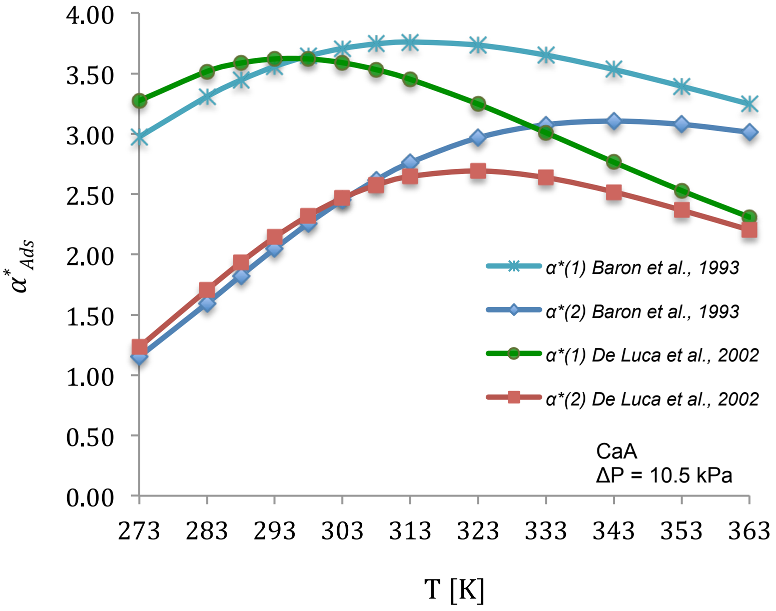

Figure 25: Adsorption selectivity of CaA modelled as function of temperature at ΔP = 10.5 kPa according to adsorption parameters obtained experimentally (Baron et al., 1993 [57]) and theoretically (De Luca et al., 2002 [52]). $\alpha^*(1)$ and $\alpha^*(2)$ stand for the values obtained by model (*1*) and (*2*) respectively.

The N_2/O_2 adsorption selectivity of CaA as function of P_F, P_P and T was predicted via models (*1*) and (*2*) with the model parameters taken from G. De Luca et al (2002). The results, obtained at constant permeate pressure (P_P = 124 kPa) and feed pressure in the interval 124.5-194.5 kPa, are shown in Figure 26. The values obtained with the two models are given also in Table 18 (obtained via model (*1*)) and Table 19 (obtained via model (*2*)). The predicted values for variation of the permeate pressure in the interval 124-194 kPa by constant feed pressure (P_F = 194.5 kPa), are shown in Figure 27, Table 20 and Table 21. The conclusions we draw remain the same as in the case of NaA zeolite and namely that the selectivity dependency on the pressure is more strongly pronounced at low temperatures and negligible at high temperatures. Increasing feed pressure (P_P = const) leads to decrease in the selectivity. For example, at 297 K model (*1*) predicts that the selectivity is decreased from 3.34 at P_F = 124.5 kPa to 2.98 at P_F = 194.5 kPa, while at 363 K the prediction indicates selectivity drop from 2.31 at P_F = 124.5 kPa to 2.29 at P_F = 194.5 kPa. Similar trend is obtained when the permeate pressure is varied. Increasing permeate pressure at constant feed pressure also lowers the selectivity due to the fact that the pressure drop decreases.

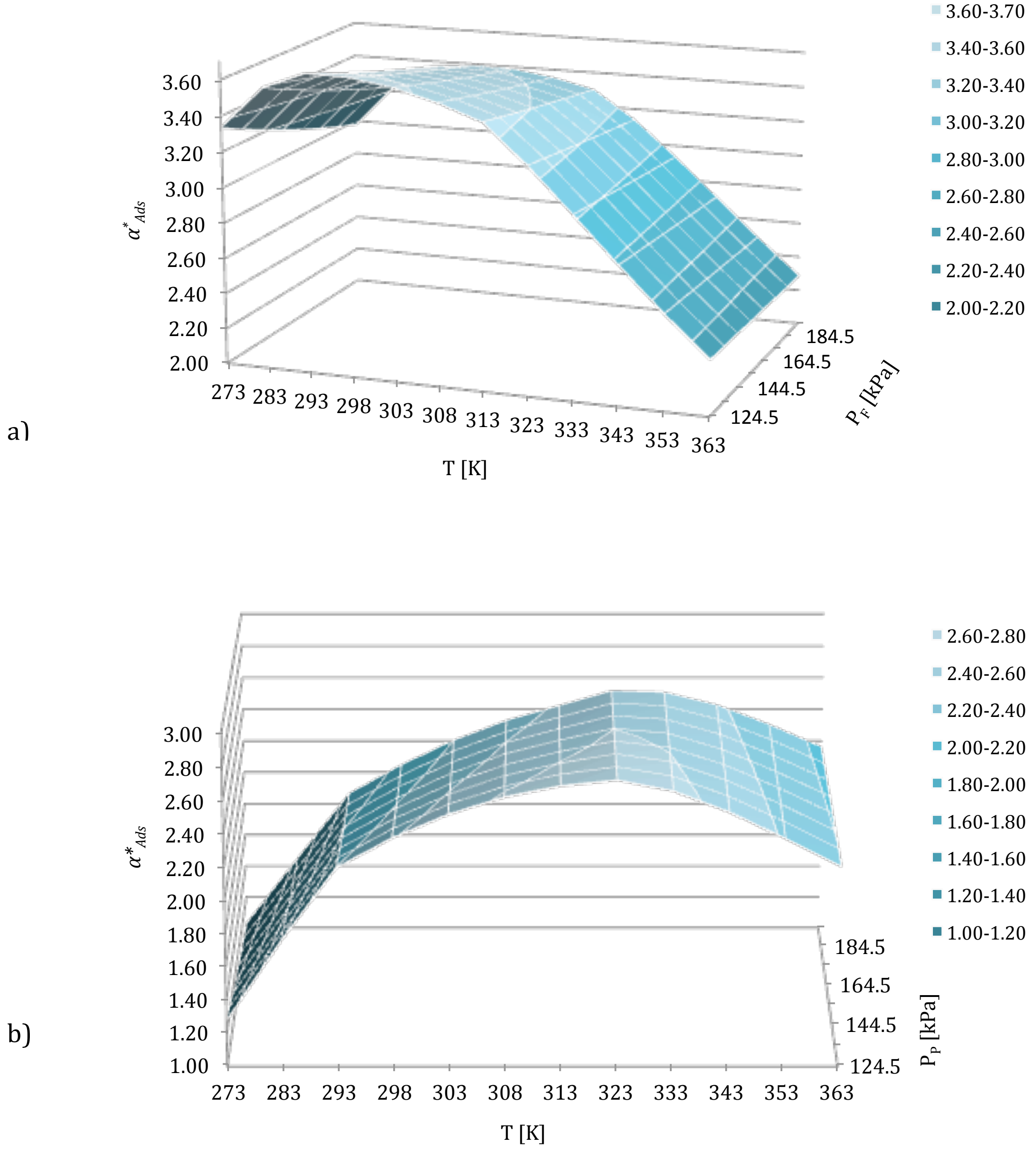

Figure 26: Adsorption selectivity of CaA calculated by a) model (*1*) and b) model (*2*) as function of temperature and pressure. Feed pressure is varied, while permeate pressure is constant (P_P = 124.0 kPa).

Table 18: Values for the predicted adsorption selectivity of CaA, calculated by model (*1*), as function of temperature and pressure. Feed pressure is varied, while permeate pressure is constant (P_P = 124.0 kPa).

T [K]	P_F [kPa]							
	124.5	134.5	144.5	154.5	164.5	174.5	184.5	194.5
273	3.34	3.27	3.22	3.16	3.11	3.06	3.02	2.98
283	3.58	3.52	3.46	3.41	3.36	3.31	3.27	3.23
293	3.67	3.62	3.57	3.53	3.49	3.44	3.41	3.37
298	3.66	3.62	3.58	3.54	3.50	3.46	3.43	3.39
303	3.63	3.59	3.55	3.52	3.48	3.45	3.42	3.38
308	3.56	3.53	3.50	3.47	3.44	3.41	3.38	3.35
313	3.48	3.45	3.42	3.40	3.37	3.35	3.32	3.30
323	3.27	3.25	3.23	3.21	3.19	3.17	3.15	3.14
333	3.02	3.01	3.00	2.98	2.97	2.96	2.94	2.93
343	2.77	2.76	2.76	2.75	2.74	2.73	2.72	2.71
353	2.53	2.53	2.52	2.52	2.51	2.51	2.50	2.49
363	2.31	2.31	2.31	2.30	2.30	2.29	2.29	2.29

Table 19: Values for the predicted adsorption selectivity of CaA, calculated by model (*2*), as function of temperature and pressure. Feed pressure is varied, while permeate pressure is constant (P_P = 124.0 kPa).

T [K]	P_F [kPa]							
	124.5	134.5	144.5	154.5	164.5	174.5	184.5	194.5
273	1.28	1.23	1.19	1.15	1.12	1.08	1.05	1.03
283	1.76	1.71	1.65	1.61	1.56	1.52	1.48	1.45
293	2.20	2.14	2.09	2.04	1.99	1.94	1.90	1.86
298	2.38	2.32	2.27	2.22	2.17	2.13	2.08	2.05
303	2.52	2.47	2.42	2.37	2.32	2.28	2.24	2.20
308	2.62	2.58	2.53	2.48	2.44	2.40	2.36	2.33
313	2.69	2.65	2.60	2.56	2.53	2.49	2.45	2.42
323	2.73	2.69	2.66	2.63	2.60	2.57	2.54	2.51
333	2.66	2.64	2.61	2.59	2.57	2.55	2.53	2.51
343	2.53	2.52	2.50	2.49	2.47	2.46	2.44	2.43
353	2.38	2.37	2.36	2.34	2.33	2.32	2.31	2.30
363	2.21	2.20	2.20	2.19	2.18	2.17	2.17	2.16

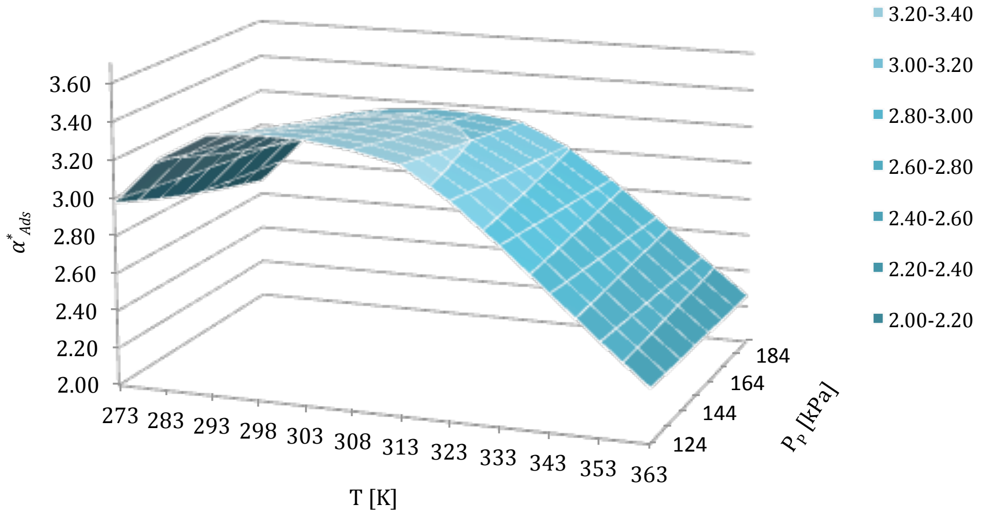

a)

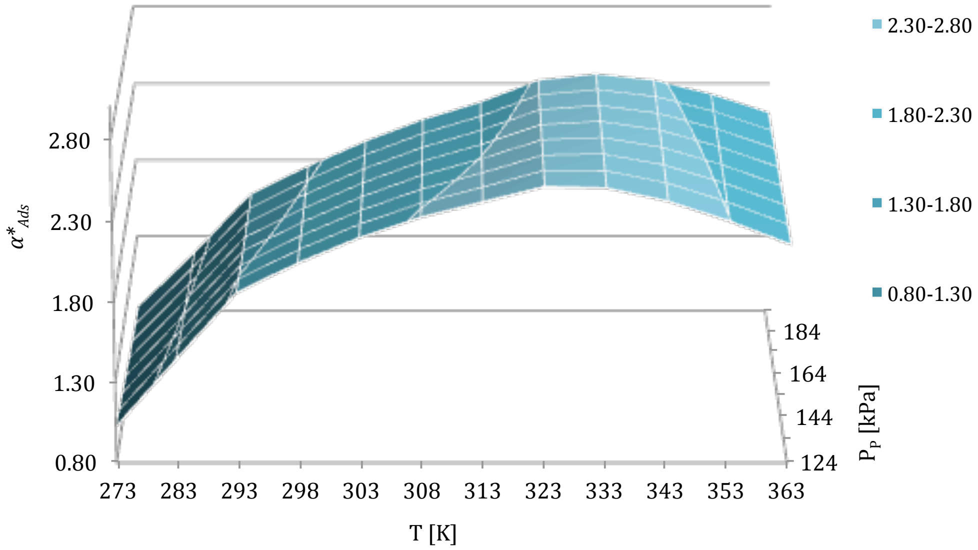

b)

Figure 27: Adsorption selectivity of CaA calculated by a) model (*1*) and b) model (*2*) as function of temperature and pressure. Feed pressure is constant and permeate pressure is varied.

Table 20: Values for the predicted adsorption selectivity of CaA, calculated by model (*1*), as function of temperature and pressure. Feed pressure is constant (P_F = 194.5 kPa) and permeate pressure is varied.

T [K]	P_P [kPa]							
	124	134	144	154	164	174	184	194
273	2.98	2.93	2.88	2.83	2.79	2.75	2.71	2.68
283	3.23	3.18	3.13	3.09	3.05	3.01	2.97	2.93
293	3.37	3.32	3.28	3.24	3.21	3.17	3.14	3.10
298	3.39	3.35	3.31	3.28	3.24	3.21	3.18	3.15
303	3.38	3.35	3.32	3.28	3.25	3.22	3.19	3.17
308	3.35	3.32	3.29	3.26	3.24	3.21	3.18	3.16
313	3.30	3.27	3.25	3.22	3.20	3.17	3.15	3.13
323	3.14	3.12	3.10	3.08	3.06	3.05	3.03	3.01
333	2.93	2.92	2.91	2.89	2.88	2.87	2.86	2.85
343	2.71	2.70	2.70	2.69	2.68	2.67	2.66	2.65
353	2.49	2.49	2.48	2.48	2.47	2.47	2.46	2.45
363	2.29	2.28	2.28	2.27	2.27	2.27	2.26	2.26

Table 21: Values for the predicted adsorption selectivity of CaA, calculated by model (*2*), as function of temperature and pressure. Feed pressure is constant (P_F = 194.5 kPa) and permeate pressure is varied.

T [K]	P_P [kPa]							
	124	134	144	154	164	174	184	194
273	1.03	0.99	0.95	0.92	0.90	0.87	0.85	0.82
283	1.45	1.40	1.36	1.32	1.28	1.25	1.22	1.19
293	1.86	1.81	1.77	1.72	1.68	1.64	1.61	1.57
298	2.05	2.00	1.95	1.91	1.87	1.83	1.79	1.76
303	2.20	2.15	2.11	2.07	2.03	1.99	1.96	1.92
308	2.33	2.28	2.24	2.20	2.17	2.13	2.10	2.06
313	2.42	2.38	2.34	2.31	2.27	2.24	2.21	2.18
323	2.51	2.48	2.45	2.43	2.40	2.37	2.35	2.32
333	2.51	2.48	2.46	2.44	2.42	2.40	2.38	2.36
343	2.43	2.41	2.39	2.38	2.36	2.35	2.33	2.32
353	2.30	2.29	2.28	2.27	2.26	2.25	2.24	2.23
363	2.16	2.15	2.14	2.14	2.13	2.12	2.12	2.11

The theoretical results take into account only the adsorption part of separation, as underlined in section 6.2. However, separation of nitrogen and oxygen by LTA zeolites is in fact an adsorption-controlled process. This statement is validated by the ideal permselectivities of NaA and CaA membranes that were obtained via experimental techniques. The single-gas permeances through the two tested 4A membranes and their Ca^{2+}-exchanged equivalents at 308 K and 10.5 kPa are reported in Table 22. Although 5A pores are larger than those corresponding to 4A, the ion-exchanged samples showed lower permeance values, perhaps due to the deposition of salts on the membrane pores. Surprisingly the experimental selectivities of the membranes in their sodium-form were higher than those of the Ca-exchanged membranes. This can be attributed to insufficient ion-exchange procedure but we can't draw clear conclusions here, since the membranes were not analysed via energy dispersive X-ray spectroscopy or another suitable procedure that would provide more information about the composition of the zeolite layer before and after ion exchange. Our models and literature data show different trend and namely that 5A molecular sieve exhibits greater separation ability than 4A. This is explained by the fact that the main adsorption force of LTA-type zeolites is the electrostatic interaction between the extra-framework cations and the gas molecules, as outlined in section 5.2. The polarization power of Ca^{2+} is higher than that of Na^{+}, which means that the interaction between Ca^{2+} ions and N_2 (the molecules with stronger quadrupole moment) is of greater power [62].

Table 22: Experimental single-gas permeances through NaA and CaA membranes at 308 K and 10.5 kPa and the corresponding ideal permselectivities.

Membrane	Permeance [mol m^{-2} s^{-1} Pa^{-1}]		α^{*}_{Perm} N_2/O_2
	N_2	O_2	
NaA – Membrane 1	$5.71 \cdot 10^{-9}$	$1.34 \cdot 10^{-9}$	4.27
NaA – Membrane 2	$3.61 \cdot 10^{-9}$	$8.18 \cdot 10^{-10}$	4.42
CaA – Membrane 1	$1.57 \cdot 10^{-9}$	$4.78 \cdot 10^{-10}$	3.28
CaA – Membrane 2	$4.32 \cdot 10^{-10}$	$1.57 \cdot 10^{-10}$	2.75

The predicted selectivity of NaA at 308 K and 10.5 kPa is 2.58 according model (*1*), and 2.32 according model (*2*). The experimentally determined permselectivities, obtained by identical operation conditions, are 4.27 and 4.42 with membranes 1 and 2, respectively, i.e. higher than the theoretical values. In the case of CaA, the selectivities modelled via the two relationships, at the same temperature and pressure drop, are 3.75 and 3.53 (with model parameters employed from [57] and [52] respectively), when $D_{MS,i} \neq f(\theta)$ is assumed, and 2.62 and 2.58 (model parameters as aforementioned), when the assumption is that $D_{MS,i} = f(\theta)$. In comparison, the values calculated from the measured single-gas permeances through the 4A membranes are 3.28 and 2.75. These values are summarized in Table 23.

Table 23: Comparison of the predicted adsorption selectivities and the experimental permselectivities of NaA and CaA at 308 K and 10.5 kPa.

Data Source	Zeolite	α^*_{Ads} **(N$_2$/O$_2$)** T = 308 K, ΔP = 10.5 kPa		α^*_{Perm} **(N$_2$/O$_2$)** T = 308 K, ΔP = 10.5 kPa	
		$D_{MS,i} \neq f(\theta)$	$D_{MS,i} = f(\theta)$	Membrane 1	Membrane 2
Chromatographic Study [57]	NaA	2.59	2.32	4.27	4.42
Chromatographic Study [57]	CaA	3.53	2.58	3.28	2.75
DFT Study [52]		3.75	2.62		

In addition, the predicted α^*_{Ads} values were compared to the pure-component adsorption selectivities of NaA and CaA towards N_2 and O_2 obtained experimentally by Y. Shang et al. (2009) [62]. Reportedly, NaA exhibits adsorption selectivity of 2.8, while α^*_{Ads} of CaA is 3.2, at 298 K and 113 kPa feed pressure. Using identical operation conditions, model (*1*) yields adsorption selectivity of NaA equal to 2.73, and model (*2*) yields 2.42. The theoretical result for CaA via model (*1*) is 3.81, and via model (*2*) it is 2.46 (parameters from G.V. Baron et al.). The results obtained by using the model parameters calculated by G. De Luca et al., gave similar results, as shown in Table 24.

Table 24: Comparison of the predicted and experimental adsorption of NaA and CaA at 298 K and 113 kPa feed pressure.

Data Source	Zeolite	**α^*_{Ads} (N_2/O_2)** T = 298 K, P_F = 113 kPa		**α^*_{Ads} (N_2/O_2)** T = 298 K, P_F = 113 kPa [62]
		$D_{MS,i} \neq f(\theta)$	$D_{MS,i} = f(\theta)$	
Chromatographic Study [57]	NaA	2.73	2.42	2.8
Chromatographic Study [57]	CaA	3.81	2.46	3.2
DFT Study [52]		3.77	2.52	

Although our predicted ideal selectivities differ in a short range depending on the adopted model parameters, the conclusions are in agreement with both experimental and literature values. However, the model derived under the assumption that the Maxwell-Stefan diffusivities depend on the occupancy predicts too low values for the ideal separation factor.

Despite the agreement of the modelled adsorption selectivities with the measured permselectivities exhibited by LTA-type membranes, our attempt to calculate the permselectivities taking into account the diffusivity coefficients was unsuccessful. N_2 is preferentially adsorbed on Linde type A zeolite but has lower diffusivity in respect to oxygen. This leads to very low diffusivity coefficient of N_2 compared to that of O_2. In the hereto-derived predictive models, the influence exerted by the diffusivity on the permselectivity is expressed as ratio of diffusivity coefficients and the impact of these parameters on the results is strong. To illustrate this statement we must report that employing the reported D_S values of $0.014 \cdot 10^{-12}$ m²/s for N_2 and $0.24 \cdot 10^{-12}$ m²/s at 298 K for O_2 diffusing through NaA, results in N_2/O_2 permselectivities in the order of 0.16, i.e. reverse selectivity (O_2/N_2). In the case of CaA, the diffusivity coefficients of the two gases under consideration exhibit more similar values ($1.5 \cdot 10^{-12}$ m²/s for N_2 and $5.0 \cdot 10^{-12}$ m²/s for O_2) and the predicted α^*_{Perm} is approximately ≈1 at 298 K as calculated via the first model, and lower according the values obtained via model (*2*). These values are in contradiction to the permselectivities obtained experimentally with NaA and CaA membranes. Instead, the ratio of the measured single-gas permeances is in a good agreement with the predicted adsorption selectivities without taking into account the diffusion coefficients. This fact suggests that adsorption effects control the N_2/O_2 separation by LTA-type membranes.

To further explore these aspects, we used both models to evaluate the ideal selectivity of ZIF-8 metal organic framework for CO_2 over CH_4. The results for the adsorption selectivities in a 273 – 363 K temperature span and 50 kPa pressure drop (P_F = 150 kPa, P_P = 100 kPa), obtained by utilizing the model parameters given in Table 13, are reported in Figure 28. The models correctly predicted preferential adsorption of CO_2 in respect to CH_4. According literature data, this adsorption trend is valid also for CO_2/CH_4 mixtures [63]. The adsorption selectivities, predicted by the two models, coincide at high temperatures. The theoretical values for the adsorption selectivity were compared to experimental ideal permselectivities of confined ZIF-8 membrane, also reported in Figure 28. The measured selectivities decrease when temperature increases. This trend was reproduced well with both models. Moreover, the predicted α^*_{Ads} values and the experimental permselectivities are in close margins, where the theoretical adsorption selectivities (referring to the ideal case, i.e. treating single-component data) are lower than the measured ideal permselectivities. The difference between them is ascribed to the diffusivity contribution, which again should be in favour of CO_2 [63].

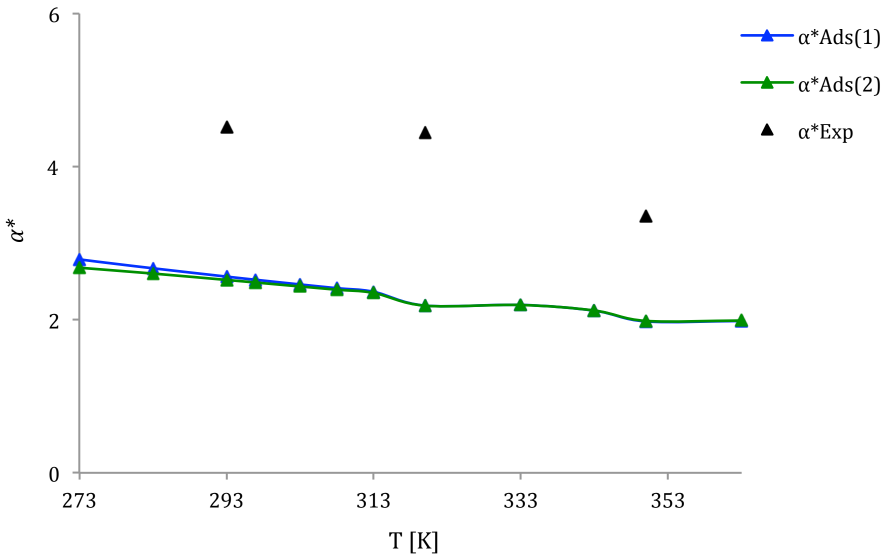

Figure 28: CO_2/CH_4 adsorption selectivity of ZIF-8 modelled as function of temperature at ΔP = 50 kPa. $\alpha^*_{Ads}(1)$ and $\alpha^*_{Ads}(2)$ stand for the values obtained by model (*1*) and (*2*). α^*_{Exp} indicates the experimental permselectivity values with identical operating conditions.

However, as in the case of LTA zeolite, quantitative forecast of the permselectivities could not be obtained because reliable values for D_{MS} are lacking. To propose analytical relationships for the contribution of the diffusivity coefficients as a function of other parameters goes beyond the scope of this work. The discrepancy among self-diffusion coefficients listed in the literature leads to difference in the results for α^*_{Perm} with a factor of 50. In order to clarify the utility of the proposed models to describe the separation performance of metal organic frameworks, measurements of the adsorption selectivity of ZIF-8 membranes or membranes made with another MOF material are required. Then direct comparison between both the theoretical and experimental values for α^{*}_{Ads} can verify the reliability of models (*1*) and (*2*) for this class of crystalline porous materials. In addition, establishing a procedure for assessment of D_{MS} is essential for a good exploitation of the models for predicting the separation properties of MOF-based membranes in terms of both adsorption and diffusion selectivities.

8 Conclusions

Implementation of the derived models, based on Maxwell-Stefan theory, showed that the adsorption selectivities of crystalline porous materials can be predicted with just few single-gas parameters obtained experimentally or computationally. These models, combined with computer accurate computational techniques can play an important role at the process design stage in the selection of zeolite or MOF materials for preparation of membranes by providing predictions of the expected (ideal) behaviour in the absence of membrane defects. Utilizing just few parameters, the proposed models are simple and their goal is to provide:

i) the order of magnitude of the adsorption selectivity of materials used for membrane preparation;

ii) the trend of the adsorption selectivity with respect to temperature and pressure.

These objectives were achieved. Modelling the separation factors for gas mixtures and taking into account defects in a real membrane was not pursued. In fact, this would require complex models with hardly obtainable parameters. The results provided by the hereto-proposed models must be considered as ideal (boundary) values. Their implementation at early research stage is aimed to recommend suitable candidate materials for membrane fabrication and to alleviate the experimental workload by exclusion of poor performing materials for target separations.

Finally, it should be pointed out that the diffusion coefficients were not the subject of this study and expression of the ratio of the diffusion coefficients in an analytical form goes beyond the scope of this thesis. Only the predicted adsorption selectivities are compared with experimental data and the results are discussed qualitatively to verify if a physical sense exists with respect to the measured permselectivities.

Bibliography

[1] J. Xiao, J. Wei, Diffusion mechanism of hydrocarbons in zeolites – I. Theory, Chemical Engineering Science, vol. 47, no. 5, 1123-1141, 1992.

[2] A.J. Burggraaf, Single gas permeation of thin zeolite (MFI) membranes: theory and analysis of experimental observations, Journal of Membrane Science, vol. 155, 45-65, 1999.

[3] J.C. Maxwell, On the dynamical theory of gases, in: The Scientific Papers of J.C. Maxwell, 1965, 26–78.

[4] J. Stefan, Über das Gleichgewicht und Bewegung, insbesondere die Diffusion von Gemischen, Sitzungsberichte der Kaiserlichen Akademie der Wissenschaften, Wien, 63, 1971.

[5] F. Kapteijn, W.J.W. Bakker, G. Zheng, J.A. Moulijn, Temperature- and occupancy-dependent diffusion of n-butane through a silicalite-1 membrane, Microporous Materials, vol. 3, 227-234, 1994.

[6] J. Kärger, S. Vasenkov, S.M. Auerbach, Diffusion in Zeolites, in: Handbook of zeolite science and technology, S.M. Auerbach, K.A. Carrado, P. Dutta (Eds.), New York, USA: Marcel Dekker, Inc., 2003.

[7] M.V. Mundschau, Hydrogen separation using dense composite membranes, in: Inorganic membranes for energy and environmental applications, A.C. Bose (Ed.), New York, NY, USA: Springer, 2009.

[8] S. Mokhatab, W.A. Poe, J.Y. Mark, Chapter 7 - Natural gas dehydration, in: Handbook of natural gas transmission and processing: Principles and practices, 3rd Ed. Amsterdam, The Netherlands: Elsevier, 2015, 223-263.

[9] P. Krokidas, E.D. Skouras, V. Nikolakis, V.N. Burganos, Simulation of sorption and transport in faujasites for gas separation tailoring, in: 4th Conference on Engineering with Membranes, Algarve, 2008.

[10] H. van Bekkum, E.M. Flanigen, P.A. Jacobs, J.C. Jansen, Studies in Surface Science and Catalysis: Introduction to zeolite science and practice, 2nd ed., B. Delmon, J.T. Yates (Eds.), Amsterdam, The Netherlands: Elsevier, vol. 137, 2001.

[11] S.-R. Lee, Y.-H. Son, A. Julbe, J.-H. Choy, Vacuum seeding and secondary growth route to sodalite membrane, Thin Solid Films, vol. 495, 92-96, 2006.

[12] J. Cejka, H. van Bekkum (Eds.), Zeolites and ordered mesoporous materials: Progress and prospects, 1st Ed., Amsterdam, The Netherlands: Elsevier, vol. 157, 2005.

[13] M. Tsapatsis, Molecular sieves in the nanotechnology era, AIChE Journal, vol. 48, no. 4, 654-660, 2002.

[14] Ch. Günter, H. Richter, I. Voigt, Zeolite membranes for hydrogen and water separation under harsh conditions, Chemical Engineering Transactions, vol. 32, 2013.

[15] J. Gascon, F. Kapteijn, B. Zornoza, V. Sebastián, C. Casado, J. Coronas, Practical approach to zeolitic membranes and coatings: state of the art, opportunities, barriers, and future perspectives, Chemistry of Materials, vol. 24, 2829-2844, 2015.

[16] Ch. Baerlocher, L.B. McCusker, Atlas of zeolite framework types, 6th Ed., D.H. Olson (Ed.) Amsterdam, The Netherlands: Elsevier, 2007.

[17] W. Yang, Y. Li, Zeolite membranes, in Inorganic membranes for energy and environmental applications, A. C. Bose (Ed.), New York, NY, USA: Springer, 2009, 275-285.

[18] G. Guan, K. Kusakabe, S. Morooka, Separation of N_2 from O_2 and other gases using FAU-type zeolite membranes, Journal of Chemical Engineering of Japan, vol. 34, no. 8, 990-997, 2001.

[19] A. Corma, F. Rey, J. Rius, M.J. Sabater, S. Valencia, Supramolecular self-assembled molecules as organic directing agent for synthesis of zeolites, Nature, vol. 431, 287-290, 2004.

[20] http://www.qzhuiying.cn, October 2015

[21] R.T. Yang, Gas separation by adsorption processes. Boston, USA: Butterworth Publishers, 1986.

[22] W.J. Thomas, B. Crittenden, Adsorption technology and design, 1st Ed., Oxford, UK: Butterworth-Heinemann, 1998.

[23] J.A. Martens, D. Ghys, M. Van de Voorde, H. Verelst, G. Baron, P.A. Jacobs, Chromatographic study of the adsorption of O_2, N_2, Ar and CH_4 in cation exchanged A, X and Y zeolites, Separation Technology, 819-828, 1994.

[24] R.J. Neddenriep, Sodium cation adsorption sites in zeolite types X and Y, Journal of Colloid and Interface Science, vol. 28, no. 2, 293-304, 1968.

[25] S. Sircar, A.L. Myers, Gas Separation by Zeolites, in Handbook of zeolite science and technology, S.M. Auerbach, K.A. Carrado, P.K. Dutta (Eds.), New York, NY, USA: Marcel Dekker, Inc., 2003.

[26] N. Burke, J. Zhang, S. Huang, S. Limd, Y. Zhue Y. Yang, Influence of charge compensating cations on propane adsorption in X zeolites: experimental measurement and mathematical modeling, Royal Society of Chemistry Advances, vol. 4, 7279–7287, 2014.

[27] Ch.-H. Nicolas, V. Moizan-Basle, C. Nieto, H. Amrouche, N. Bats, N. Audebrand, D. Farrusseng S. Aguado, Facile synthesis of an ultramicroporous MOF tubular membrane with selectivity towards CO_2, New Journal of Chemistry, vol. 35, 41-44, 2011.

[28] H. Wu, W. Zhou, T. Yildirim, Hydrogen storage in a prototypical zeolitic imidazolate framework-8, Journal of the American Chemical Society, vol. 129, 5314-5315, 2007.

[29] Y.-S. Li, F.-Y. Liang, H. Bux, A. Feldhoff, W.-S. Yang, J. Caro, Molecular sieve membrane: supported metal–organic framework with high hydrogen selectivity, Angewandte Chemie International Edition, vol. 49, 548 –551, 2010.

[30] N. Liédana, A. Galve, C. Rubio, C. Téllez, J. Coronas, CAF@ZIF-8: One-step encapsulation of caffeine in MOF, ACS Applied Materials and Interfaces, vol. 4, no. 9, 5016-5021, 2012.

[31] A. Caravella, P.F. Zito, A. Brunetti, E. Drioli, G. Barbieri, Adsorption properties and permeation performance of DD3R zeolite membranes, Chemical Engineering Transactions, vol. 43, 1075-1080, 2015.

[32] B. Liu, B. Smit, Comparative molecular simulation study of CO_2/N_2 and CH_4/N_2 separation in zeolites and metal-organic frameworks, Langmuir, vol. 25, no. 10, 5918-5926, 2008.

[33] T. Seike, M. Matsuda, M. Miyake, Preparation of FAU type zeolite membranes by electrophoretic deposition and their separation properties, Journal of Materials Chemistry, vol. 12, 366–368, 2002.

[34] K. Kusakabe, T. Kuroda, K. Uchino, Y. Hasegawa, S. Morooka, Gas permeation properties of ion-exchanged faujasite-type zeolite membranes, AIChE Journal, vol. 45, no. 6, 1220-1226, 1999.

[35] K. Kusakabe, T. Kuroda, S. Morooka, Separation of carbon dioxide from nitrogen using ion-exchanged faujasite-type zeolite membranes formed on porous support tubes, Journal of Membrane Science, vol. 148, 13-23, 1998.

[36] A. Battisti, S. Taioli, G. Garberoglio, Zeolitic imidazolate frameworks for separation of binary mixtures of CO_2, CH_4, N_2 and H_2: A computer simulation investigation, Microporous and Mesoporous Materials, vol. 143, 46–53, 2011.

[37] F. Cacho-Bailo, S. Catalan-Aguirre, M. Etxeberria-Benavides, O. Karvan, V. Sebastian, C. Tellez, J. Coronas, Metal-organic framework membranes on the inner-side of a polymeric hollow fiber by microfluidic synthesis, Journal of Membrane Science, vol. 476, 277-285, 2015.

[38] K. Aoki, K. Kusakabe, S. Morooka, Gas permeation properties of A-type zeolite membrane formed on porous substrate by hydrothermal synthesis, Journal of Membrane Science, vol. 141, 197-205, 1998.

[39] X. Xu, W. Yang, J. Liu, L. Lin, Synthesis of a high-permeance NaA zeolite membrane by microwave heating, Advanced Materials, vol. 12, 195-198, 2000.

[40] A. Navajas, R. Mallada, C. Téllez, J. Coronas, M. Menéndez, J. Santamaría, Study on the reproducibility of mordenite tubular membranes used in dehydration of ethanol, Journal of Membrane science, vol. 299, no. 1, 166-173, 2007.

[41] J.L. Falconer, R.D. Noble, R. Krishna S. Li, Interpreting unary, binary and ternary mixture permeation across a SAPO-34 membrane with loading-dependent Maxwell-Stefan diffusivities, The Journal of Physical Chemistry C, vol. 111, 5075-5082, 2007.

[42] L. Riekert, Sorption, diffusion, and catalytic reaction in zeolites, Advances in Catalysis, vol. 21, 281-321, 1970.

[43] J. Kärger, H. Pfeifer, N.m.r. self-diffusion studies in zeolite science and technology, Zeolites, vol. 7, 90-107, 1987.

[44] N.A. Al-Baghli, K.F. Loughlin, Adsorption of Methane, Ethane, and Ethylene on Titanosilicate ETS-10 Zeolite, Journal of Chemical and Engineering Data, vol. 50, 843-848, 2005.

[45] A. Caravella, P.F. Zito, A. Brunetti, E. Drioli, G. Barbieri, Evaluation of pure-component adsorption properties of DD3R based on the Langmuir and Sips models, Journal of Chemical and Engineering Data, vol. 60, 2343–2355, 2015.

[46] A. Caravella, P.F. Zito, A. Brunetti, G. Barbieri, E. Drioli, Evaluation of pure-component adsorption properties of silicalite based on the Langmuir and Sips models, American Institute of Chemical Engineers Journal, 2015.

[47] L.J.P. van den Broeke, F. Kapteijn, J.A. Moulijn, Transport and separation properties of a silicalite-1 membrane – II. Variable separation factor, Chemical Engineering Science, vol. 54, 256-269, 1999.

[48] Z. Mao, S.B. Sinnott, Separation of organic molecular mixtures in carbon nanotubes and bundles: molecular dynamics simulations, Journal of Physical Chemistry B, vol. 105, 6916-6924, 2001.

[49] A. Julbe, Zeolite membranes – synthesis, characterization and application, in: Introduction to zeolite molecular sieves, 3rd Ed., J. Cejka, H. van Bekkum, A. Corma, F. Schüth (Eds.), Elsevier, 2007, 181-219.

[50] R. Krishna, R. Baur, Analytic solution of the Maxwell-Stefan equations for multicomponent permeation across a zeolite membrane, Chemical Engineering Journal, vol. 97, 37-45, 2004.

[51] F. Kapteijn, J.A. Moulijn, R. Krishna, The generalized Maxwell-Stefan model for diffusion in zeolites: sorbate molecules with different saturation loadings, Chemical Engineering Science, vol. 55, 2923-2930, 2000.

[52] G. De Luca, P. Pullumbi, N. Russo, Density functional theory calculations of Henry's constant for N_2, O_2 and Ar in Ca-A and Ca-LSX zeolites, Studies in Surface and Catalysis, vol. 142, 2003-2010, 2002.

[53] A.I. Skoulidas, D.S. Sholl, Direct tests of the Darken approximation for molecular diffusion in zeolites using equilibrium molecular dynamics, The Journal of Physical Chemistry B, vol. 105, no. 16, 3151-3154, 2001.

[54] D.M. Ruthven, Diffusion in zeolites – a continuing saga, Adsorption, vol. 16, 511–514, 2010.

[55] J. Kärger, Measurement of Diffusion in Zeolites – A Never Ending Challenge?, Adsorption, vol. 9, 29–35, 2003.

[56] H.A. Boniface, D.M. Ruthven, Selectivity of some zeolites for adsorption atmospheric gases, Gas Separation and Purification, vol. 7, no. 3, 183-184, 1993.

[57] G.V. Baron, M. Van de Voorde, J. Martens, P. Jacobs, Diffusion in zeolite adsorbents: measurement, modelling and structure – performance relation, in: Fundamentals of Adsorption, M. Suzuki (Ed.), Kyoto, Japan: Elsevier, 1993, vol. 80, 45-49.

[58] P.M. Mathias, R. Kumar, J.D. Moyer, J.M. Schork, S.R. Srinivasan, S.R. Auvil, O. Talu, Correlation of multicomponent gas adsorption by the dual-site Langmuir model. Application to nitrogen/oxygen adsorption on 5A-zeolite, Industrial and Engineering Chemistry Research, vol. 35, 2477-2483, 1996.

[59] J. Perez-Pellitero, H. Amrouche, F.R. Siperstein, G. Pirngruber, C. Nieto-Draghi, G. Chaplais, A. Simon-Masseron, D. Bazer-Bachi, D. Peralta, N. Bats, Adsorption of CO_2, CH_4, and N_2 on zeolitic imidazolate frameworks: experiments and simulations, Chemistry: A European Journal, vol. 16, 1560-1571, 2010.

[60] H. Kita, K. Horii, Y. Ohtoshi, K. Tanaka, K.-I. Okamoto, Synthesis of a zeolite NaA membrane for pervaporation of water/organic liquid mixtures, Journal of Materials Science Letters, vol. 14, no. 3, 206-208, 1995.

[61] M. Drobek, M. Bechelany, C. Vallicari, A.A. Chaaya, Ch. Charmette, C. Salvador-Levehang, Ph. Miele, A. Julbe, An innovative approach for the preparation of confined ZIF-8 membranes by conversion of ZnO ALD layers, Journal of Membrane Science, vol. 475, 39–46, 2015.

[62] Y. Shang, J. Zhu, Y. Wang, C. Meng, Study on adsorption of N_2 and O_2 by magnesium(II)-exchanged zeolite A, Journal of Alloys and Compounds, vol. 478, 15-17, 2009.

[63] Ch. Chmelik, J. van Baten, R. Krishna, Hindering effects in diffusion of CO_2/CH_4 mixtures in ZIF-8 crystals, Journal of Membrane Science, vol. 397-398, 87–91, 2012.

Scientific activities

Institutions and Mobility periods

Home university

University of Calabria (UNICAL):	1 November 2012 – 28 February 2013 (16 months)
	1 September 2015 – 31 October 2015 (2 months)
	1 May 2015 – 31 October 2015 (6 months)

At UNICAL the research has been conducted at the Department of Environmental and Chemical Engineering (DIATIC) in cooperation with the Institute on Membrane Technology (ITM-CNR).

Host universities

University of Zaragoza (UNIZAR):	1 March 2014 – 31 August 2014 (6 months)
University of Montpellier (UM):	1 November 2014 – 30 April 2015 (6 months)

The research at UNIZAR was carried out at the Chemical & Environmental Engineering Department & Nanoscience Institute of Aragon (INA). The work at UM was undertaken at the Institut Européen des Membranes (IEM).

Exchange Period as Visiting scientist

Commonwealth Scientific & Industrial Research Organisation (CSIRO):

13 July 2015 – 13 August 2015 (1 month)

Courses and workshops

Membrane course, organized by ITM-CNR (Rende, Italy), January – March 2013 (20 hours).

29th EMS Summer School on ‘Membranes for liquid separations from an industrial & academic point of view’, organized by Universität Duisburg-Essen (Essen, Germany), 22 – 26 July 2013.

XXXI EMS Summerschool on ‘Innovative Membrane Systems’, organized by ITM-CNR, Cetraro, Italy, 28 September – 3 October 2014.

Advanced Markov Modeling, organized by Ecole Doctorale I2S (Montpellier, France), February 2015 (17 hours).

Français Langue Étrangère (FLE), organized by Collège Doctoral Languedoc Roussillon (Montpellier, France), February – May 2015 (28 hours).

XXXII EMS Summer Membrane School 'Integrated and Electromembrane processes', organized by the Czech Membrane Platform (Stráž pod Ralskem / Liberec, Czech Republic), 21 – 26 June 2015.

4th MSA Workshop & Networking: Cheramic based membranes for gas separation applications, organized by Queensland University (Brisbane, Australia), 07. August 2015

Business model and business plan, organized by Tappa Formativa (Cosenza, Italy), November 2015 (8 hours).

Conference Poster Presentations

'Predictive ab-initio study of the selectivity of crystalline nano-porous materials with respect to light gases', J. Evtimova, G. De Luca, J. Coronas, E. Drioli. 10th International Conference on Membrane and Membrane Processes, Suzhou, China, 20 – 25 July 2014.

'Hydrogen trapping in metal alloys used in gas separation membranes', G. De Luca, J. Evtimova, E. Drioli. 10th International Conference on Membrane and Membrane Processes, Suzhou, China, 20 – 25 July 2014.

'A study of the selectivity of crystalline nano-porous materials and on non-Pd metal alloys used in gas separation membranes', J. Evtimova, G. De Luca, J. Coronas, E. Drioli. EMS Summerschool, Cetraro, Italy, 28 September – 3 October 2014.

'A density functional theory study of V-based metal alloys for hydrogen separation membranes', J. Evtimova, G. De Luca, Enrico Drioli. EMS Summerschool, Prague, Czech Republic, 21 – 26 June 2015.

'First-principles Screening of VNiTi alloys used in hydrogen separation membranes', J. Evtimova, G. De Luca, E. Drioli. Euromembrane conference hosted by RWTH, Aachen, Germany, 6 – 10 September 2015.

‘Theoretical models for predicting the ideal gas selectivities of crystalline porous materials’, J. Evtimova, M. Drobek, F. Cacho-Bailo, A. Julbe, J. Coronas, E. Drioli, G. De Luca. Euromembrane conference hosted by RWTH, Aachen, Germany, 6 – 10 September 2015.

Oral Presentations

Conference Oral Presentations

‘Screening Non-Pd Metal Alloys and Crystalline Porous Materials used in Gas Separation Membranes‘, J. Evtimova, G. De Luca, M. Drobek, A. Julbe, E. Drioli. Presented at “The Chemical Browser”, Workshop ENSCM-Montpellier, France, 27 – 28 April 2015.

‘A density functional theory study of VNiTi alloys used in hydrogen separation membranes’, J. Evtimova, G. De Luca, E. Drioli. Pitch presentation at the Euromembrane conference hosted by RWTH, Aachen, Germany, 6 – 10 September 2015.

Oral Presentations at Scientific Events

‘Theoretical and experimental study of zeolites and metal alloys used in membranes for gas separation’, J. Evtimova, G. De Luca, E. Drioli. Presented at the INDIGO & EUDIME Workshop, KULEUVEN, Leuven, Belgium, 17 – 20 September 2013.

6-months, 1-year, 2-years and final progress reports presented at Seminars cycle XXVIII, Dipartimento di Ingegneria per l’Ambiente e il Territorio e Ingegneria Chimica Università della Calabria, Rende, Italy, 2013 – 2015.

‘Study of the selectivity of crystalline nano-porous materials and metal alloys used in gas separation membranes’, J. Evtimova, G. De Luca, E. Drioli, I Kumakiri, H. Kita, F. Cacho-Bailo, C. Tellez, J. Coronas. Presented at the Joint Workshop EUDIME-EM3E, hosted by IEM, Montpellier, France, 2-4 September 2014.

’Study of hydrogen occupation in VNi-based alloys’, J. Evtimova. Presented at CSIRO and UQ, Brisbane, Australia, 10 August 2015.

‘Study on V-based alloys and crystalline porous materials for gas separation membranes’. J. Evtimova. Presented at the 4th Scientific Annual Meeting of the EUDIME Doctorate School, hosted by ITM-CNR, Rende, Italy, 1 – 3 October 2015.

Publications

J. Evtimova, E. Drioli, G. De Luca, 'A density functional theory study of hydrogen occupation in VNiTi alloys used for dense metal membranes', Journal of Alloys and Compounds, submitted (Manuscript Number: JALCOM-D-15-07866).

J. Evtimova, M. Drobek, A. Julbe, J. Coronas, E. Drioli, G. De Luca, 'Theoretical model for predicting the ideal selectivity of crystalline porous membrane materials towards light gases', in preparation.

Appendix A

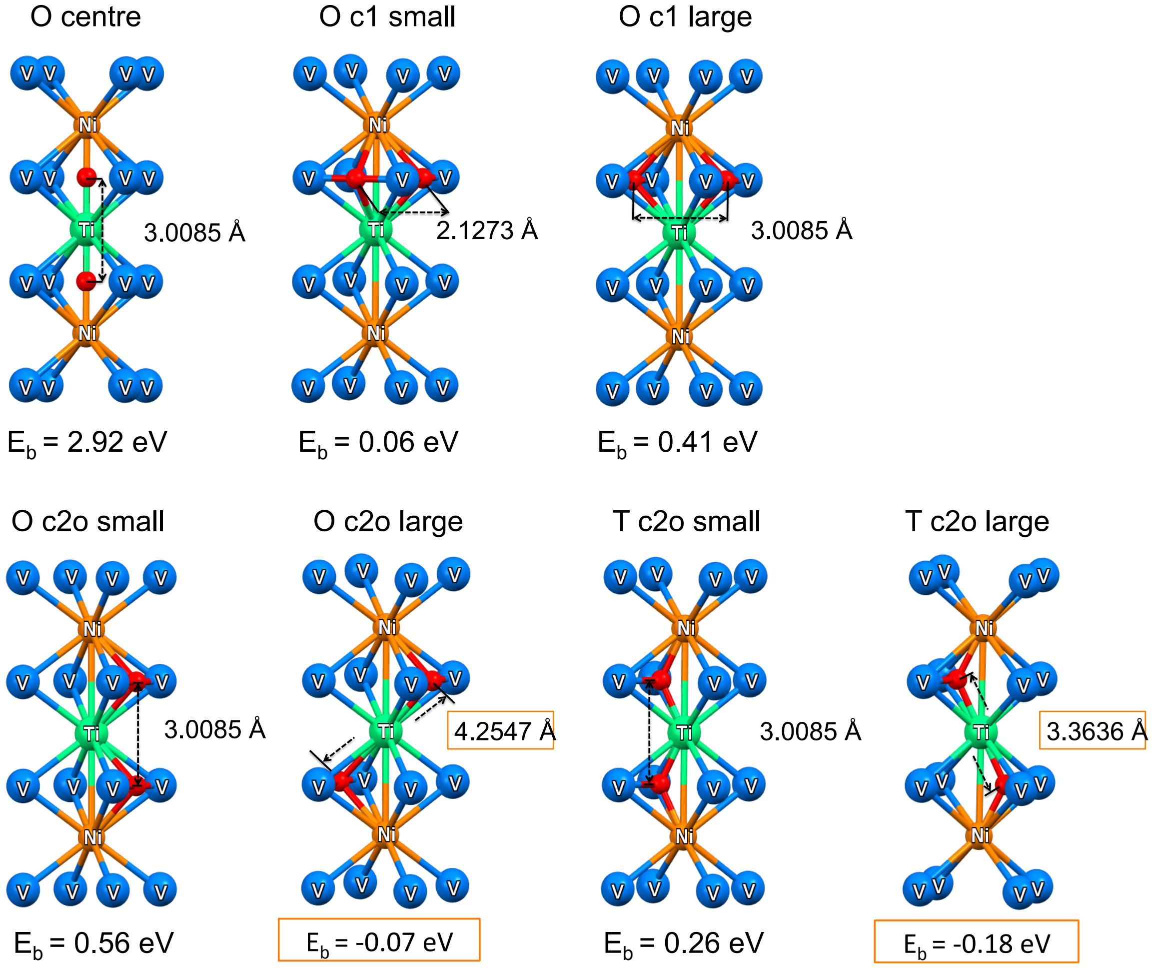

Figure A 1: Non-equivalent H configurations of a pair of H atoms in the utilized $V_{84.2}Ni_{10.5}Ti_{5.3}$ cluster.

Appendix B

B.1 Models boundary conditions

A schematic representation of a gas separation device that utilizes a zeolite membrane is shown in Figure B 1. The support layer is supposed to have sufficiently large pore sizes and therefore to provide a negligible effect to mass transfer limitation.

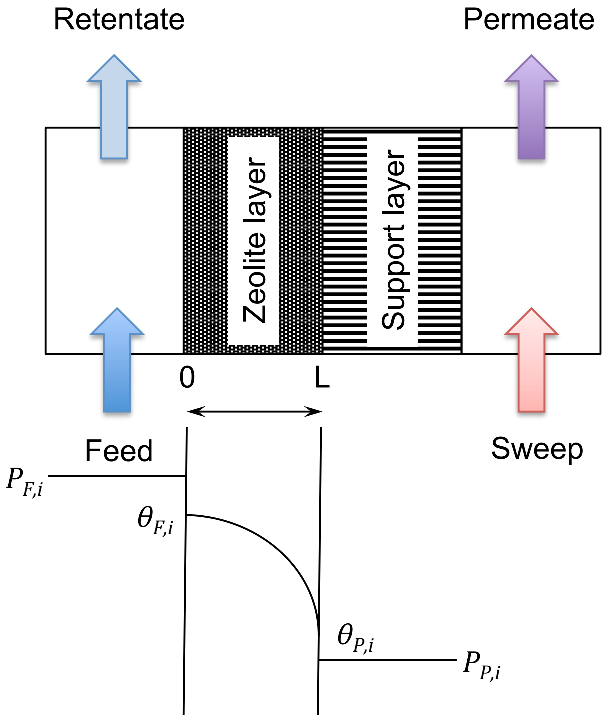

Figure B 1: Schematic representation of a zeolite membrane separation device and the boundary conditions considered for modelling studies of the zeolite layer.

B.2 Procedure for Ca^{2+} ion exchange of NaA powder samples

Source materials:

- Distilled water;
- Calcium chloride: $CaCl_2 \cdot 2H_2O$ (147.1 g/mol);
- 4A zeolite powder: $Na_2O:Al_2O_3:2SiO_2$ (284 g/mol, 20 wt% moisture).

Ion exchange procedure:

(A) 0.25 M aqueous solution of $CaCl_2$ was prepared by dissolving 4.15 g calcium chloride in 115 mL distilled water; this corresponds to 28.21 mmol;

(B) 5 g zeolite powder were added to (A) and the solution was mixed on magnetic stirrer for 2 h at 50 °C;

(C) [(B)] was filtered to recover solids;

(D) The product was washed with distilled water until filtrate conductivity was below 2 mS/cm and then dried on filter paper and watch glass at 100 °C over night.

The amount of Na^+ in the solution corresponds to 14.08 mmol. Therefore 7.04 mmol are stoichiometrically needed for 100 % ion exchange. The amount of Ca^{2+} in the solution corresponds to 28.21 mmol, which is in 400 % excess from the stoichiometrically needed amount.

B.3 Characterization of the powder samples

B.3.1 Titration

Ethylenediaminetetraacetic acid (EDTA) titration of the initial solution of $CaCl_2$ and the mother liquor obtained after ion exchange was performed as follows:

(A) 1 mL NH_3 and ~10 gram NH_4ClO_2 were added to 10 ml of the initial solution/mother liquor in an Erlenmeyer flask and diluted with distilled water;

(B) 1 indicator buffer tablet (Merck, colour: olive green) was dissolved in [(A)];

(C) 0.1 M EDTA solution was filled in a volumetric flask;

(D) [(B)] was titrated with [(C)] until colour change from green to yellow.

The Ca^{2+} concentration determined in initial solution by titration was 0.207 M, while in the mother liquor it was reduced to 0.165 M. This indicates that 4.83 mmol were ion exchanged, corresponding to 68 % ion exchange.

B.3.2 X-ray powder diffraction

X-ray diffraction (XRD) patterns of the initial NaA and the ion-exchanged CaA powder samples were recorded on D-Max Rigaku diffractometer operated at 40 kV and 80 mA, using Cu Kα (λ = 1.5418 Å) radiation. The patterns were collected in a range of 2θ from 4° to 40° at a step of 0.03°. The XRD spectra confirm that the powder samples have LTA crystal structure (with characteristic peaks at 2θ = 7.20; 10.19; 12.49; 14.40; 16.11; 17.65; 23.99; 31.70; 32.54; 34.18 and 33.37[1]) as can be observed by comparing the ideal crystallographic structure patterns and the experimental data. The LTA structure remains essentially unchanged after substitution of Na^+ with Ca^{2+}. There are some differences in the peak intensities due to the different scattering power of the cations.

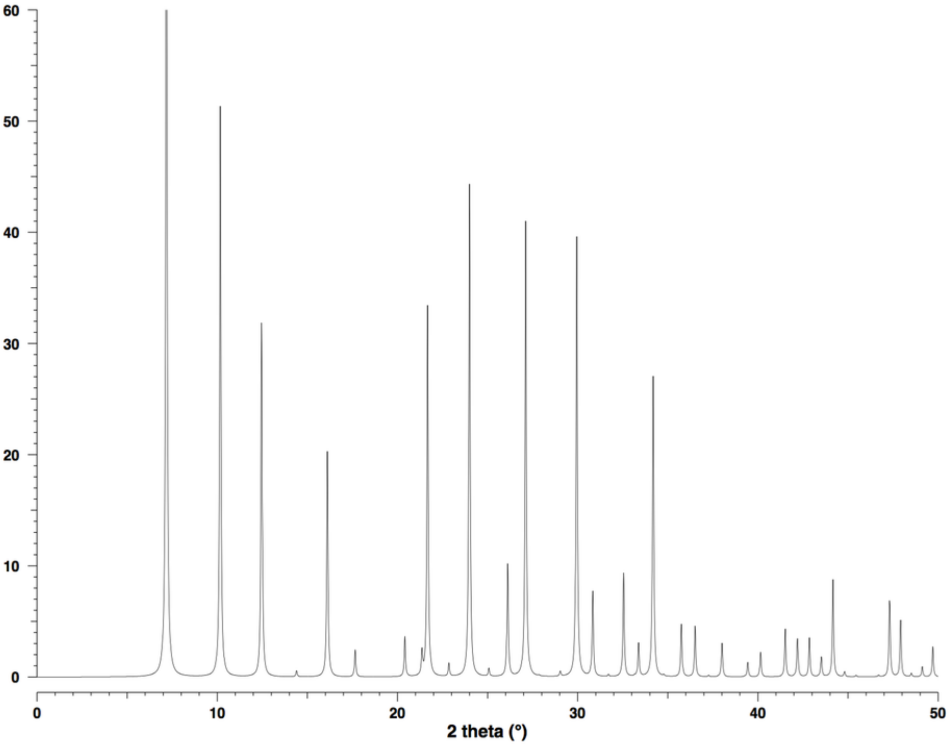

Figure B 2: Simulated X-ray diffraction pattern corresponding to the LTA-type structure.

Source*: M.M.J. Treacy, J.B. Higgins (Eds.), Collection of simulated XRD powder patterns for zeolites, Elsevier, 2001*.

---

[1] M.M.J. Treacy, J.B. Higgins (Eds.), Collection of simulated XRD powder patterns for zeolites, Elsevier, 2001.

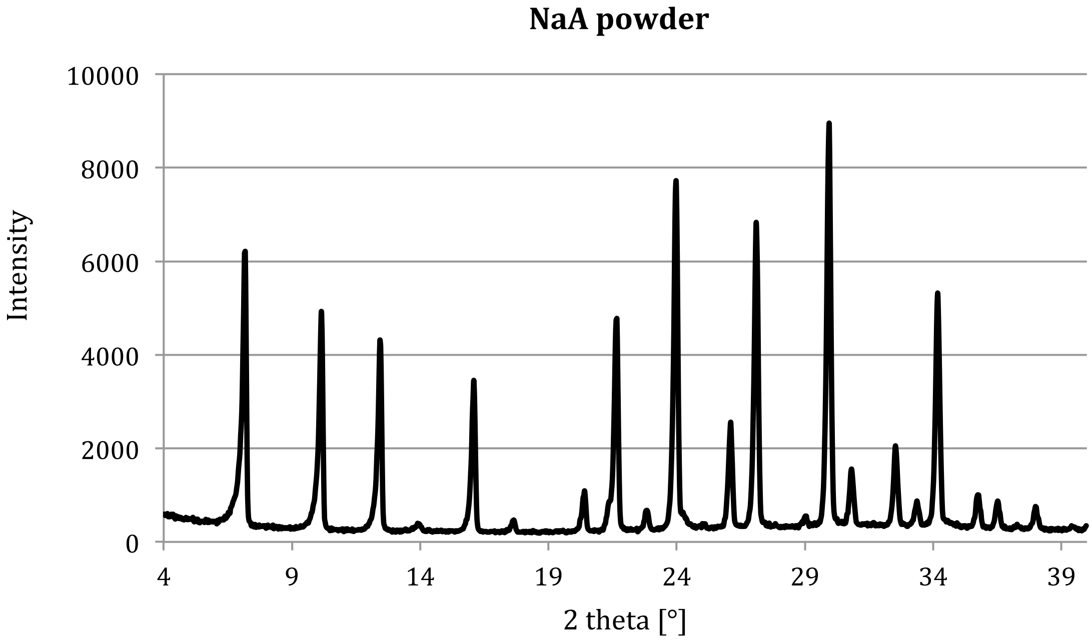

Figure B 3: X-ray diffraction pattern of the NaA powder used for ion exchange.

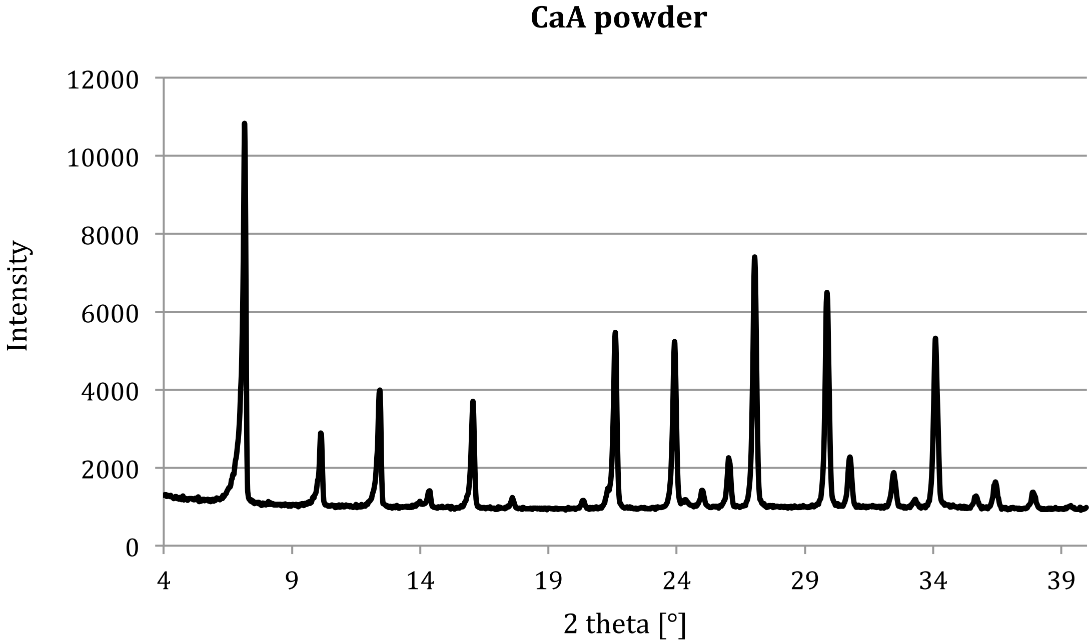

Figure B 4: X-ray diffraction pattern of the ion exchanged CaA powder.

B.3.2 Thermogravimetric analysis

Powder samples from the NaA zeolite and the ion-exchanged CaA sample were analysed on a Mettler Toledo Thermogravimetric (TG) and differential thermal analysis (DTA) equipment to determine the dehydration dynamics of 4A and 5A zeolites. The samples were heated in nitrogen atmosphere from 25 °C to 850 °C at a rate of 10 °C min^{-1}. It is visible from Figure B 5 that temperatures over 150 °C for NaA and 200 °C for CaA are sufficient for dehumidification of the zeolite as pre-treatment before permeation measurements.

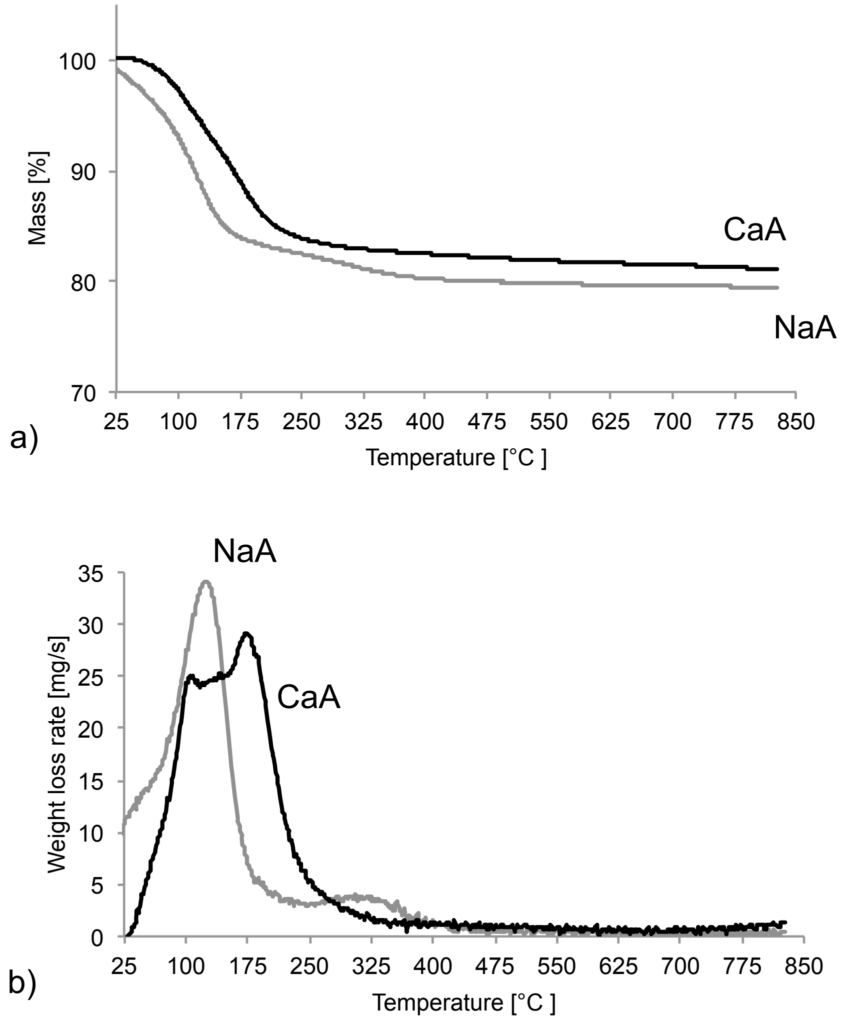

Figure B 5: TGA curves of NaA and CaA powders: a) Evolution of sample mass per cent as a function of temperature; b) corresponding weight loss rate as function of temperature.